

# Design of a Red Bull Flugtag Aircraft

A project present to  
The Faculty of the Department of Aerospace Engineering  
San Jose State University

in partial fulfillment of the requirements for the degree  
*Master of Science in Aerospace Engineering*

By

**Martin R. Sullivan**  
**Jennifer E. Sutton**

May 2014

approved by



Dr. Nikos Mourtos  
Faculty Advisor



# Design of a Red Bull Flugtag Aircraft

Martin R. Sullivan<sup>1</sup> and Jennifer E. Sutton<sup>2</sup>  
San Jose State University, San Jose, CA, 95112

**This project details the process used to engineer a glider for the Red Bull Flugtag competition. It will be the first manned C-wing aircraft in existence, boasting a span efficiency 50% greater than a conventional planar aircraft.**

## Nomenclature

$W$	=	weight
$AR$	=	aspect ratio
$b$	=	span
$S$	=	wing area
$c$	=	chord length
$\rho$	=	density
$\alpha$	=	angle of attack
$CG$	=	center of gravity
$e$	=	wing efficiency factor
$L/D$	=	lift to drag ratio
$c_{ref}$	=	reference chord length
$Re$	=	Reynold's number
$V_\infty$	=	free stream velocity
$V$	=	local velocity
$V_s$	=	stall speed
$V_{L/Dmax}$	=	velocity at maximum L/D

---

<sup>1</sup>Student, Aerospace Engineering Department, 1 Washington Square, San Jose, CA, 95112.

<sup>2</sup>Student, Aerospace Engineering Department, 1 Washington Square, San Jose, CA, 95112.

$c_{lmax}$	=	airfoil maximum lift coefficient
$c_l$	=	airfoil lift coefficient
$c_d$	=	airfoil total drag coefficient
$c_{d\ cruise}$	=	airfoil drag coefficient at cruise angle of attack
$c_m$	=	airfoil pitching moment coefficient
$c_p$	=	airfoil pressure coefficient
$C_{LMAX}$	=	wing maximum lift coefficient
$C_L$	=	wing lift coefficient
$C_{Di}$	=	wing induced drag coefficient
$C_{Do}$	=	wing zero lift drag coefficient
$C_D$	=	wing total drag coefficient
$C_m$	=	wing pitching moment coefficient
$C_p$	=	wing pressure coefficient
$C_x$	=	axial force coefficient, body axes, x-axis about which the craft rolls
$C_y$	=	axial force coefficient, body axes, y-axis about which the craft pitches
$C_z$	=	axial force coefficient, body axes, z-axis about which the craft yaws
$C_n$	=	yawing moment coefficient
$C_{roll}$	=	rolling moment coefficient
$M$	=	mach
$\beta$	=	sideslip
$\hat{p}$	=	roll rate
$\hat{q}$	=	pitch rate
$\hat{r}$	=	yaw rate
$R_A$	=	reaction force at point A
$q_w$	=	wing loading
$q_{wl}$	=	winglet loading
$q_{wc}$	=	wing cap loading
$l_w$	=	length of 1 side of the wing, half span

$W_{wl/wc}$	=	weight of the winglet and wing cap
$M_A$	=	reaction moment at point A
$M_{wl}$	=	resultant wing cap moment
$M_{wc}$	=	resultant winglet moment
$l_{wc}$	=	length of the wing cap
$l_{wl}$	=	length of the winglet
$M_y$	=	internal moment at point x about y axis
$V_z$	=	internal shear force at point x in z direction
$EI$	=	bending stiffness constant, material specific
$v$	=	deflection
$v'$	=	angle of rotation
$A$	=	wing sweep

### **Project Goal**

Design a flight distance world record setting Red Bull Flugtag aircraft, the “Red Bull Flugtag Glider 1” (RBFGL-1).

### **Competition Parameters**

The Red Bull Flugtag is a competition held several times a year in different locations around the world. The concept of the competition is for approximately 32 teams to design and build human powered aircraft to be launched off of a pier into water whether it be the ocean, a lake, et cetera. Scoring is based on a combination of flight distance, creativity and showmanship [1].



**Fig. 1 Competitor launch/flight at Red Bull Flugtag event [1].**

The rules governing the event vary from location to location and from year to year. Specific rules for upcoming events have not yet been made available, however; the rules for recent US events appear consistent enough to begin design of a craft.

The following are the rules expected based on previous events:

1. Height of the flight deck above the water to be 30 ft.
2. Maximum wing-span of craft is not to exceed 28 ft.
3. Height of vehicle inclusive of launch system, is not to exceed 10 ft.
4. Maximum weight including pilot and launch system cannot exceed 450 lbs.
5. Teams are to have 5 members including the pilot.
6. No stored power, gears, pulleys, or catapult systems are allowed. The craft must be entirely powered from team members pushing.
7. The pilot cannot be strapped to the craft.



**Fig. 2 Competitor flight at Red Bull Flugtag event [1].**

The competitors that participate can easily be split into two categories, those that are attempting to fly to a maximum distance and those who are not. Those who make no attempt at having a long distance flight typically have craft more reminiscent of parade floats rather than flight vehicles. Because scoring is not solely based on flight distance, a non-aerial craft is a perfectly reasonable approach and teams using this strategy make up a good percentage, if not the majority, of those competing. Those who do attempt max distance flight typically do not perform significantly better than those who do not try at all. The subtle nuances of aircraft design along with lack of proper construction materials and fabrication techniques, often time's ends with a given craft plummeting quickly into the water in spectacular fashion. An extremely limited number of competitors have achieved recognizable flight.

### **Achieving Record Flight**

The world record flight distance currently stands at 258 ft [2]. It is the expectation of this team to fly a distance of 300 ft  $\pm$ 25 ft. The competition's singular flight based goal, simply to fly as far as possible, allows for a straightforward mission specification with non-competing criteria. Minimizing if not eliminating the need for compromise is a rarity in aircraft design. The main design criteria for the RBF-1 are:

1. Maximum lift over drag ratio.
2. Minimum weight.

Another major component to the flight is how the craft is launched from the flight deck. Since the only potential energy sources are gravity times the 30ft tall flight deck and the team-members, in the form of pushing a vehicle while running, both have to be maximized. Large, physically fit pushers will be used along with the tallest allowable launch cart.

With a simple cart and typical pushing configuration, it is expected that a launch speed of approximately 22 ft/sec can be achieved. To increase that speed, the RBF-1 is planned to be launched from a staged two-tier launch cart. This means instead of 4 people pushing the cart, craft, and pilot; it will be 3 people pushing the bottom cart, top cart, second pusher, craft, and pilot. The second pusher will then be pushing the top cart, craft, and pilot. The sum of the max speed achieved by the bottom 3 pushers along with the single top pusher is expected to be approximately 30 ft/sec. Though this system is more complicated and more susceptible to error, it will significantly increase maximum achievable flight distance.

## Mission Profile

1. Cart is pushed by four team members to maximum achievable velocity off edge of flight deck.
2. Aircraft dives to reach  $V_{L/D \max}$ .
3. Once  $V_{L/D \max}$  is achieved, aircraft maneuvers nose up to maintain max L/D glide slope.
4. Aircraft glides at optimal L/D as far as possible.
5. Aircraft performs "belly" landing on water.

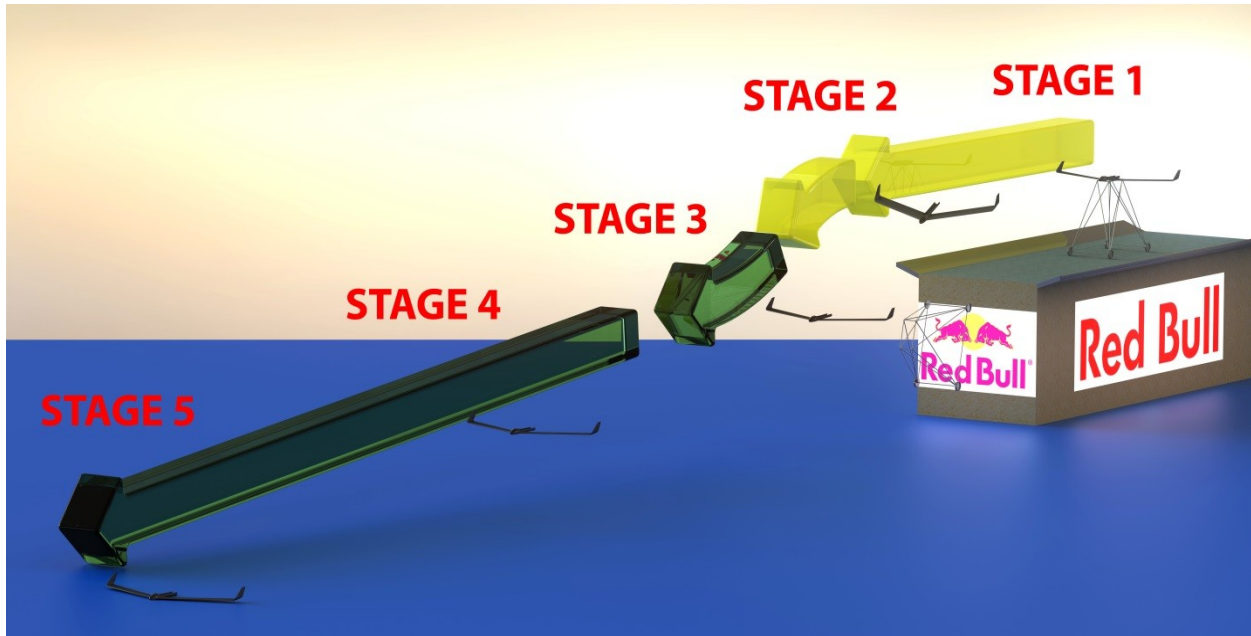


Fig. 3 RBF-1 Mission profile depiction.

## Configuration Discussion

The configuration of the RBF-1 was decided to be tailless early on. The implications of this design choice are far reaching and all encompassing. Though more difficult to design and more sensitive to error, it is believed to be superior to all other possible configurations. Within this section of the report other common configurations are discussed and the reasons why they were not used are explained.

### Conventional Configuration

Because of the small size and ultra-light nature of the RBF-1, a conventional configuration would have come with a possible weight penalty in the way of a tail boom [3]. Also, the tail would likely strike first when flaring while landing in the water, detracting from the total flight distance.

### **Canard Configuration**

A canard configuration, though aerodynamically elegant due to all lift vectors being positive, would suffer from a lower than optimal wing  $C_{Lmax}$  as a design necessity to prevent deep stall. Likewise,  $C_{Lmax}$  values would suffer at an attempt to maximize span efficiency. [4]

### **Biplane Configuration**

The last option is a biplane configuration, considered by many to be the most intuitive choice. A biplane though ideal for high lift situations would likely have a L/D than all other options. This is because a biplane does not add surface area as is commonly believed, but rather reduces chord length thereby increasing aspect ratio.

As can be seen in Eq. 1, increasing aspect ratio can be tremendously advantageous since drag is inversely proportional to AR, however, second order consequences negate this benefit. First, the wings of a biplane would weigh more than a mono-wing of the same area due to the lower airfoil thickness that comes with having a shorter chord. Second, a robust structure would have to be added interconnecting the two wings which would otherwise not be needed on a mono-wing. Lastly, a decrease in chord length will result in a decrease in Reynolds number which would likely prove to be detrimental to airfoil performance in the way of laminar separation bubbles since the aircraft is already flying at a relatively low Reynolds number of approximately 800,000. [4]

$$C_{Di} = \frac{C_L^2}{\pi A R e} \quad ( \text{SEQ Equation } 1 )$$

Though no formal trade study was performed, by analytically weighing the pros and cons of each configuration, it is the belief of the team that the correct configuration was chosen. Even if a tailless design proved to be less optimal than another configuration, it would likely not be by a significant margin. Additionally, scholastically speaking, the added challenge associated with designing the theoretically more complex and sophisticated tailless design is merit enough for its choice over the other more pedestrian options.

### **Layout**

The layout of the RBFQ-1 is very simple when compared with most other aircraft. The only choice that must be made is where to place the pilot with respect to the wing. Without an empennage, engines, landing gear or cargo-hold, layout can be determined post-haste without significant analysis.

## **Pilot Position**

The location of the pilot with respect to the craft can be highly consequential to the total flight distance. The options for pilot location are realistically only above or below the wing. Placing the pilot in front or behind the wing are not available options due to the static margin and aerodynamic performance sensitivity associated with tailless designs. Hang gliders along with rigid wing hang gliders such as the SWIFT typically place the pilot below the wing. This option though appealing aerodynamically is not ideal for the water based belly landing the RBFG-1 will be performing.

There also exists a rule in the competition that the pilot cannot be strapped or attached to the aircraft in anyway [1]. Without a harness, an enclosure would have to be built to house the pilot, making it difficult for the pilot to escape after performing the water based landing and would add unnecessary weight and complexity to the craft. As such, the chosen location of the pilot was determined to be above the wing.

Apart from necessity, aerodynamic advantages and disadvantages come with placing the pilot on top of the wing. An advantage is a more pronounced ground effect towards the end of the glide because the wing can get closer to the water before touching. A disadvantage is the loss of lift at the root of the wing where the pilot will be placed. Also, airfoil moment elevation through lowering the aircraft's center of gravity, a major benefit exploited to great extent by hang gliders, will not be available to the RBFG-1. As such, an airfoil with virtually zero moment coefficient must be used unless another means of moment elevation can be found.

The pilot, placed on the top of the wing, lies prone. This option was chosen over the sitting and supine position to minimize drag and maximize visibility. Issues such as poor ergonomics and lack of sensory orientation encountered with prone flying in previous aircraft like the Horten IV should not be of concern for the short flight duration experienced by the RBFG-1 [5].



**Fig. 4 Picture of Horten IV aircraft and pilot position [6].**

What will need special attention is pilot safety in the event of a nose-first crash landing. The prone position is more precarious than a feet first position in that particular instance. Safety will be a driving factor in cockpit design to prevent injury to the pilot regardless of how the craft hits the water.

### **Preliminary Sizing**

Determining the wing area of the aircraft is only dependent on one constraint, sizing to stall. Other normal considerations like sizing to climb and cruise speed are completely ignored with the short and precise mission profile of the RBF-1. Sizing to stall is based on the single lowest value of two factors, the maximum speed at which it is safe to land, and the maximum achievable speed through the initial push and dive in the beginning of the flight. Landing speed was chosen to be no more than 18.5 knots. This speed was inspired by high performance hang gliders which have similar stall speeds. The maximum achievable takeoff speed was determined by a combination of rudimentary physics and empirical testing. Various objects, specifically motorcycles and bicycles, were pushed as fast as humanly possible and the times were recorded. The average speed from these tests was 13 knots. Taking into account the 2-stage launch cart used and assuming a second pusher can gain an extra 5 kts minimum, a launch speed of 18 knots is reasonable. Since the launch speed is lower than the safe landing speed, it becomes the sizing to stall design parameter.

Preliminary sizing calculations were performed based on the above criteria. An estimated value for  $C_{Lmax}$  was input in conjunction with the estimated stall speed, based off of maximum achievable launch velocity. This, in turn, output the required wing loading for the aircraft. The wing area was then calculated from dividing the craft weight,

estimated at 185 lbs (including weight of the structure and weight of the pilot), by the wing loading calculated in Eq. 2.

$$\frac{W}{S} = \frac{1}{2} \rho V_s^2 C_{Lmax} \quad (1)$$

$$\frac{W}{S} = S \quad (2)$$

The wing area was then restricted by the 28 foot span limitation to achieve the following preliminary sizing values:

**Table 1 Preliminary sizing parameters driven by initial wing area and span constraints.**

<b>Parameter</b>	<b>Preliminary Sizing Value</b>
$C_{Lmax}$	1.4
<b>S</b>	116.4 ft <sup>2</sup>
<b>c</b>	3.88 ft
$V_s$	18.0 kts

## Wing Design

### Nonplanar Wings

An artifact of the rules for the Red Bull Flugtag competition is the aerodynamic advantage nonplanar wing designs have over their much more ubiquitous planar counterparts. In the competition, the wing span is limited to 28 ft and take-off speed, though not explicitly limited, is limited consequently by the banning of any type of mechanical launch system. These factors inevitably lead to an aircraft where the optimal span can never be met with a planar design. Nonplanar wings, however, in terms of inviscid drag efficiency, simulate planar wings of greater span. This means a properly designed nonplanar aircraft should fly farther than a properly designed planar aircraft.

Choosing the correct nonplanar wing for this application was not as difficult of a task as would be expected. With an early commitment to a tailless configuration, winglets were a must from the start, already making the RBF-1 nonplanar. There was still, however, opportunity to be had in the form of a C-wing. Fig. 5 lists span efficiencies for optimally loaded nonplanar systems [7]. As expected, the box wing in the bottom right corner is most efficient, with a span efficiency of 1.46. What is more interesting is the virtually identical performance of the C-wing directly above it. A box wing aircraft is not well suited for this application because of the amount of extra

wetted area and the need for a long fuselage to connect to the back of the wing box. A C-wing, on the other hand, has opportunity to provide the RBF-1 several benefits.

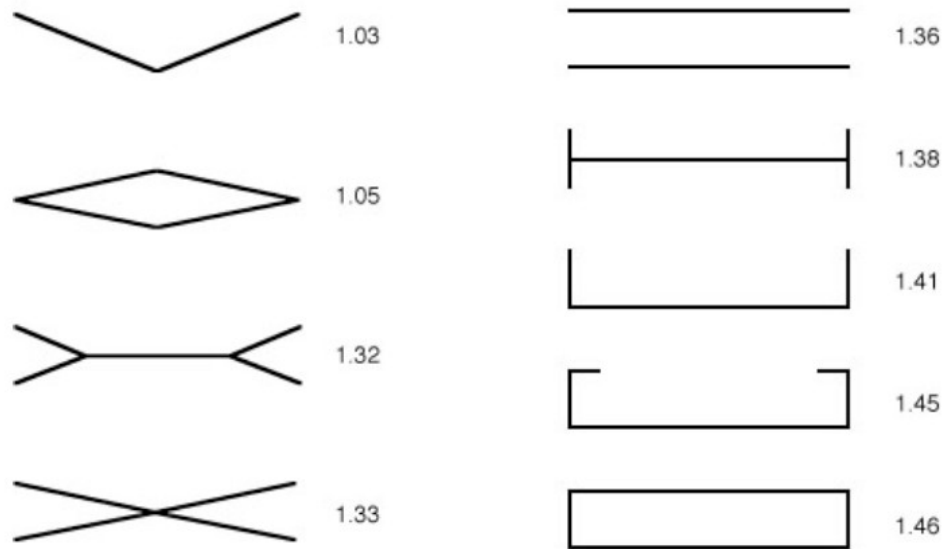


**Fig. 5 Different wing configurations and associated span efficiency [7].**

### C-wings

C-wings elegantly serve the RBF-1 in two ways. First, they increase the effective span reducing inviscid drag [8]. Second, they provide pitch trim. Shown in Fig. 6 the loading on the “wing cap” (the name created by our team to denote the inward jutting lifting surface at the top of the winglet as no official name could be found) is downward. Utilizing this downward force on the wing cap for trim alleviates the amount of twist needed on the wing which in turn improves span efficiency. Since the wing cap is pointed aft instead of parallel with the wing, the trimming moment is provided farther back, thus lessening the amount of sweep needed for the main wing. Less sweep equates to less structural weight, offsetting some of the weight increase the C-wing itself adds. It also means more lift per unit span, a further added benefit.

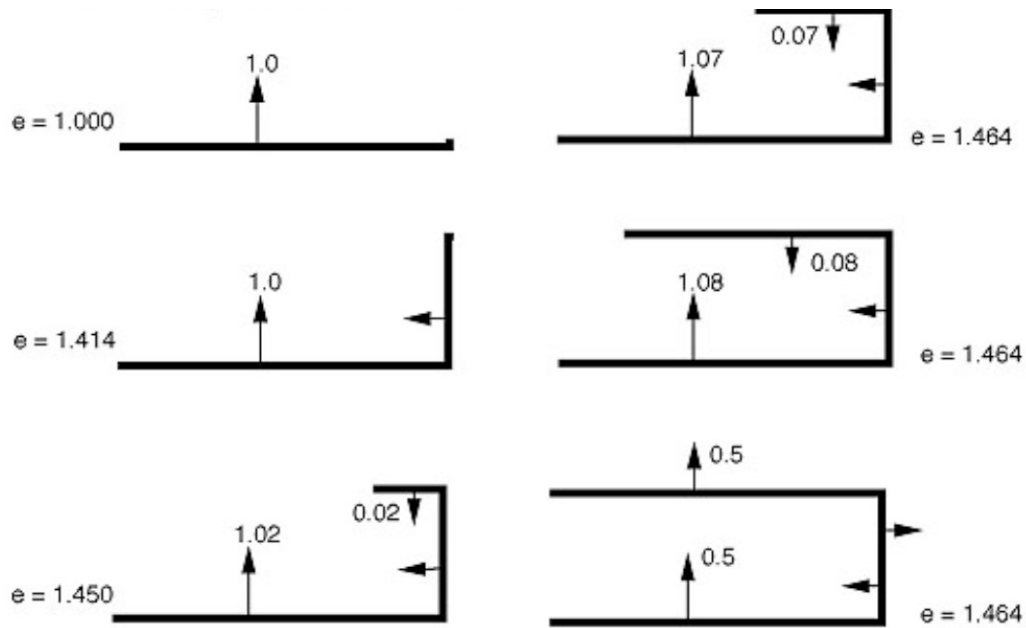


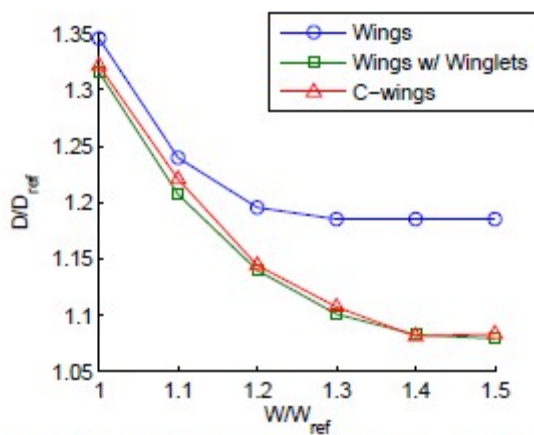
Fig. 6 Span efficiency and load factors for various wing configurations [7].

The graphs and configurations shown in

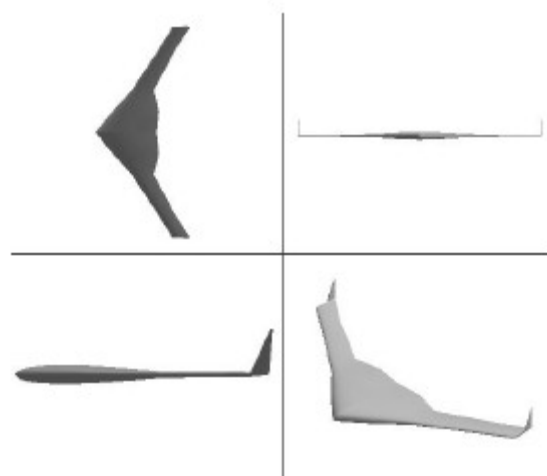
(a) (b) through

(a) (b) correspond to pitching moments about the aerodynamic center of -0.1, 0.0, and 0.1, respectively, for tailless aircraft. These wings were optimized with a fixed constraint on winglet and C-wing geometry leading this team to believe further improvements can be made by eliminating the geometric constraint and by custom tailoring each C-wing shape to each particular wing. With that stated, it is shown C-wings provide little to no benefit for negative and neutral pitching moment constrained designs. The positive pitching moment design, which corresponds to the requirements of the RBFG-1, shows significant decrease in vortex drag however. Furthermore,

(a) (b) shows that by eliminating the sweep constraint of 32 degrees present on Fig. 7 through Fig. 9, total drag savings increases over the planar wing and wing with winglet designs as sweep decreases.



(a)



(b)

Fig. 7 (a) Pareto front for optimized span constrained designs ( $C_{mac} = -0.1$ ). (b) Optimized wing with winglet ( $C_{mac} = -0.1$  and  $W/W_{ref} = 1.3$ ). [8]

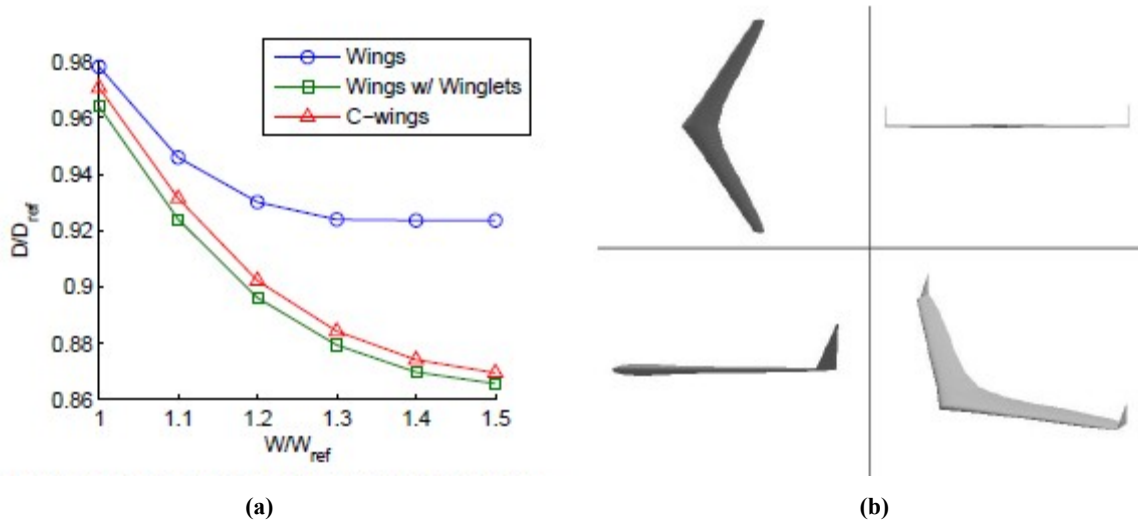
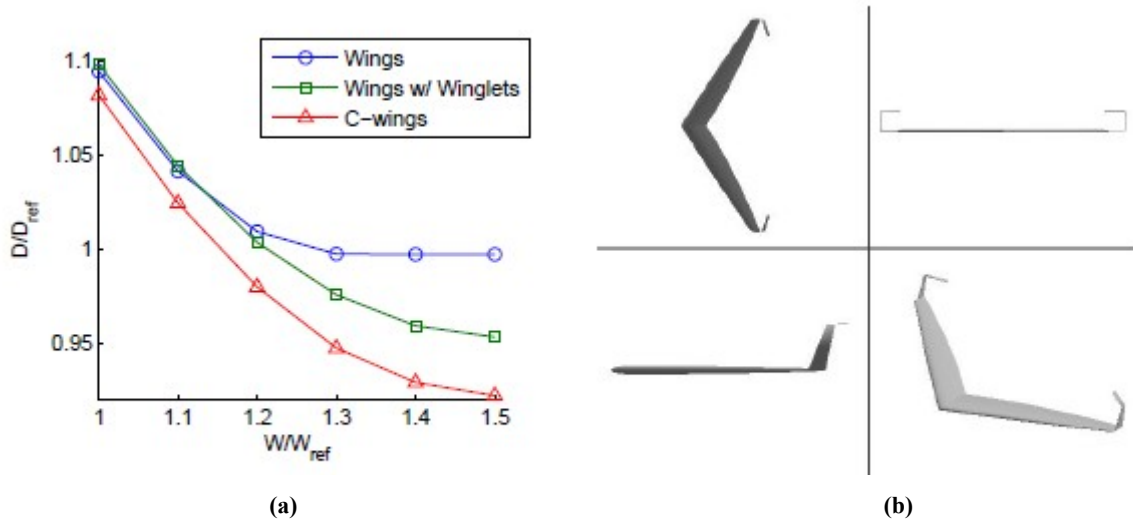
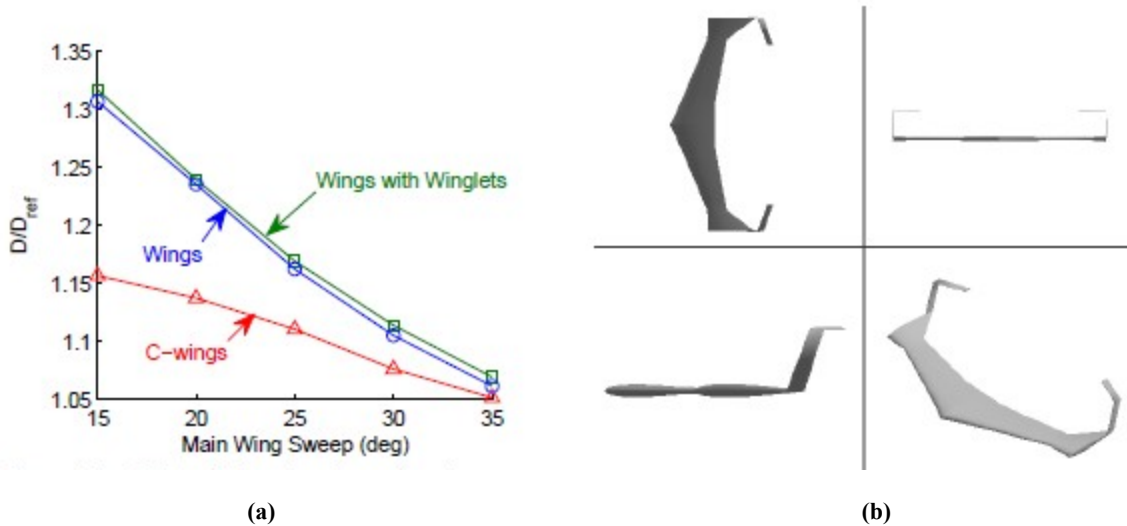


Fig. 8 (a) Pareto front for optimized span constrained designs ( $C_{mac} = 0$ ). (b) Optimized wing with winglet ( $C_{mac} = 0$  and  $W/W_{ref} = 1.3$ ). [8]



**Fig. 9 (a) Pareto front for optimized span constrained designs ( $C_{mac} = 0.1$ ). (b) Optimized C-wing ( $C_{mac} = 0.1$  and  $W/W_{ref} = 1.3$ ). [8]**



**Fig. 10 (a) Effect of changing the main wing sweep ( $C_{mac} = +0.1$ ). (b) Optimized C-wing with winglet ( $C_{mac} = +0.1$  and  $A = 20^\circ$ ). [8]**

To determine the size of the winglet and wing cap, a parametric study was performed varying span, chord, and sweep. The optimized design has the lowest total L/D. With a fixed stall speed, weight will also be taken into consideration as an increase in weight equates to an increase in required planar area. The increase in area will consequently increase the chord length, decreasing the aspect ratio, and thus increasing the induced drag. Through the papers written on C-wings from Dr. Kroo and Dr. Ning, the team feels a good starting point has been established to begin refinement.

It is important to note that this team has found no evidence that a C-wing has ever been utilized on a manned aircraft. The use of C-wings on the RBF-1 will likely be the most interesting and technologically significant aspect of an otherwise humble mission and aircraft.

### Preliminary 3-D Wing Design

An initial 3-D wing design exercise was performed to verify the legitimacy of the decisions made during the configuration and preliminary design phases. Desktop Aeronautics' vortex-lattice solver, LinAir, was used for this process. Inputs into the program are geometry and flow properties, while the outputs are element forces, moments, and stability derivatives. Several assumptions were made for this exercise, they include:

1. An airfoil  $c_{lmax}$  of 1.4, the same  $c_{lmax}$  of the SWIFT's airfoil.
2. Profile drag coefficients are zero.

3. Wing span is 30 ft as opposed to 28 ft.
4. CG is only varied longitudinally with a z value of zero, coincident with the aircraft's centerline.

The main goals set for the initial 3D-wing design were the following:

1. Become comfortable and familiar with the software.
2. Design a trimmed wing stable in pitch.
3. Maximize span efficiency as much as possible without use of an optimizer.

All goals were met. For this initial design phase, the results are as follows:

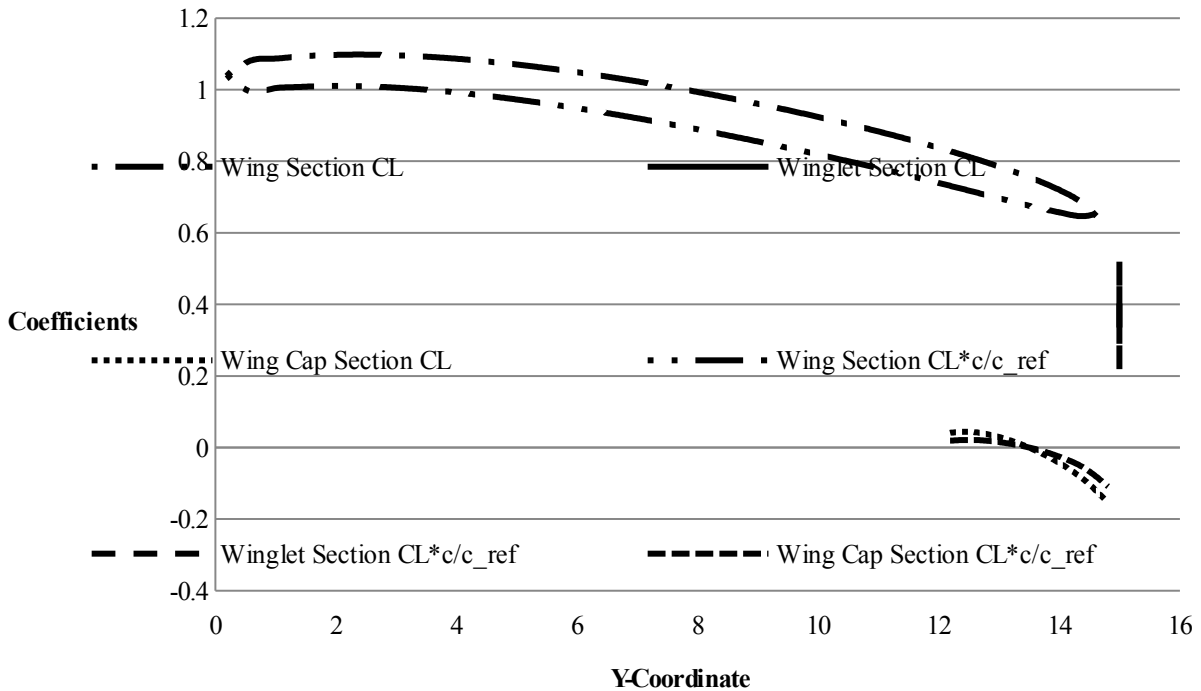


**Fig. 11 Lift distribution for preliminary wing design of RBF1.**

### *Lift Distribution*

Contrary to the typical aircraft design doctrine, the lift distribution shown in Fig. 11 is not elliptical, however, targeting an elliptical lift distribution is not always optimal [7]. The span efficiency for this wing is an approximate value of 1.2 at the angles of attack relevant to the mission. A value of 1.2 is significantly higher than the theoretically perfect value of 1.0 achieved by planar elliptically loaded wings. The maximum section  $C_L$  value is slightly above 1.0 and is well below the assumed airfoil maximum of 1.4. This allows room to modify the neutral control surface pitch trim either up or down to maximize L/D.

### Alpha Sweep

The alpha sweep graphs in Fig. 12 and Fig. 13 show the effects of varying angle of attack (AOA) from 0 degrees to 15 degrees on  $C_L$ ,  $C_D$ ,  $C_m$ , and  $e$  (span efficiency). Most notably, it shows span efficiency to be maximized around an AOA of 5 degrees. For the wing incidence used, an AOA of 5 degrees will result in a relatively low  $C_L$  forcing the glider to fly faster to achieve necessary lift.

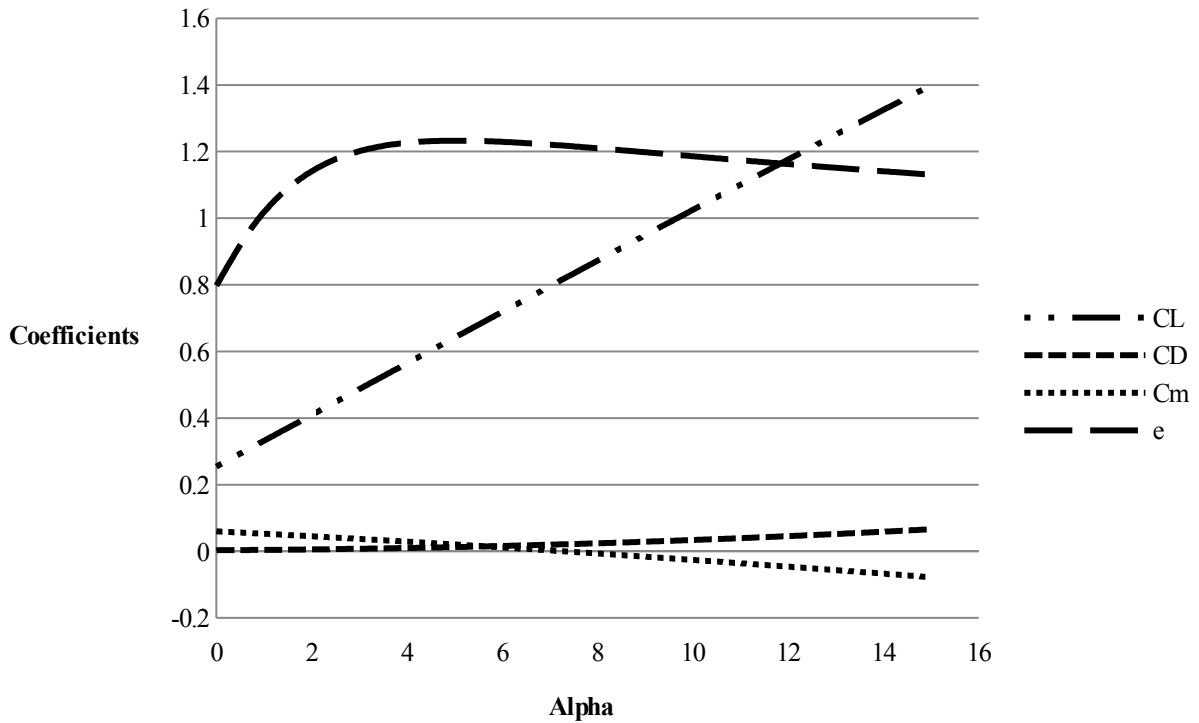


Fig. 12 Alpha sweep graph for preliminary wing design of RBF1-1.

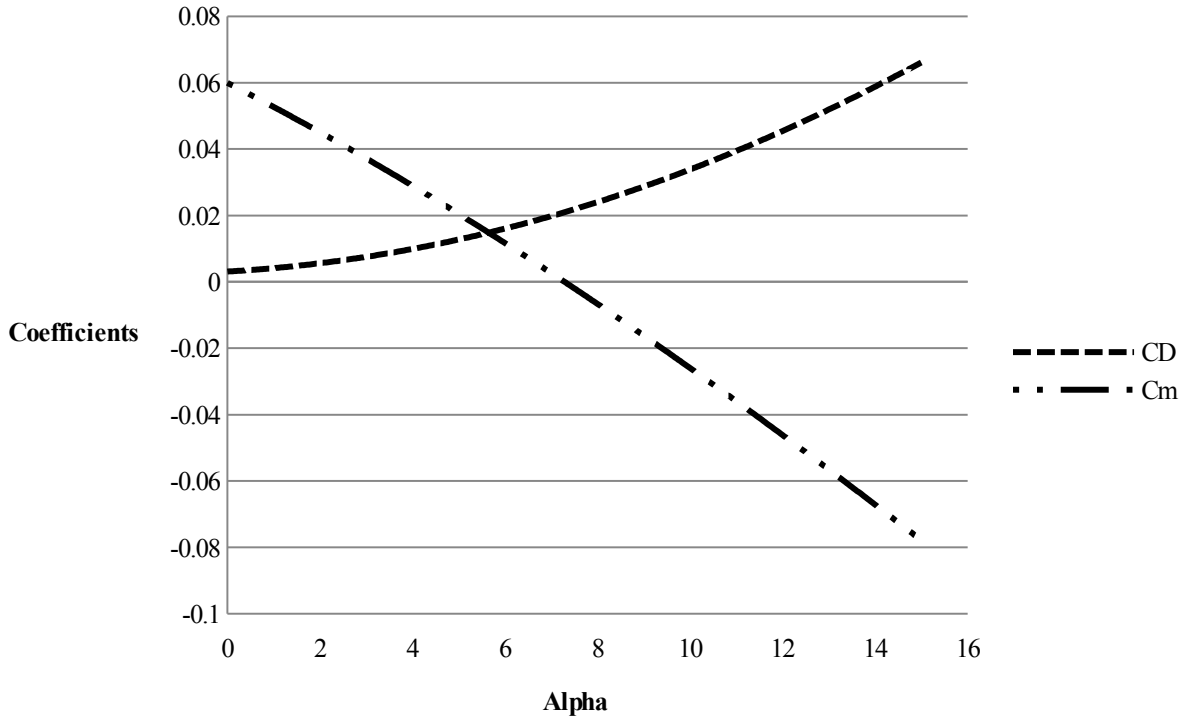


Fig. 13 Alpha sweep graph for preliminary wing design of RBF-1 with higher fidelity for  $C_D$  and  $C_m$ .

*Stability Derivatives*

The basic stability derivatives are shown in Table 2. The only outputs currently being considered are  $C_m-\alpha$  and  $C_L-\alpha$ . Dividing  $C_m-\alpha$  by  $C_L-\alpha$  will provide the static margin of the craft as shown in Eq. 4.

Table 2 Stability derivative table results and static margin calculation for preliminary wing design of RBF-1.

Parameters	$C_L$	$C_D$	$C_x$	$C_z$	$C_y$	$C_m$	$C_n$	$C_{roll}$	Static Margin
$\alpha$	4.35	0.31	-1.47	4.19	0	-0.6	0	0	13%
$M$	0	0	0	0	0	0	0	0	
$\beta$	0	0	0	0	-0.7	0	0.046	-0.219	
$\hat{p}$	0	0	0	0	-0	0	-0.2	-0.664	
$\hat{q}$	4.57	0.41	-0.39	4.57	0	-3.7	0	0	
$\hat{r}$	0	0	0	0	0.38	0	-0.04	0.214	

$$Static\ Margin = \left( \frac{-C_{m\alpha}}{C_{L\alpha}} \right) \cdot 100 \tag{3}$$

A negative value indicates a statically stable craft [4]. This was found to be mostly a function of the longitudinal location of the center of gravity for this particular craft. The CG was placed to produce a static margin of approximately 13%. Less static margin equates to less forces being exerted by the craft on the air around it, resulting in less drag. It is difficult to determine, analytically, a reasonable static margin for a craft flying this slow. Likely the final location of the static margin will be chosen through full scale gimbal testing and/or by the sage advice of those in the know. Fortunately, it can be varied right up until minutes before its flight by adjusting the location of the pilot forward or backward by a few inches.

### **$C_m$ vs. $C_L$**

Graphed in Fig. 14 is  $C_m$  vs.  $C_L$  for a series of wings with twist varying from 5 degrees to 10 degrees. The first interesting fact is that all lines have a negative slope indicating a longitudinally stable craft. Also all lines intersect  $C_m = 0$  but at different  $C_L$  values. The twist chosen will be the instance which provides  $C_L$  corresponding to the lowest  $C_D$ . Changing the location of the CG longitudinally proves to have large impacts on this graph. With the CG too far aft, the lines slope upward resulting in an unstable aircraft. With the CG too far forward the lines begin below  $C_m = 0$ , never intersecting it. Placing the CG in the correct location for the given planform was discovered to be absolutely vital prior to analyzing this aspect of the design.

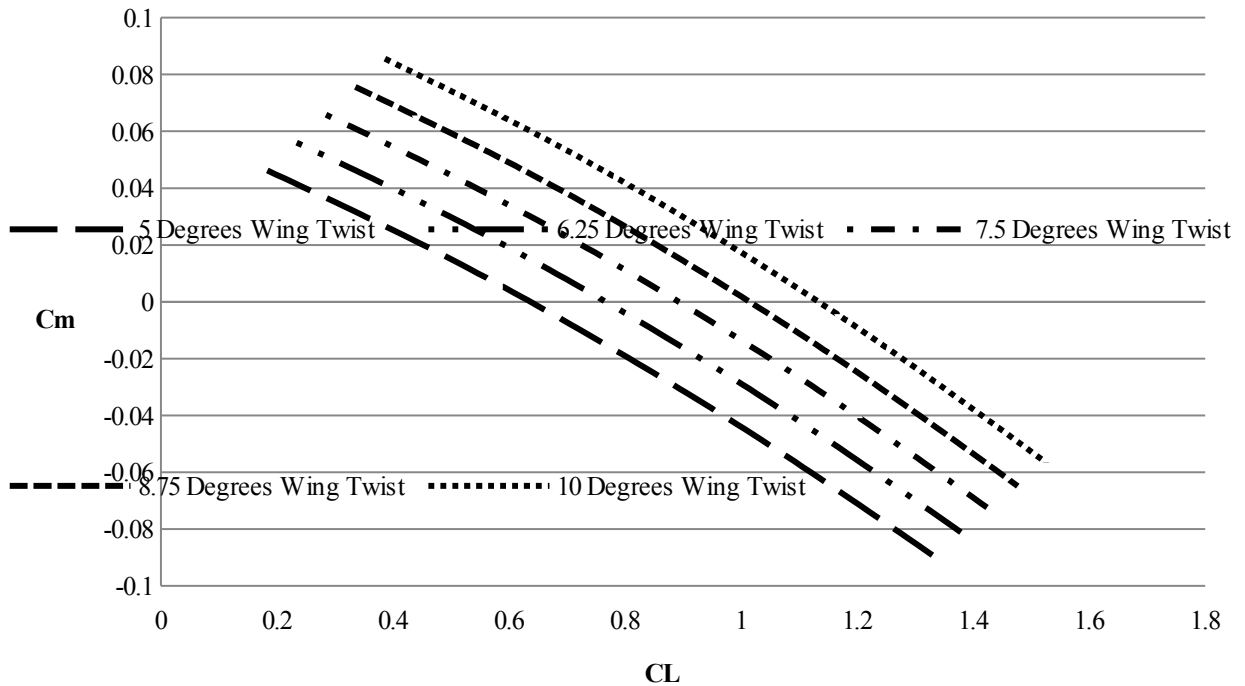


Fig. 14  $C_m$  versus  $C_L$  graph.

#### *Discussion of Preliminary 3-D Wing Design Results*

The results of the preliminary 3-D wing design reinforce the choices made early on. The craft at this phase is functional, though far from optimal. In addition, the lessons learned from varying different aspects of the geometry are extremely valuable, though largely anecdotal. How can one definitively attribute geometric variables to discrete performance changes? How can one truly optimize such a highly coupled and unconventional design? The method chosen by this team was to run a Design of Experiments (DOE). Further description and analytical details of the DOE are contained within the *3-D Wing Design Optimization* section of this report.

#### **Airfoil Selection**

For safety, practicality, and structural reasons; virtually all aircraft flying use airfoils that have compromised aerodynamic performance to some degree. A supersonic fighter needs an airfoil that works both at landing and take-off speeds; a general aviation aircraft needs an airfoil that has gentle and forgiving stall characteristics for novice pilots. These types of compromises are not required for the RBF-1. This allows our team to take advantage of delicate, finicky, but extremely high performance airfoils.

## Wing Airfoil Design

The desired characteristics for the RBF-1's airfoil are listed below.

1. A low moment coefficient.
2. A high  $C_{L,max}$ .
3. A low  $C_D$  at  $C_L$  values between 0.5 and 1.0.

### Initial Design Approach

The team decided to start by analyzing the SWIFT's airfoil. The SWIFT's airfoil has a low pitching moment, a decently high  $c_l$  of 1.4 and low drag. Unfortunately, the coordinates for the airfoil are proprietary preventing us from computing its polars; however, we were able to closely mimic it by heavily modifying a NACA 4416 to exhibit the same pressure coefficient distribution which was dubbed "FlugFoil-9", as shown in Fig. 15 through Fig. 17. As a result, the shape,  $c_l$ ,  $c_m$ , and  $c_d$  were fairly similar. In the process of performing this mimicking exercise, it became clear the SWIFT's airfoil was not a perfect shoe in for the application. Though it exhibits all the traits desired, the RBF-1 has the opportunity to utilize higher performance airfoils due to its unique mission profile.

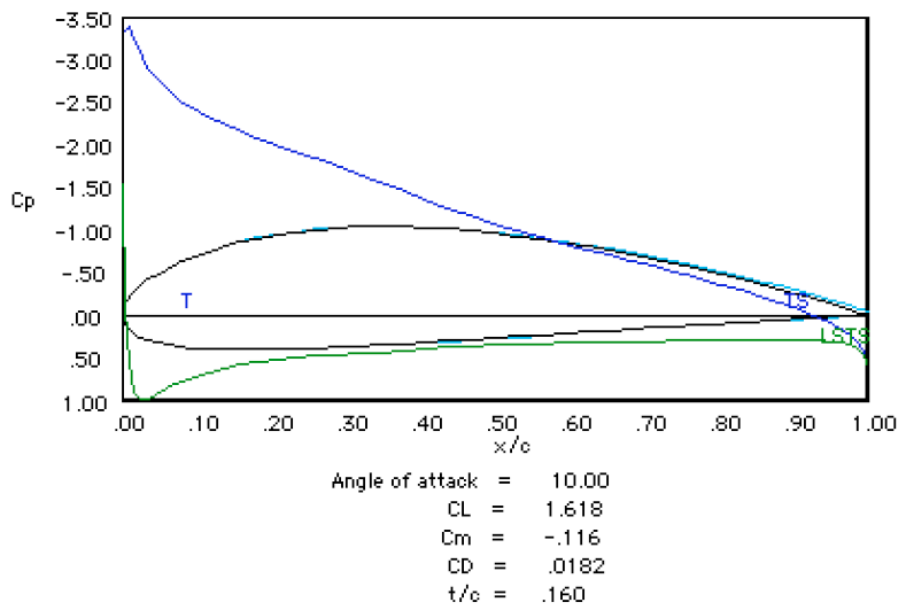


Fig. 15 NACA 4416 airfoil shape with pressure distributions.

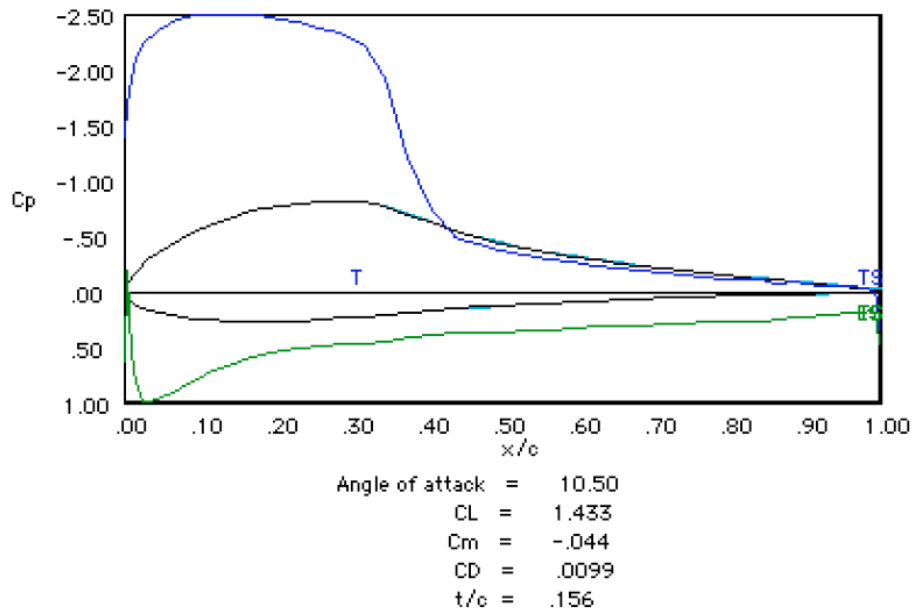


Fig. 16 Flugfoil 9 airfoil shape and pressure distribution.

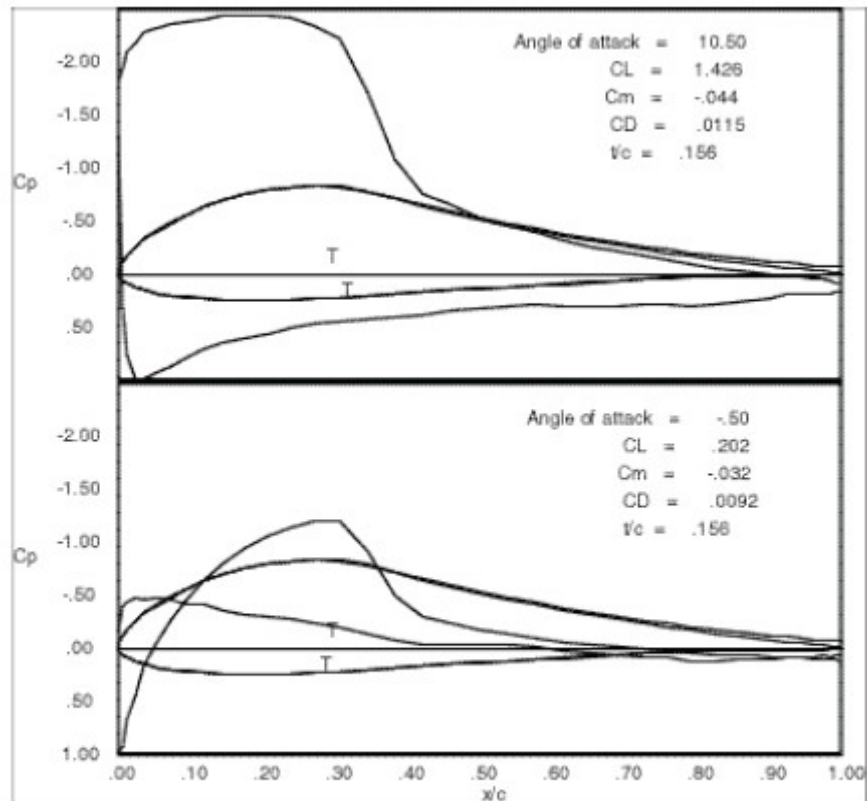
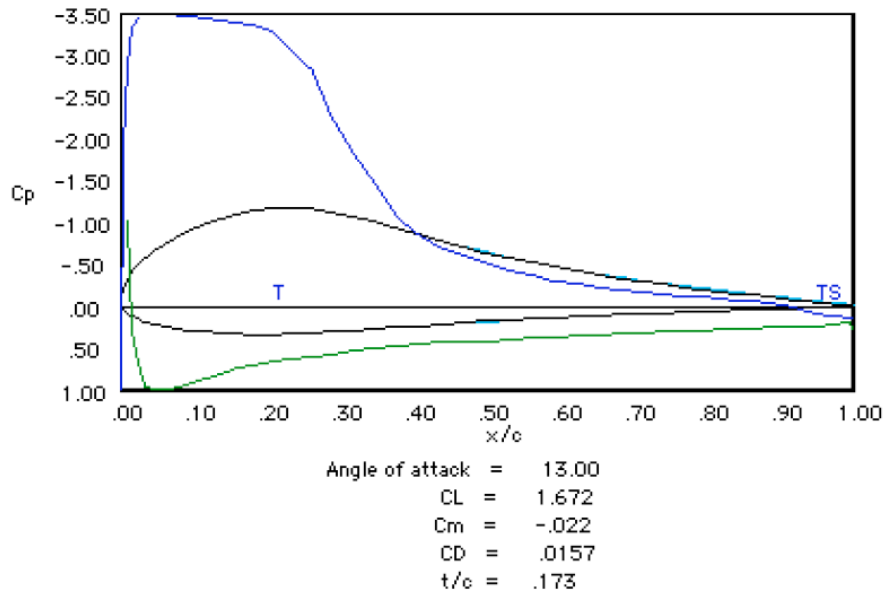


Fig. 17 SWIFT airfoil shape and pressure distributions.

The SWIFT's airfoil, originally being considered for use on the RBF-1, uses an upper surface  $c_p$  distribution very similar to the ideal canonical distribution illustrated in the Stratford pressure recovery graph assuming turbulent

flow. Though it is known that the SWIFT's airfoil utilizes laminar flow whenever possible, it appears to be designed to still perform well in turbulent flow. This is a compromise made by most aircraft airfoils that does not need to be made for the RBF-1. The SWIFT is designed to fly in real life conditions where the leading edge can get marred by bugs, nicks and water droplets. The RBF-1 airfoil is afforded the privilege of being designed assuming exclusive laminar flow since its mission is incredibly brief and is only performed once.

Taking Flugfoil-9, our best attempt at mimicking the SWIFT's airfoil, we began the process of modifying it to hold higher upper surface  $c_p$  values to increase its lift assuming laminar leading edge flow. The exercise produced only lackluster results however with a  $c_{lmax}$  of only 1.5 and a boundary layer that separated at reduced  $\alpha$  values. This airfoil, Flugfoil-13, is depicted in Fig. 18.



**Fig. 18 Flugfoil 13 airfoil shape and pressure distribution.**

The next step taken was to abandon the SWIFT's airfoil all together and begin the search for other airfoils which maximize the design points desired by the RBF-1. The airfoils most closely looked at were the Liebeck LA5055, L1003, LA203A, and LNV109A. Airfoils by Eppler, Selig, and Wortmann were also investigated but all had prohibitively high moment coefficients. The one airfoil that stood out above the rest was the Liebeck LNV109A.

#### *Liebeck Airfoils and Stratford Pressure Recoveries*

The mission for the RBF-1 is to fly approximately 300 ft, once. In addition, that single mission would likely happen on a calm fair weather day. Likely no other aircraft in the world has the luxury of such a simple and short

lived mission. This in turn means that most aircraft airfoils would be unnecessarily compromising when applied to the RBF-1 limiting its potential performance.

The pursuit for high lift, low moment coefficient airfoils led to the discovery of Liebeck's family of airfoils. The SWIFT's airfoil mentioned above, though not technically part of this family; is largely based on Liebeck airfoils and leverages a lot of the same principles, just not to the same degree. Liebeck airfoils utilize laminar flow coupled with Stratford pressure recoveries to generate amazingly high lift to drag ratios. This methodology lends itself well to low moment coefficients due to the nature of the front loaded  $c_p$  distribution. Also, Liebeck airfoils are generally designed to achieve their  $c_{l_{max}}$  without separated flow, which differs from more traditional airfoil designs [9]. This means they carry very low  $c_d$  values up to the point of stall. The graph for  $c_l$  vs.  $c_d$  shows a distinct drag bucket on most Liebeck airfoils as opposed to a simple parabola seen on more conventional airfoils. The differences can be easily seen in parts a and b of Fig. 19.

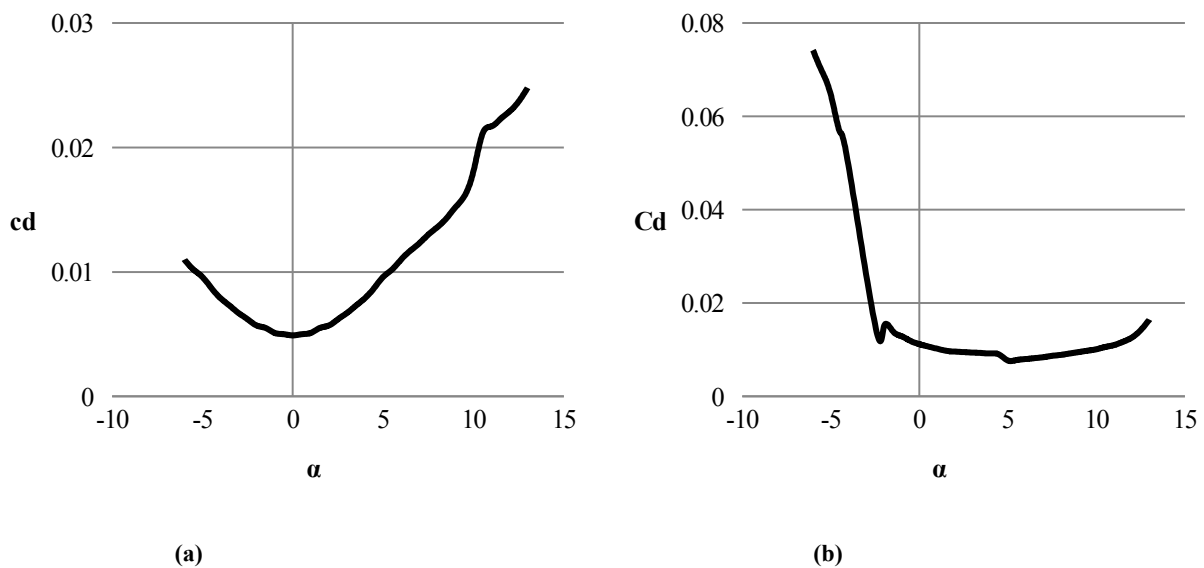


**Fig. 19 (a) Drag bucket for NACA M3 airfoil, representative of typical airfoil drag bucket shapes. (b) Drag bucket for the LNV109A airfoil.**

Fig. 20 shows the ideal velocity distribution to maximize  $c_l/c_d$  around an airfoil geometrically starting with the trailing edge at  $x = 0$  and working clockwise around the perimeter of the airfoil. There are several aspects to this velocity distribution which cannot be recreated in reality. First, velocity is held at 0 along the entire underside of the airfoil creating a large stagnation zone as opposed to a realistic stagnation point. Second, the  $c_p$  rooftop has sharp squared off corners; something not physically possible in the real world. Modifications to this perfect model were performed by allowing a velocity on the underside of the airfoil and a rounding of the leading edge of the rooftop to

create a favorable pressure gradient preserving attached flow. The results of these modification resulted in the airfoils shown below.

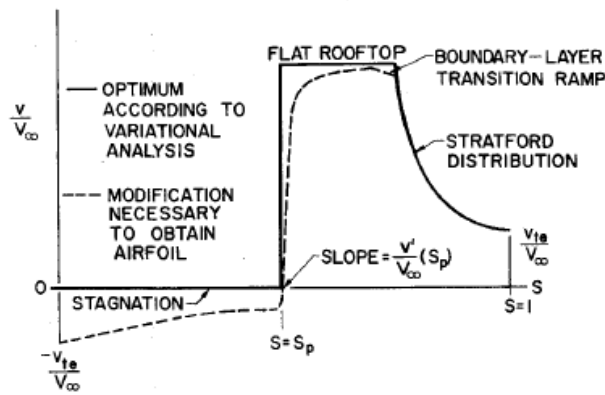


Fig. 20 “Optimized form of airfoil velocity distribution including modification necessary for obtaining an airfoil shape.” [9]

In Liebeck's early designs he utilized Weber's second-order inverse airfoil method to determine the ideal pressure distribution which in turn drove the geometric shape [9]. Fig. 21 is Liebeck's theoretical best geometry for achieving highest lift to drag values. It is quite impressive with an L/D of 600. Being so thin, it has very little practicality in current aircraft design due to its extremely poor structural qualities however. Fig. 22 is the airfoil with a realistic thickness. Though its lift to drag decreases from the ideal case, it is still extremely high at 420.

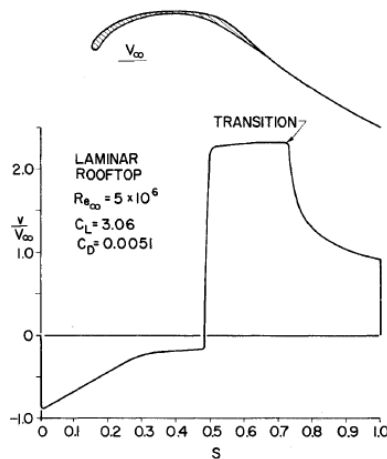
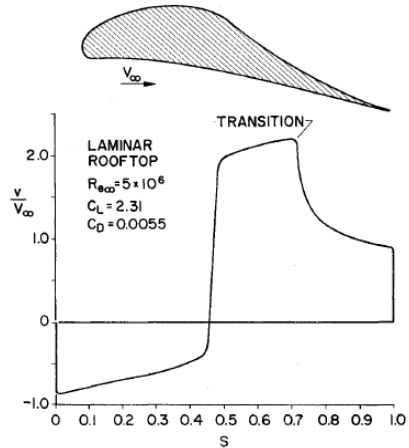


Fig. 21 Liebeck airfoil theoretically designed with velocity distribution, neglects practical consideration. [9]



**Fig. 22 Liebeck airfoil design and velocity distribution, with practical thickness and geometry. [9]**

There are two main characteristics to a Liebeck airfoil, a high  $c_p$  “rooftop” and a Stratford pressure recovery zone; both of which exist on the top surface of the airfoil. The concept is to maximize area under the  $c_p$  curve while still allowing the flow to transition to turbulent and recover smoothly without separating. The height of the roof top is determined by the location of transition along the chord and whether the flow leaving the leading edge is laminar or turbulent.

(a) and (b) Error: Reference source not found show Stratford  $c_p$  distributions along the chord length assuming laminar and turbulent flow respectively. These graphs can be viewed as the ideal distribution for the top surface of an airfoil for maximum  $c_l$ . The higher the  $c_p$ , the sooner recovery is necessary. Conversely, with a low  $c_p$ , recovery does not need to begin until very far down the chord length. For the turbulent distribution, the highest possible  $c_l$  is 1.0 with a  $c_p$  rooftop value of approximately -2.6 and a transition location of approximately 0.35c. The laminar distribution has a  $c_l$  double the turbulent case, with a  $c_p$  of -3.9 and a transition of approximately 0.52c. This shows that if one were intending to maximize lift one would want to design the airfoil for laminar flow.

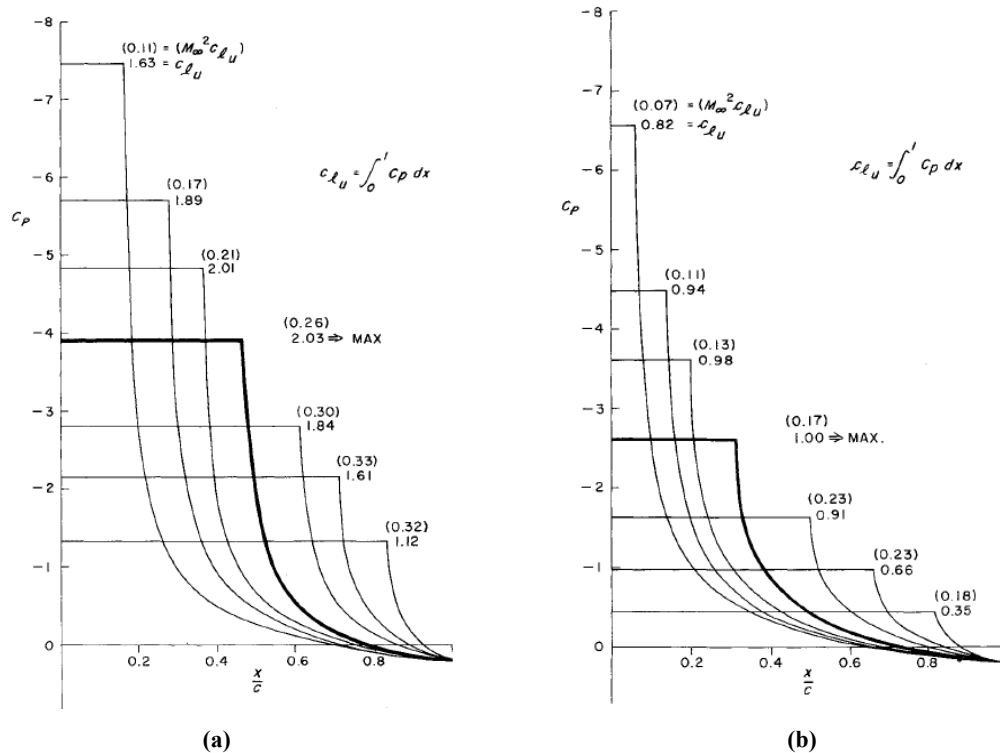


**Fig. 23 (a) “Suction side pressure distributions using Stratford pressure recovery to  $c_p=0.20$  at trailing-edge. Laminar rooftop,  $Re=5 \times 10^6$ . Values beside each curve indicate the lift that is developed.” [10] (b) “Suction side pressure distributions using Stratford pressure recovery to  $c_p=0.20$  at trailing-edge. Turbulent rooftop.  $Re=5 \times 10^6$ . ” [10]**

#### Selection of LNV109A

The LNV109A has the unique property of a very high  $c_{l_{max}}$  of 1.83 with a very low  $c_m$  of only -0.0474 at the RBF-1’s design Reynold’s number of  $1.0 \times 10^6$ . This comes from its forward loaded  $c_p$  rooftop. Generally laminar flow airfoils use lower rooftops that span more chord to prevent laminar separation bubbles [11]. The original design Reynold’s number for the LNV109A was  $4.0 \times 10^5$ . At that Reynolds number it is prone to laminar separation bubbles, which doesn’t hurt lift but does increase drag [12].

A design similar to the LNV109A but with better laminar separation mitigation is the LA203A. It uses the same basic design points as the LNV109A except with the moment coefficient limitation removed [13]. This allows for a longer and shorter rooftop increasing the local Reynolds number at the location of transition but drastically increasing the moment coefficient making it unusable for the RBF-1. To mitigate the LNV109A’s inherent laminar separation bubble problem, and thus improve its performance; a turbulator had to be added.

*Optimization of LNV109A*

After computing the polars for the LNV109A, it was apparent in the  $c_l$  versus  $c_d$  graph that the airfoil was suffering from a laminar separation bubble at  $c_l$  values below 1.0 which was corroborated by previous empirical studies, as shown in Fig. 24 [9]. To further improve performance, a turbulator was added to the upper surface of the airfoil to forcibly trip the boundary layer from laminar to turbulent flow. The turbulator's location was varied until the highest  $c_l/c_d$  was achieved. This location ended up being at 34% of the chord length, as can be seen in the progression of trends in Fig. 25. The performance graphs for the LNV109A airfoil are depicted in Fig. 26 through Fig. 29.

**Table 3 Liebeck LNV109A Airfoil Performance Parameters.**

<b>Parameter</b>	<b>Performance Value</b>
$c_{lmax}$	1.8208
$c_m$	-0.0487
$c_d$ cruise	0.0092

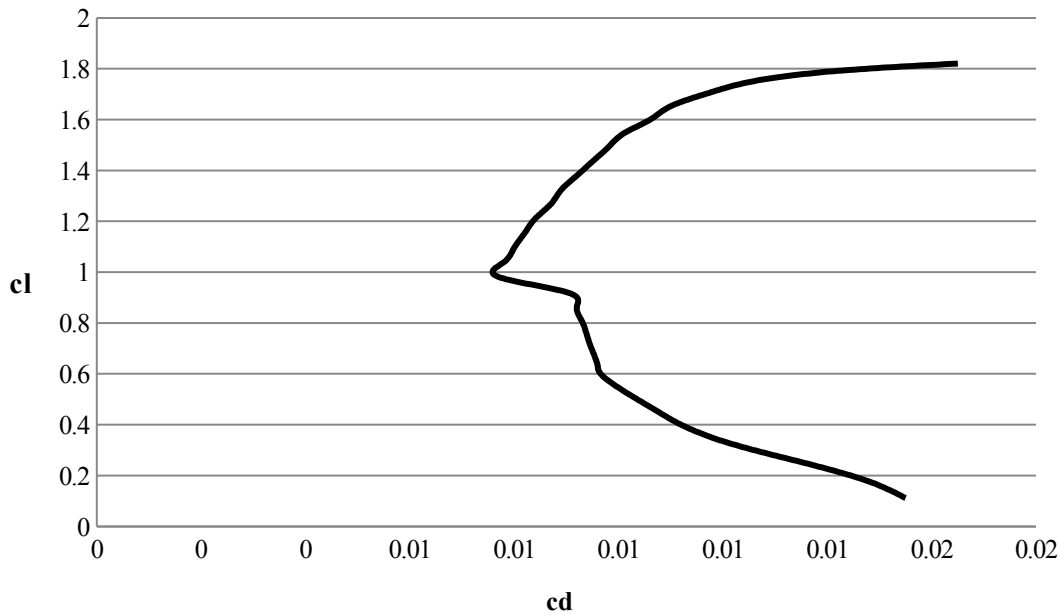


**Fig. 24  $c_l$  versus  $c_d$  for LNV109A airfoil with a turbulator located at 34% chord length.**

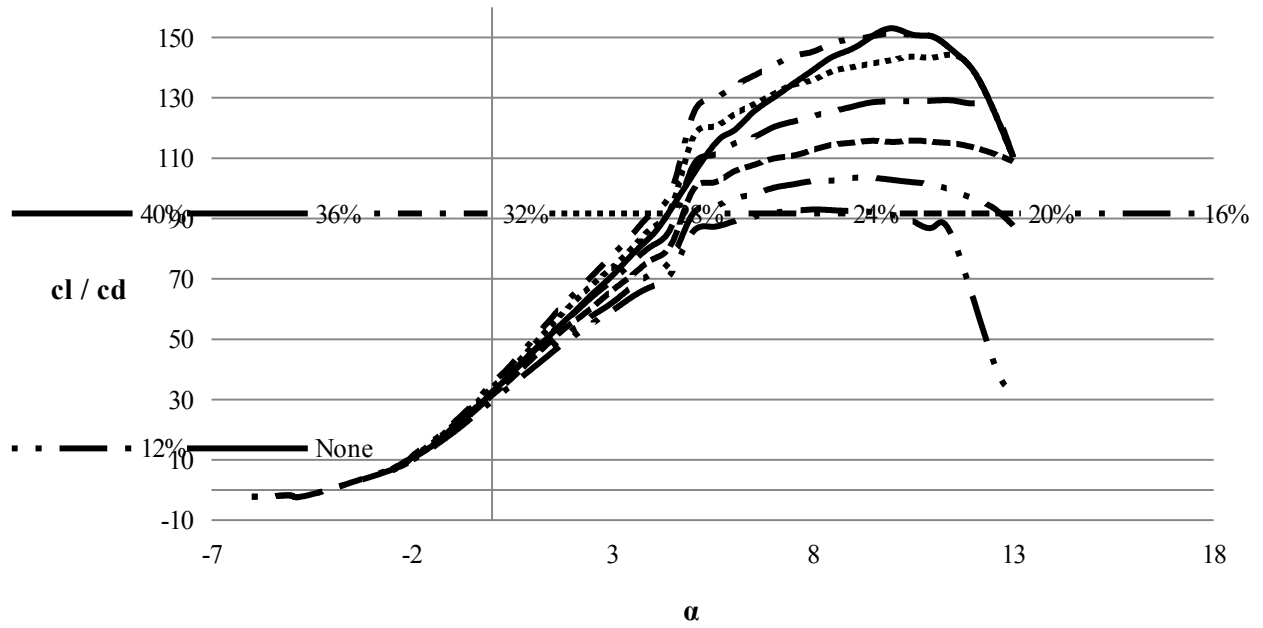


Fig. 25  $c_l/c_d$  versus  $\alpha$  for LNV109A airfoil.

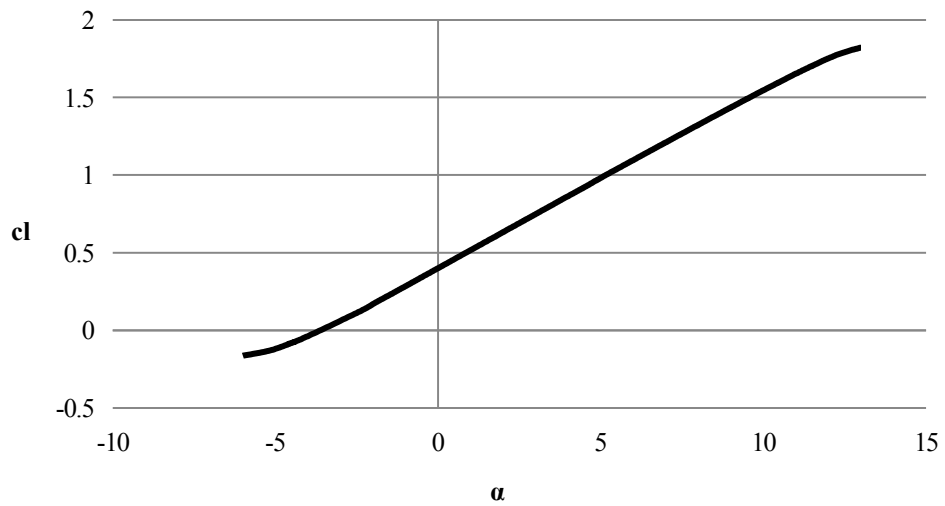
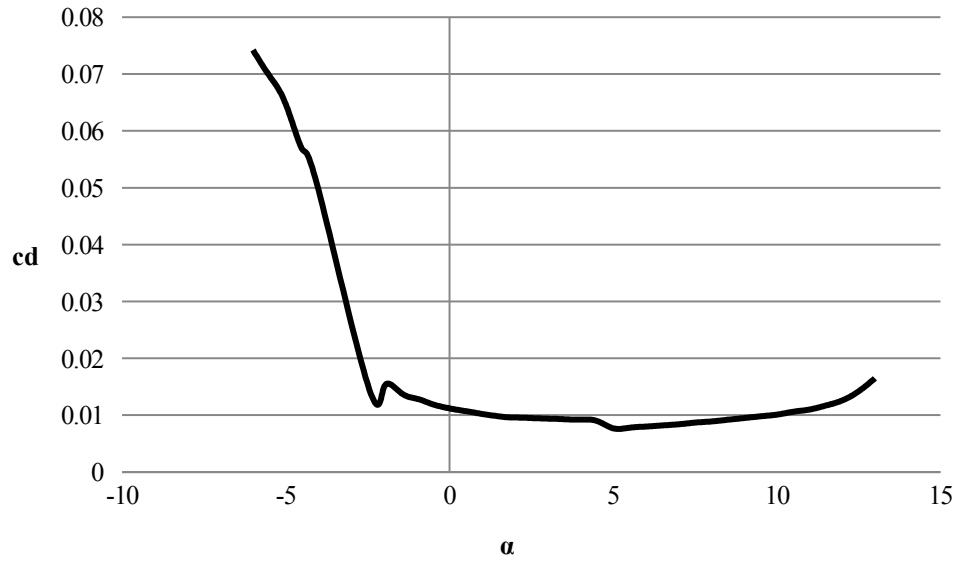
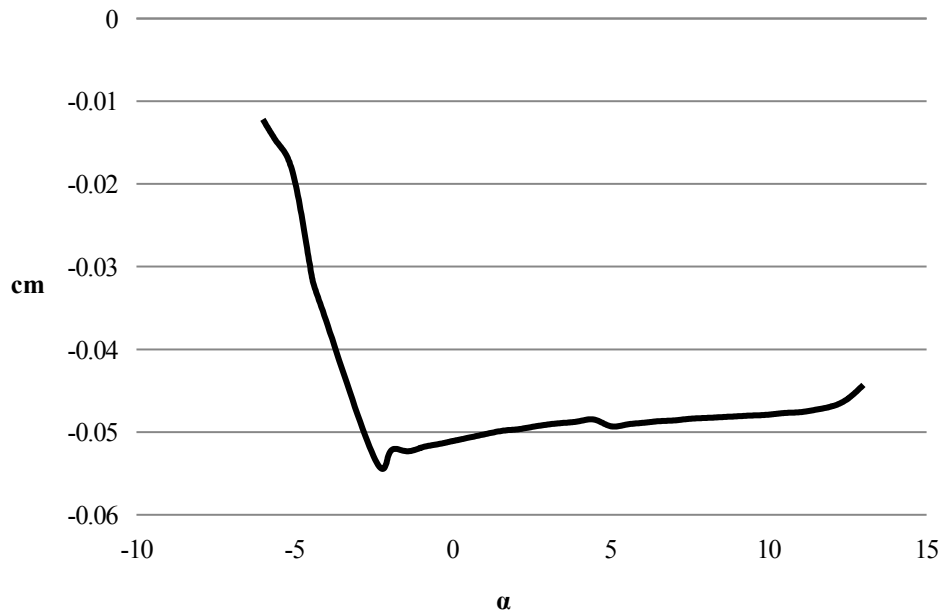


Fig. 26  $c_l$  versus  $\alpha$  for LNV109A airfoil with a turbulator located at 34% chord length,  $Re = 1,000,000$ .



**Fig. 27  $c_d$  versus  $\alpha$  for LNV109A airfoil with a turbulator located at 34% chord length,  $Re = 1,000,000$ .**



**Fig. 28  $c_m$  versus  $\alpha$  for LNV109A airfoil with a turbulator located at 34% chord length,  $Re = 1,000,000$ .**

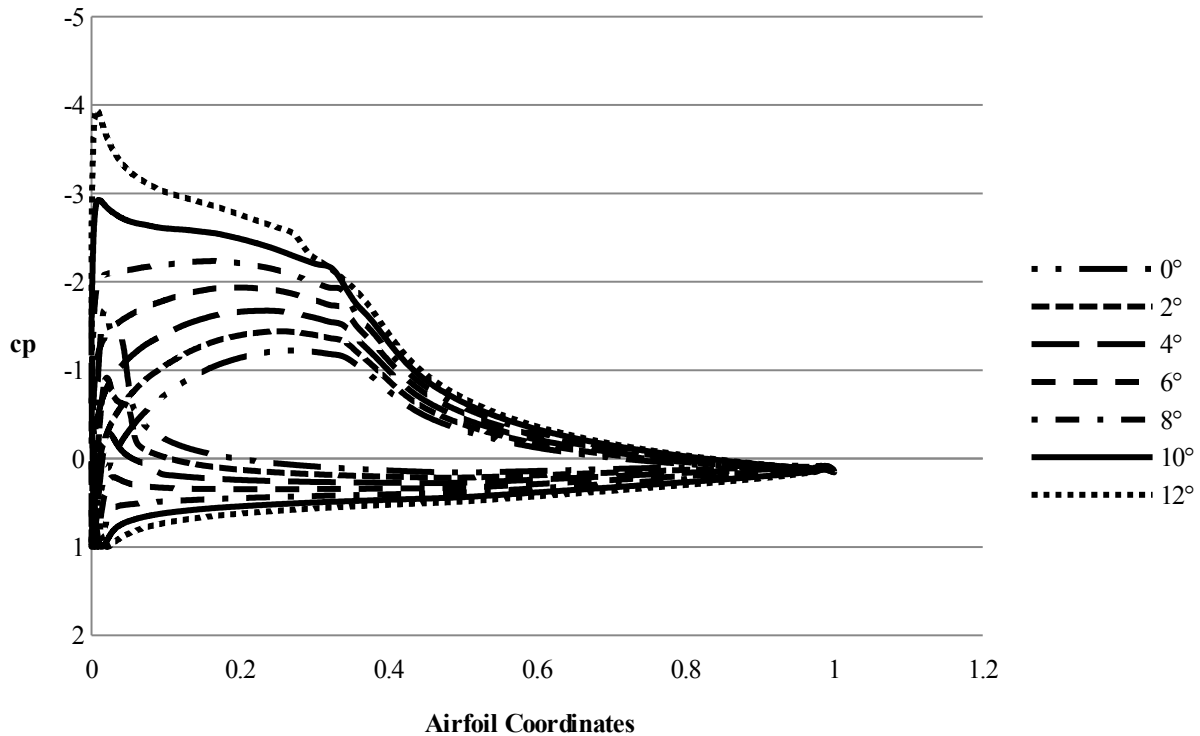


**Fig. 29  $C_p$  distribution for LNV109A airfoil with a turbulator located at 34% chord length,  $Re = 1,000,000$ .**

As can be seen in Fig. 25 the turbulator improved L/D dramatically for alphas between 5 degrees and 9 degrees, coincident with the local free stream alphas the RBF-1 will be cruising in. No loss of performance in any other manner was apparent as a consequence of adding the turbulator.

The LNV109A has a great  $c_{lmax}$ , and very good drag qualities; however, it has its drawbacks. First, it requires laminar leading edge flow to achieve its high  $c_{lmax}$  value and if does not get it, its performance drops off considerably. This requires very precise manufacturing methods for fabricating the leading edge of the wing along with very careful handling of the wing. Also, since it uses a true Stratford pressure recovery, its stall is abrupt and severe. This is because Stratford pressure recoveries are specifically designed to be on the edge of separation all the way down the pressure gradient [14]. Once flow separates, it quickly migrates up the length of the chord causing the majority of the airfoil to stall all at once, instead of slowly and gradually as with more conventional airfoils. These complications will be accounted for and dealt with as no other airfoil comes close to matching the LNV109A's performance.

#### **Winglet and Wing Cap Airfoil Selection**

The choosing of the airfoil sections for the winglets and wing caps was more straight forward. The methodology used was to find the operating range of  $C_L$ 's which each lifting surface experiences and choose an airfoil that has the lowest drag over that range of  $C_L$ 's. This resulted in the choosing of the NACA 63-215 airfoil for both the winglets and the wing cap. The performance graphs for the NACA 63-215 airfoil are depicted in Fig. 30 through Fig. 33.

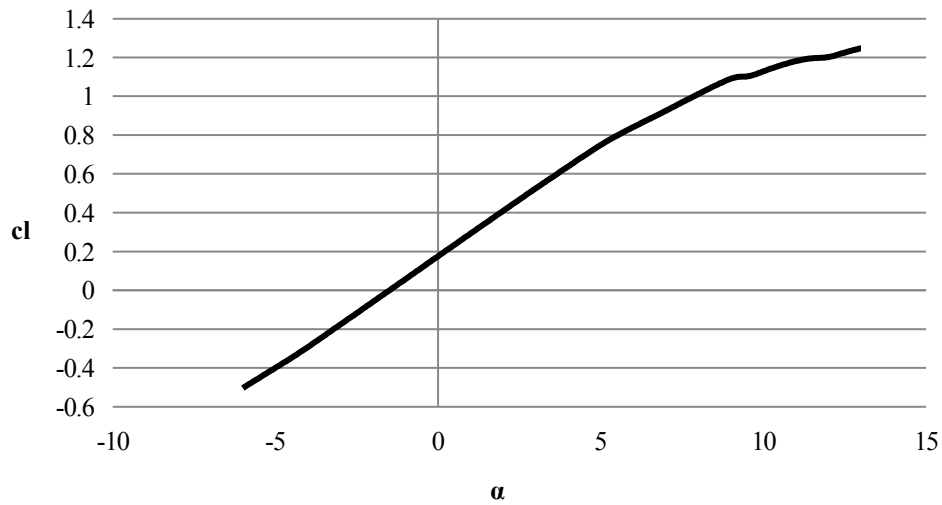


Fig. 30  $c_l$  versus  $\alpha$  for NACA 63-215 airfoil,  $Re = 1,000,000$ .

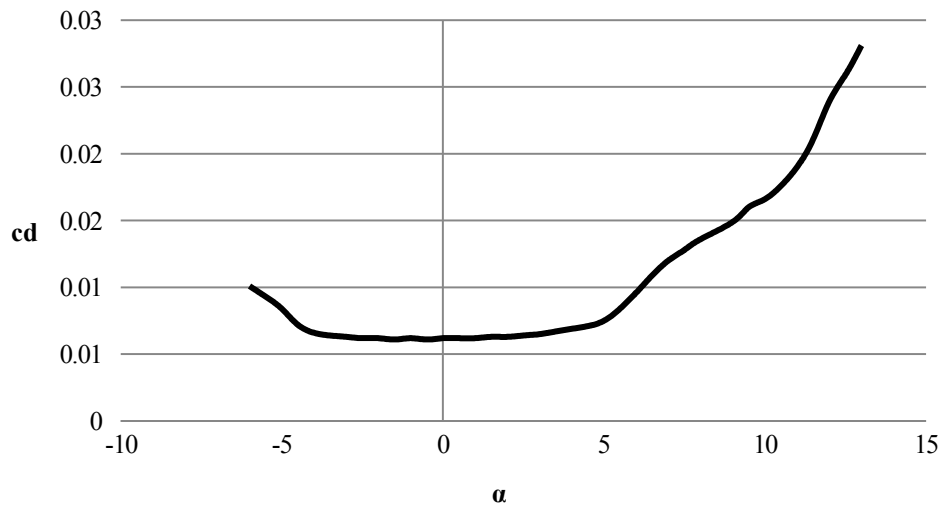


Fig. 31  $c_d$  versus  $\alpha$  for NACA 63-215 airfoil,  $Re = 1,000,000$ .

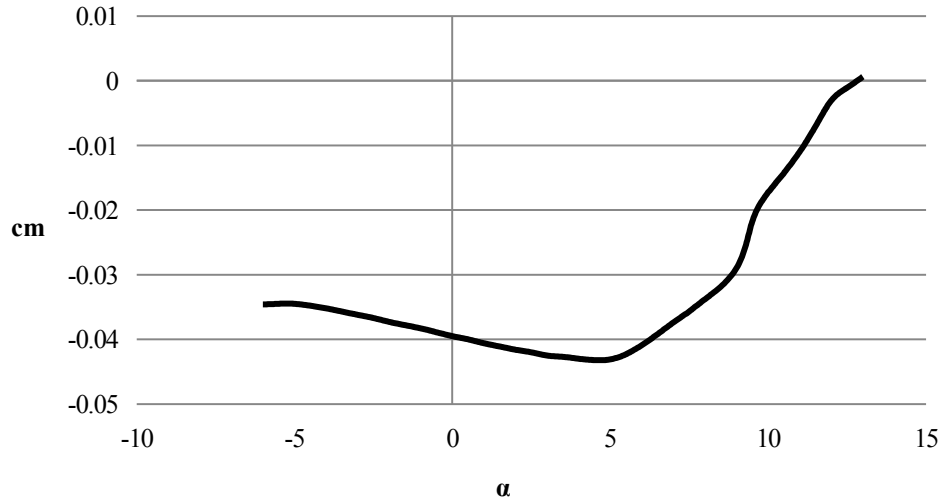


Fig. 32  $c_m$  versus  $\alpha$  for NACA 63-215 airfoil,  $Re = 1,000,000$ .

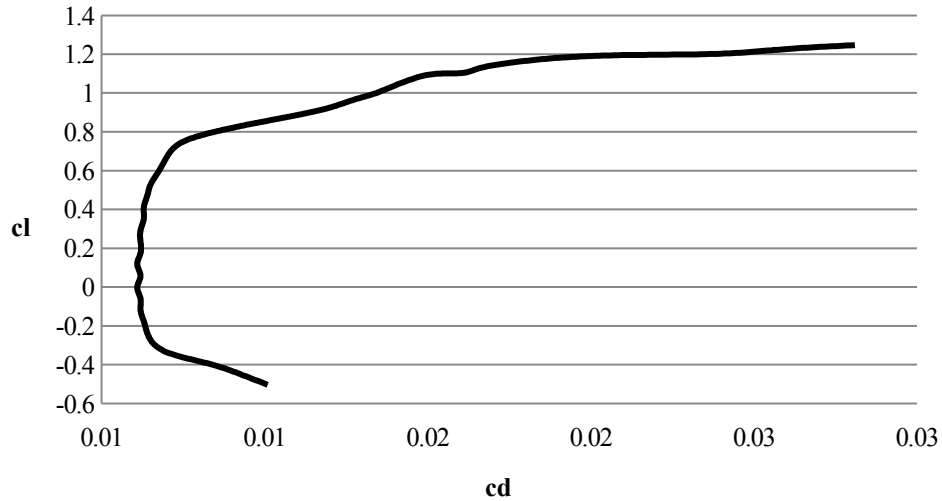


Fig. 33  $c_l$  versus  $c_d$  for NACA 63-215 airfoil,  $Re = 1,000,000$ .

### 3-D Wing Design Optimization

Typically in the design of a wing on a conventional aircraft, the variables are as follows: surface area, span, sweep, taper, twist, and incidence. Unless the spectrum of each variable is inordinately large, the aircraft's tail should be able to trim whatever combinations of the wing's variables are chosen. In the case of a tailless aircraft, the variables become much more highly coupled and many combinations thereof produce an un-flyable aircraft, thus adding significant complication to the wing design. In the case of the RBF-1, having no tail, but with winglets and the first ever use of 'wing caps'; the number of variables are two exponent powers larger than the already delicate and finicky tailless aircraft. In addition, the root of the winglet must be held equal to the tip of the wing, as is the

case for the relationship between wing cap and winglet. This further adds layers of coupling. Lastly, add in second order effects, such as structural and Reynolds number considerations, and the design becomes well outside the range of a simple numeric optimizer. As such, to determine the best design out of a seemingly infinite number of variable combinations, Design of Experiments (DOEs) were created and ran in conjunction with LinAir's built in optimizer which identified ideal lifting surface twists.

### **LinAir Optimizer**

LinAir's optimizer allows for a user defined number of inputs and constraints. The objective of the optimizer is to minimize  $C_D$ . In the case of the RBF-1 the variables used were:

1. Wing Root Incidence
2. Wing Tip Incidence
3. Winglet Root Incidence
4. Winglet Tip Incidence
5. Wing Cap Root Incidence
6. Wing Cap Tip Incidence.

The constraining variables were  $C_L$  and  $C_m$ .

LinAir can also vary geometric location of lifting surface corner points, for example, the leading edge of the wing tip; however, it cannot attach dependency of one surface point onto another. This proved problematic in attempting to vary coupled surface points. For example, if one wanted to vary sweep of the wing, there does not exist a way to make the wing tip trailing edge dependent on the wing tip leading edge. One would have to allow both points to float freely, consequently allowing surface area and taper to vary along with sweep. Only twist and CG were varied in the optimizer, because of the inability to fully control geometric relationships. Static margin was manually held to approximately 5% for all runs. Since the optimizer only designs for lowest drag instead of lowest  $C_L/C_D$ ,  $C_L$  was held constant as to not contaminate the results of the DOEs.

### **Plackett-Burman Factorial DOE**

A Plackett-Burman Factorial DOE was run to attach cause and effect to a wide range of geometric variables. By design, the Plackett-Burman DOE uses a minimal number of runs to determine causation but does so without identifying synergic variable combinations. This is valuable for differentiating between important and unimportant

variables but does not provide the fidelity to optimize the RBF-1's design to the desired level. All input variable limits were determined based off a combination of the outcome from the preliminary 3-D design, and an understanding of aircraft design fundamentals. The responses set in the DOE were  $C_L/C_D$  and the span efficiency.

Each design number shown in Table 4 dictated the values for factors A through G. The factors were then input into LinAir and the optimizer ran. The alpha sweep for each optimized Design No. was then analyzed and the highest  $C_L/C_D$  with the accompanying efficiency value was recorded. Because static margin is not a fixable constraint, each Design No. was run multiple times while the CG was manually varied to maintain a relatively constant static margin.

**Table 4 Plackett-Burman factorial optimized design list.**

<b>Design No.</b>	<b>A: Wing Surface Area</b>	<b>B: Wing Sweep</b>	<b>C: Winglet Height</b>	<b>D: Winglet Sweep</b>	<b>E: Winglet Taper Ratio</b>	<b>F: Wing Cap Sweep</b>	<b>G: Wing Cap Taper Ratio</b>	<b><math>C_L/C_D</math></b>	<b>e</b>
<b>1</b>	150	22.5	5.6	35	0.6	35	1.0	21.1	1.3
<b>2</b>	120	22.5	4.0	35	0.6	20	0.6	24.4	1.3
<b>3</b>	120	27.5	5.6	45	0.6	35	0.6	26.5	1.6
<b>4</b>	120	22.5	5.6	45	1.0	20	1.0	25.4	1.6
<b>5</b>	150	27.5	5.6	35	1.0	20	0.6	22.1	1.5
<b>6</b>	150	22.5	4.0	45	1.0	35	0.6	21.3	1.3
<b>7</b>	150	27.5	4.0	45	0.6	20	1.0	22.2	1.4
<b>8</b>	120	27.5	4.0	35	1.0	35	1.0	24.7	1.4

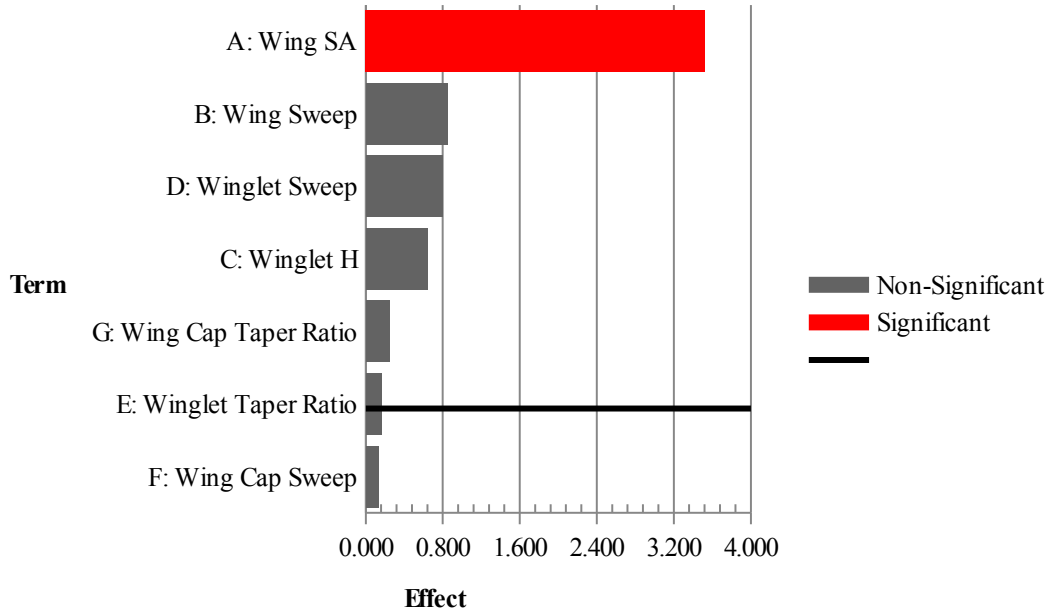


Fig. 34 Pareto chart-regression for Plackett-Burman factorial DOE.

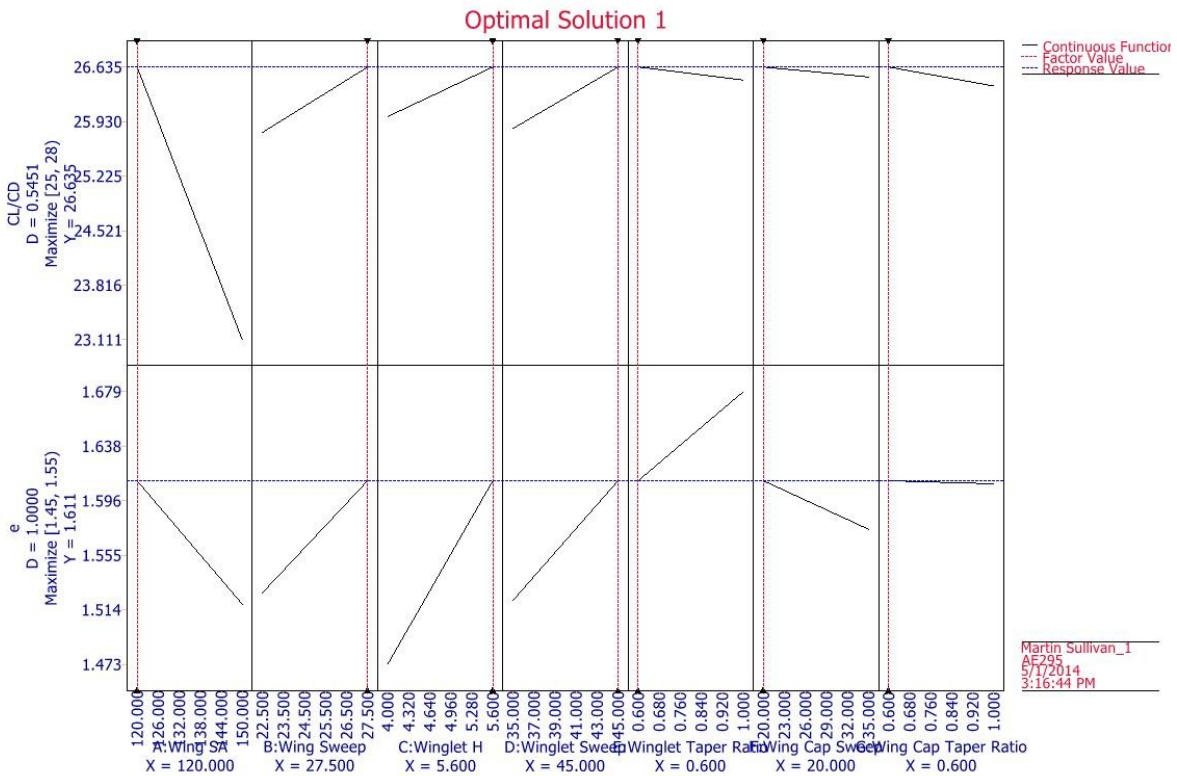


Fig. 35 Plackett-Burman factorial DOE optimal solution graph.

It can be seen in Fig. 34 and Fig. 35 that wing surface area is the only discernibly significant variable in relation to all others for this experiment. It also shows that surface area is proportional to drag. This is a highly intuitive

result since the equation for  $C_{Di}$  states that aspect ratio is inversely proportional to drag. With a fixed span, an increase in surface area results in a decrease of AR ultimately increasing drag.

### Taguchi Factorial DOE

The second DOE was a Taguchi Factorial which accounted for interplay between variables. The first DOE varied 7 factors in 8 runs whereas the 2<sup>nd</sup> DOE varied 5 factors in 27 runs. This provided a higher fidelity result and provided deeper insight into the effect of each variable.

Table 5 shows the list of results.

**Table 5 Taguchi factorial optimized design list.**

<b>Design No.</b>	<b>A: Wing Sweep</b>	<b>B: Wing Taper</b>	<b>C: Winglet Taper</b>	<b>D: Wing Cap Sweep</b>	<b>E: Wing Cap Taper</b>	<b><math>C_l/C_D</math></b>	<b>e</b>
<b>1</b>	27.5	0.8	0.60	30	0.7	26.3	1.5
<b>2</b>	22.5	0.8	0.90	30	0.6	25.3	1.5
<b>3</b>	22.5	1.0	0.90	25	0.8	25.2	1.5
<b>4</b>	25.0	1.0	0.75	25	0.7	25.6	1.5
<b>5</b>	25.0	0.9	0.60	30	0.6	26.1	1.5
<b>6</b>	25.0	0.9	0.75	20	0.6	25.8	1.5
<b>7</b>	22.5	1.0	0.60	30	0.8	25.9	1.5
<b>8</b>	25.0	0.9	0.90	25	0.6	25.5	1.5
<b>9</b>	27.5	0.9	0.90	30	0.8	25.5	1.5
<b>10</b>	22.5	0.9	0.75	30	0.7	25.7	1.5
<b>11</b>	25.0	0.8	0.60	25	0.8	26.1	1.5
<b>12</b>	25.0	1.0	0.60	20	0.7	25.9	1.5
<b>13</b>	27.5	1.0	0.90	20	0.6	25.4	1.5
<b>14</b>	22.5	0.8	0.75	25	0.6	25.8	1.5
<b>15</b>	25.0	0.8	0.90	20	0.8	25.6	1.5
<b>16</b>	25.0	0.8	0.75	30	0.8	25.9	1.5
<b>17</b>	22.5	0.8	0.60	20	0.6	26.1	1.5
<b>18</b>	22.5	1.0	0.75	20	0.8	25.5	1.5
<b>19</b>	27.5	0.9	0.75	25	0.8	25.8	1.5
<b>20</b>	27.5	1.0	0.60	25	0.6	26.0	1.5
<b>21</b>	27.5	1.0	0.75	30	0.6	25.7	1.5
<b>22</b>	27.5	0.8	0.90	25	0.7	25.7	1.5
<b>23</b>	27.5	0.8	0.75	20	0.7	26.0	1.5
<b>24</b>	25.0	1.0	0.90	30	0.7	25.4	1.6
<b>25</b>	22.5	0.9	0.60	25	0.7	26.0	1.5
<b>26</b>	27.5	0.9	0.60	20	0.8	26.0	1.5
<b>27</b>	22.5	0.9	0.90	20	0.7	25.0	1.5

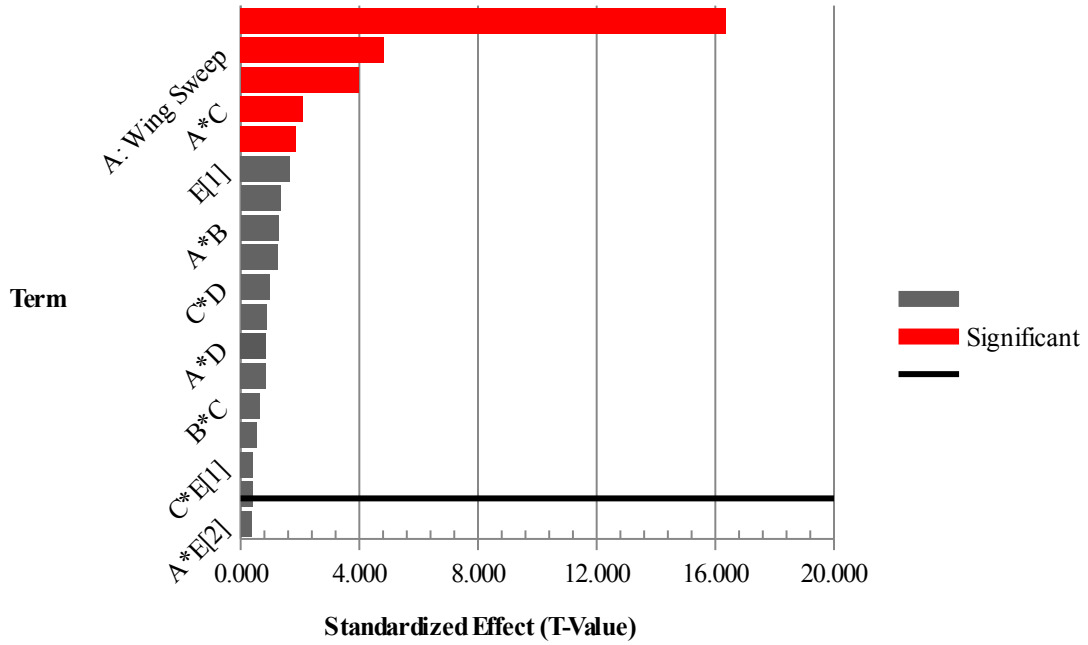


Fig. 36 Pareto chart-regression for Taguchi factorial DOE.

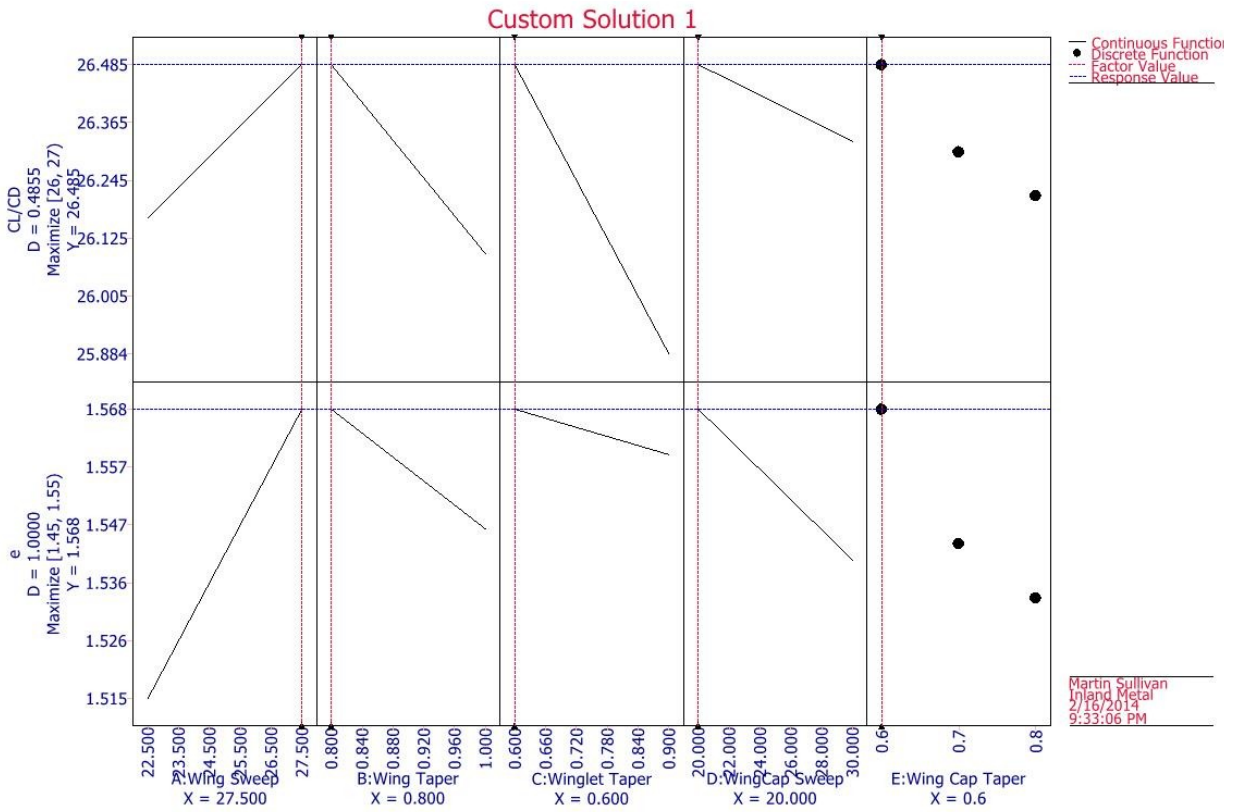


Fig. 37 Taguchi factorial DOE optimal solution graph.

It can be seen in Fig. 36 and Fig. 37 that the most significant factor amongst the variables for DOE#2 is winglet taper. Counting as measurably significant but to a much lesser degrees are, wing sweep, wing taper, wing sweep + wing taper, and lastly wing cap sweep + wing cap taper. winglet taper's high degree of influence is likely attributable to its effect on the aircraft's total wetted area. Having low taper increases surface area of both the winglets and wing caps which negatively effects performance in much the same way wing area was shown to negatively affect performance in DOE#1.

The second DOE drove the design towards a maximized sweep and winglet taper ratio. Due to second order constraints, such as Reynold's number effects, laminar flow degradation, and weight increase, which were not accounted for in the DOE; sweep was minimized instead of maximized.

### Final 3-D Wing Design

The final 3-D wing design and thus final aircraft design was born out of the DOE optimization process. The geometry is shown in figure Fig. 38. Performance was dramatically improved over the preliminary 3-D wing design. Most notably, span efficiency was increased 22%, from 1.22 to 1.49. The lift distribution of, and an alpha sweep for, the final wing geometry are shown in Fig. 39 3-D wing lift distribution for the RBF-1. Fig. 39 and Fig. 40 respectively.

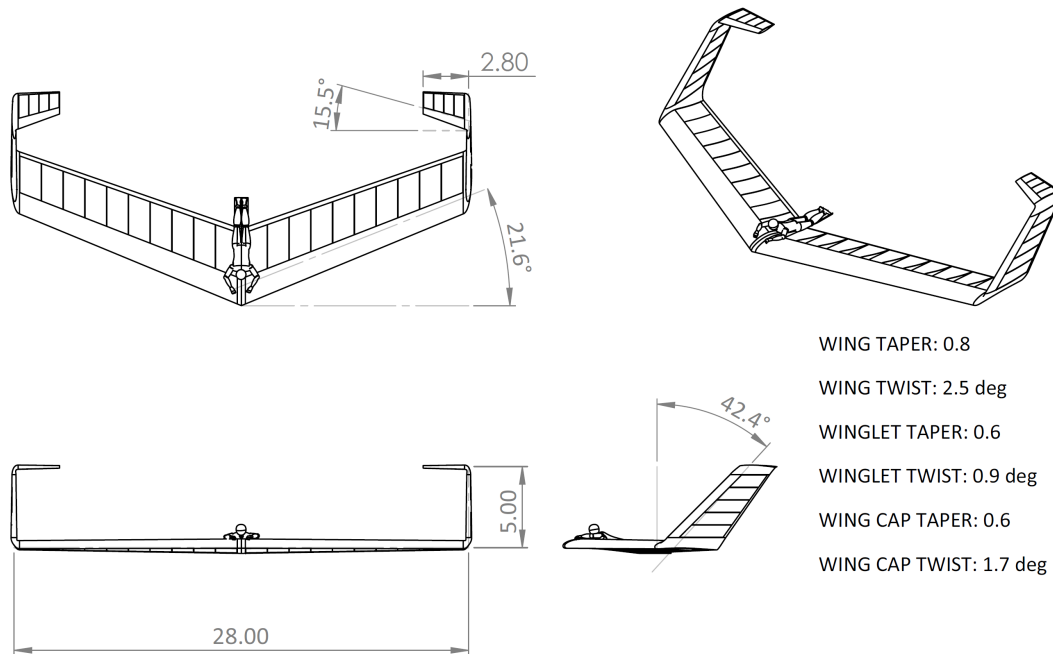


**Fig. 38 3 view drawing of the RBF-1.**

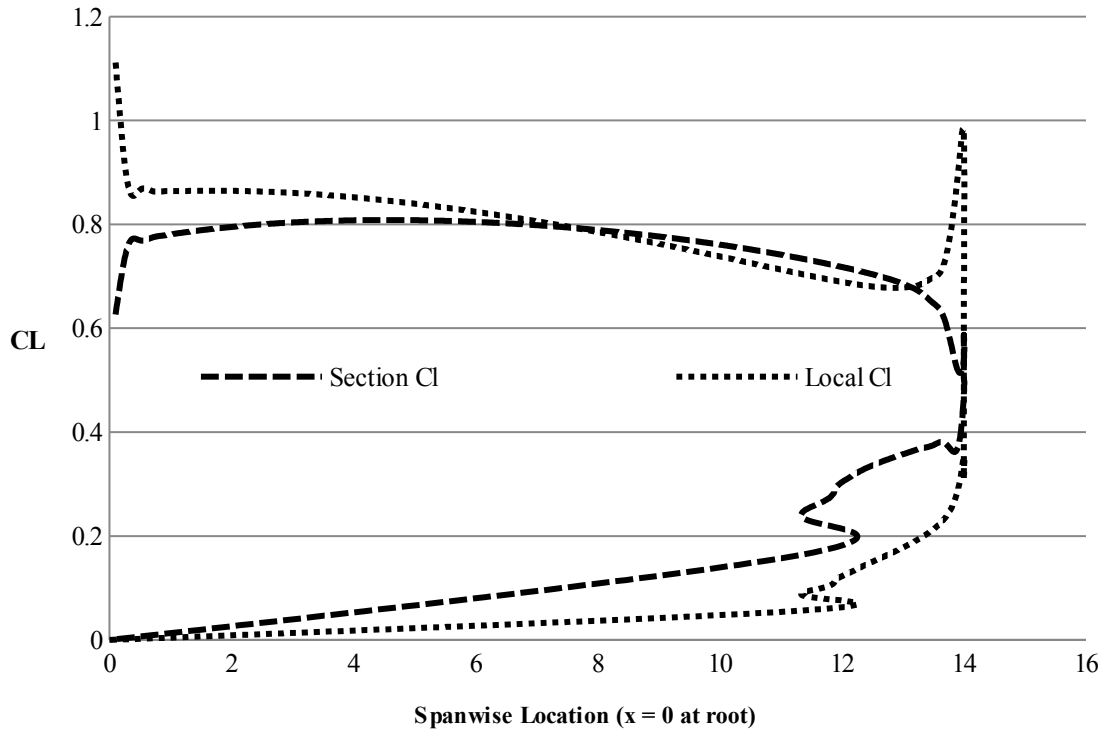


Fig. 39 3-D wing lift distribution for the RBF-1.

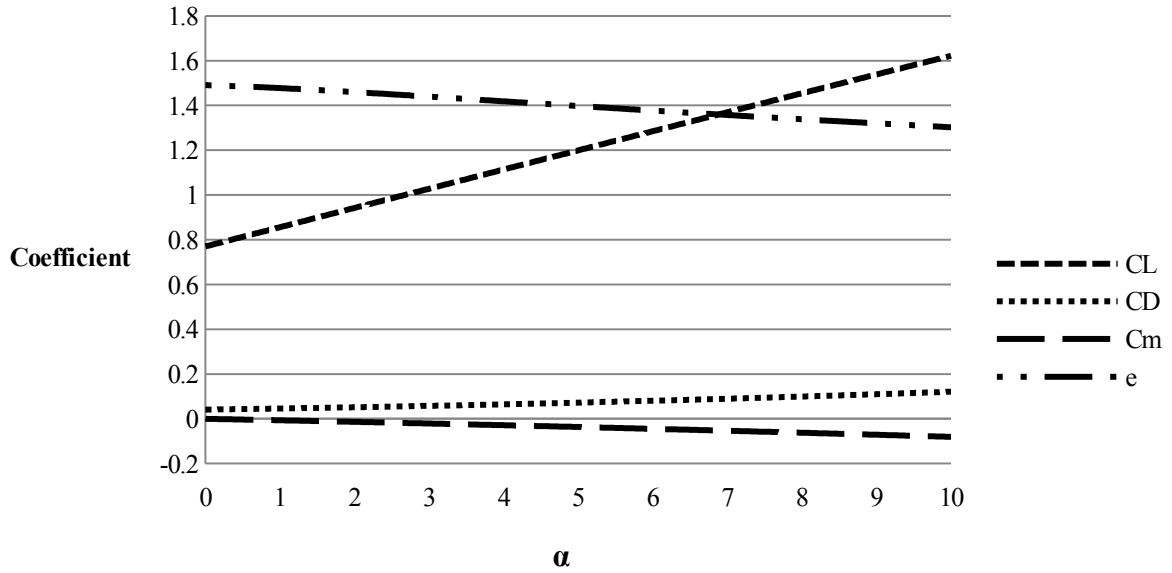
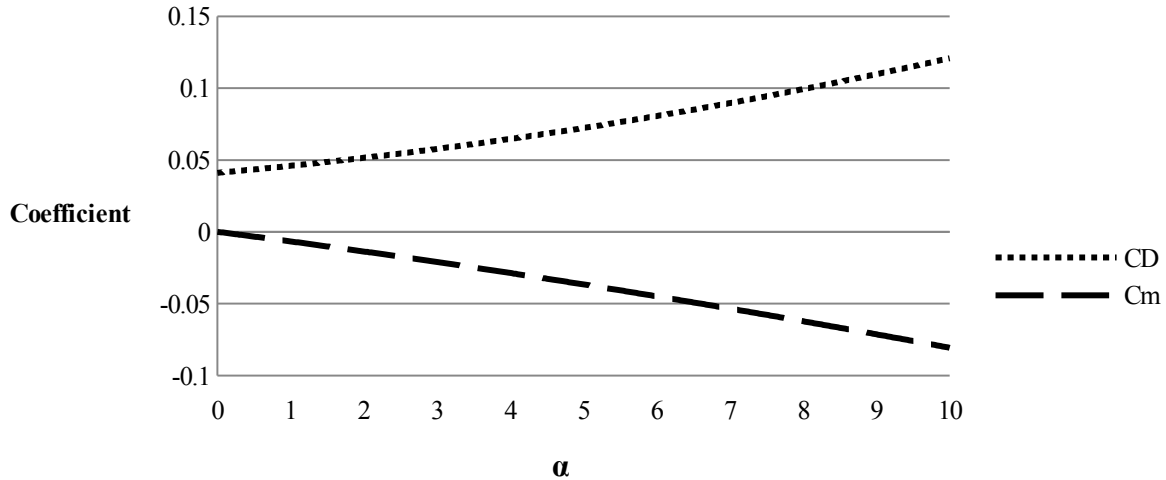


Fig. 40 Alpha sweep graph for final design of RBF-1.



**Fig. 41 Alpha sweep graph for final design of RBF-1 with higher fidelity for  $C_D$  and  $C_m$ .**

The Element forces shown in Table 6 provide deeper insight into the function of each lifting surface. Most interestingly, the  $C_D$  values for both the winglets and wing caps are negative! As unintuitive as it seems, this is correct. The free stream local to both lifting surfaces is influenced by the substantial span wise flow from the swept wing. The resultant forces are thus angled forward and the lift component cancels out the drag component. Also shown, is the negative lift created by the wing caps. This is in keeping with the theory and why the C-wing is able to add span efficiency while trimming the wing harmoniously.

**Table 6 Element forces of final wing design for RBF-1.**

Element Name	$x_{root LE}$	$y_{root LE}$	$z_{root LE}$	$C_L$	$C_D$	$C_Y$	$C_{roll}$	$C_m$	$C_n$
<b>Wing</b>	0.0	0	0	0.7915	0.0482	0	0	-0.0381	0
<b>Winglet</b>	5.8	14	0	0.0131	-0.0125	0	0	-0.0174	0
<b>WingCap</b>	10.8	14	5	-0.0316	-0.0028	0	0	0.0569	0
<b>Jen (Pilot)</b>	1.0	0	0	-0.0030	0.0082	0	0	-0.0014	0

## Stability and Control

### Longitudinal Static Stability

Longitudinal static stability bounced between 0-10% throughout the various iterations of the design but was decided to be held at 7.5% for the final version of the craft. The reasoning has not earned much more substantiation since the beginning of the project, and as stated earlier; will require gimbal testing to qualify the choice. 7.5% is

considered low for a traditional aircraft, however the RBF-1's comparatively slow velocity allows for the reduction in stability.

### Roll and Directional Static Stability

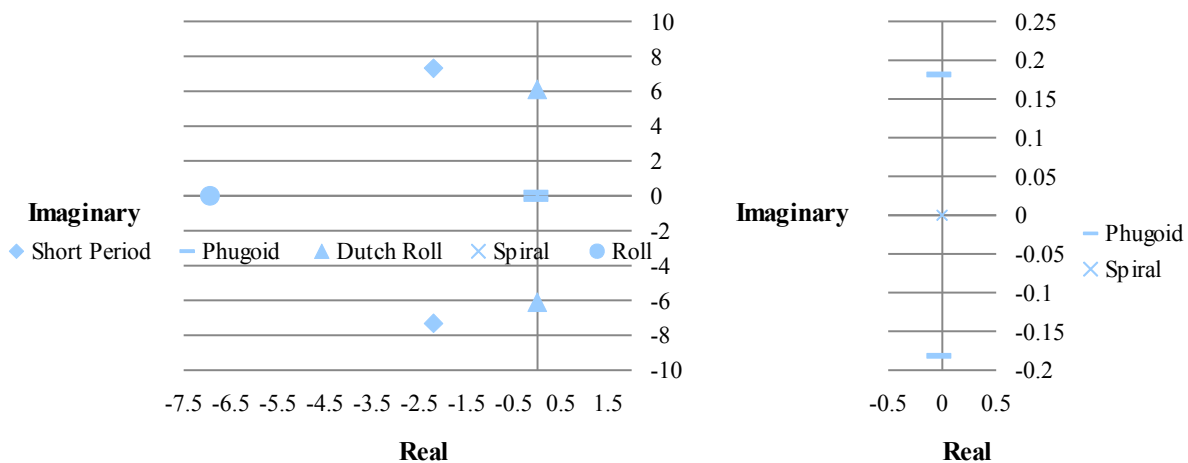
Roll and directional static stability are maintained by the large winglets and the sweep used on both the wings and winglets. The induced dihedral created by the RBF-1's planform naturally makes the aircraft very stable, if not overly so.

**Table 7 RBF-1 stability derivatives for final wing design as calculated using LinAir.**

	$C_L$	$C_D$	$C_x$	$C_z$	$C_y$	$C_m$	$C_n$	$C_{roll}$
$\alpha$	4.9267	0.2611	-0.5089	4.9678	0.0000	-0.3731	0.0000	0.0000
$M$	0.0000	0.0000	0.0000	0.0000	0.0000	0.0000	0.0000	0.0000
$\beta$	0.0000	0.0000	0.0000	0.0000	-0.9333	0.0000	0.0978	-0.2652
$\hat{p}$	0.0000	0.0000	0.0000	0.0000	-0.3210	0.0000	-0.0505	-0.7032
$\hat{q}$	5.6310	0.3746	0.3746	5.6310	0.0000	-2.6283	0.0000	0.0000
$\hat{r}$	0.0000	0.0000	0.0000	0.0000	0.7118	0.0000	-0.1097	0.2925

### Dynamic Stability

The Dynamic Stability analysis showed the craft to be stable in all 3 axes with only one truly interesting quality. The roll stability is uncharacteristically high when compared to conventional aircraft configurations. The poles of the system is graphed in (a) (b). The cause for this is very likely the C-wing configuration which exerts much higher aerodynamic loads at the tips of the wings, making the aircraft want to fly straight. This is a boon to us because of our one dimensional mission, but would be a complication for virtually any other aircraft.



(a)

(b)

**Fig. 42 (a) System poles associated with dynamic modes. (b) System poles associated with dynamic modes zoom around phugoid and spiral modes.**

### Control Surfaces

Three locations were available on the aircraft to integrate control surfaces; the wing root, the wing tips and the wing caps. Each option was aerodynamically modeled at both 0 degrees deflection and 5 degrees deflection to create an alpha sweep. After verifying the deflected response was relatively flat over the full sweep, the deltas were taken at the cruise AOA. The results of this study output as lift, drag and moment factors are shown in Table 8.

**Table 8 Results of control surface study shown as impact to lift, drag and moment coefficients.**

	$C_L$	$C_D$	$C_m$
<b>Flapperon</b>	0.02388	0.00122	-0.00018
<b>Elevon</b>	-0.01174	-0.00033	0.00582
<b>Wing-caperon</b>	-0.00450	0.00009	0.00841

It can be seen by the negative  $C_L$  value that both elevon configurations suffer from non-minimum phase responses when attempting to pitch up which is a well-documented consequence of tailless craft [5, 15].<sup>3</sup> The inboard flapperon does not suffer from a non-minimum phase response but due to the lack of pitching moment; it is largely ineffectual as a control surface. After eliminating the flapperon as an option, the choice between the wing tip and wing cap for a control surface location is an easy one; the wing cap has a larger pitching moment, lower non-minimum phase response, and lower drag making it the all-around superior control surface.

Instead of leaving the wing caps fixed and adding an actuating trailing edge, the entire wing caps will articulate eliminating drag caused by jack-knifing control surfaces. Conventional cable and pulley controls would be too heavy and difficult to rig because of the wing caps' location, therefore control inputs will be done electronically. Servos will articulate the wing caps which will be controlled by the pilot via a digital joystick.

### Flight Simulation

The flight of the RBF-1 was simulated using a 6 degree of freedom (DOF) ballistic modeling program for written in MATLAB by Gonzalo Mendoza [16]. Though the program models the dynamics of the flight completely with quaternion based equations of motion; it is unable to account for midflight flight path adjustments. As such, a PID controller was integrated mimicking the pilot's commands, to as accurately as possible, simulate the RBF-1's

<sup>3</sup> Smith, S. (2013, March 12). Pancaking Discussion. (M. J. Sullivan, Interviewer)

flight. By inputting the craft's initial conditions, computed aerodynamic and moment of inertia data, an expected flight path was created. Aerodynamic data was calculated and exported out of LinAir. Moment of inertia data was generated by modeling the RBF-1 in CAD and attributing accurate mass properties to each component.

The 2-D flight trajectory starting at 35 feet of elevation and gliding while trimming to best glide slope is shown in Fig. 43. The elevator deflection and pitch attitude versus time, one set for the actual flight time and one set for an extended flight time are graphed in Fig. 44 and Fig. 47 respectively. It is important to note that ambient conditions for the simulated flight has wind velocity set to zero. Depending on the direction and magnitude of the wind during actual flight, performance can increase or decrease from what is simulated.

Fig. 43 depicts a simulated flight distance of 424 ft, well past the current record of 258 ft. Ground effect and the pilot flaring towards the end of the flight was not taken into account in the simulation. The simulation has the pilot landing at 35 ft/sec when in actuality landing would likely happen at or near stall speed. As such, it is arguable the simulation is conservative in expected flight distance.

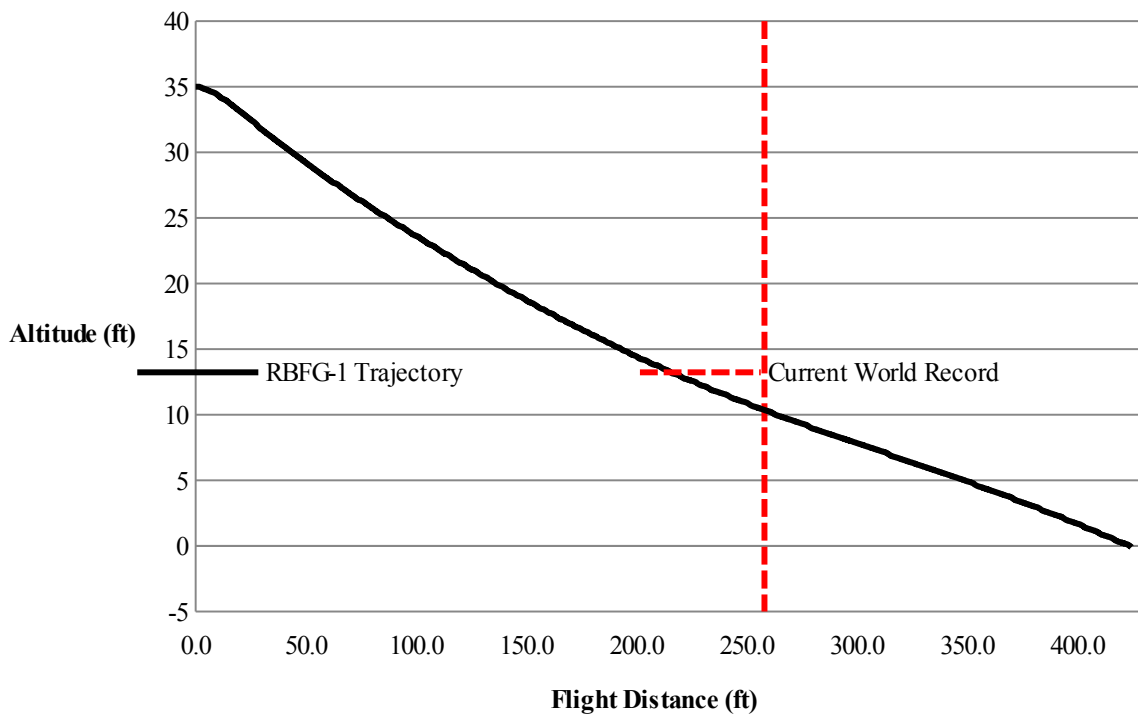


**Fig. 43 RBF-1 6-DOF simulated flight trajectory.**

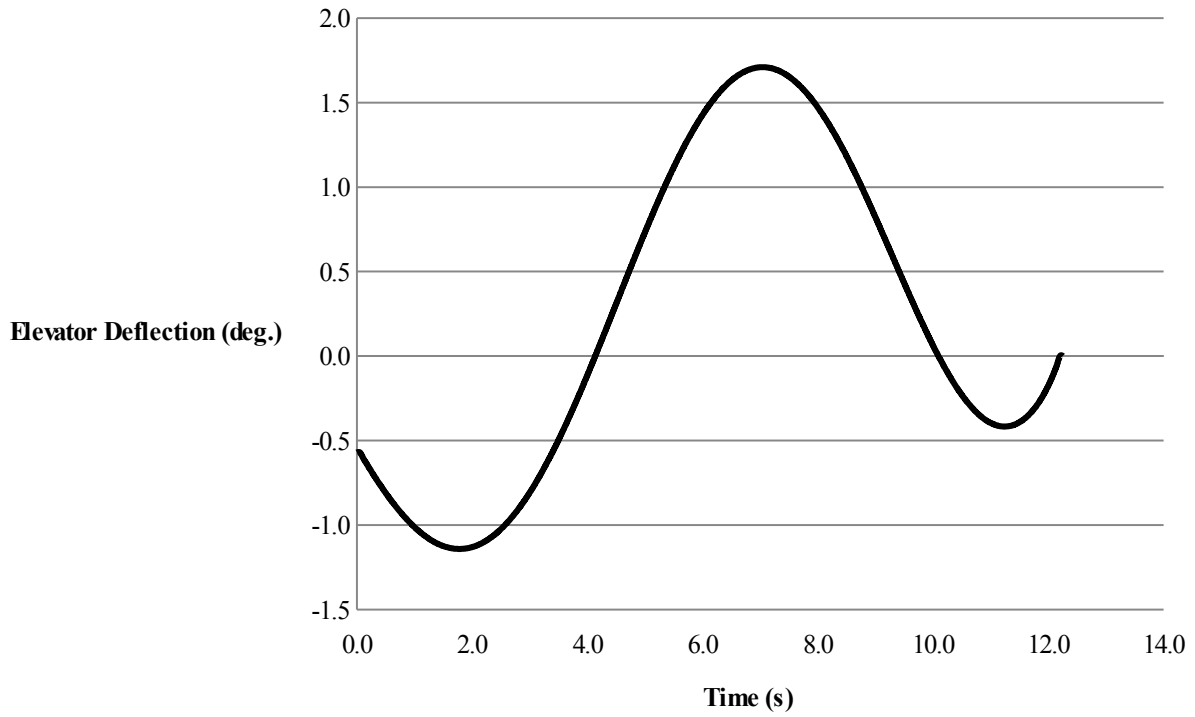


**Fig. 44 Elevator deflection versus time using 6-DOF simulator for actual flight window.**

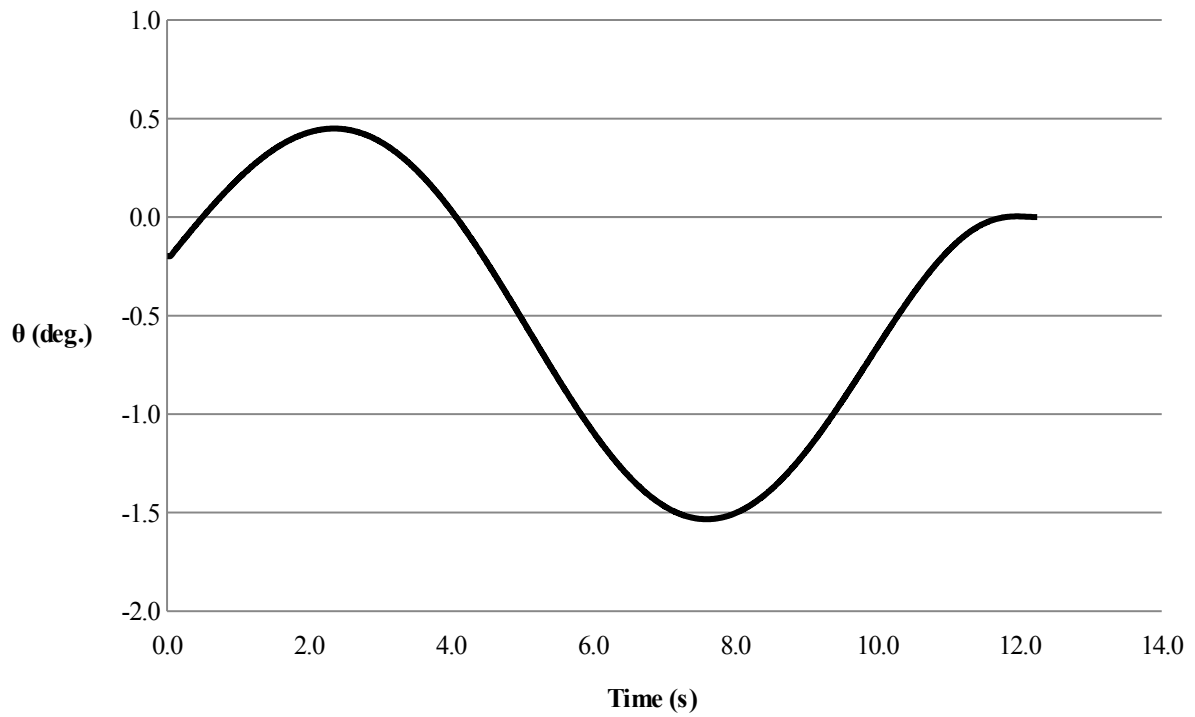


**Fig. 45 Pitch deflection versus time using 6-DOF simulator for actual flight window.**

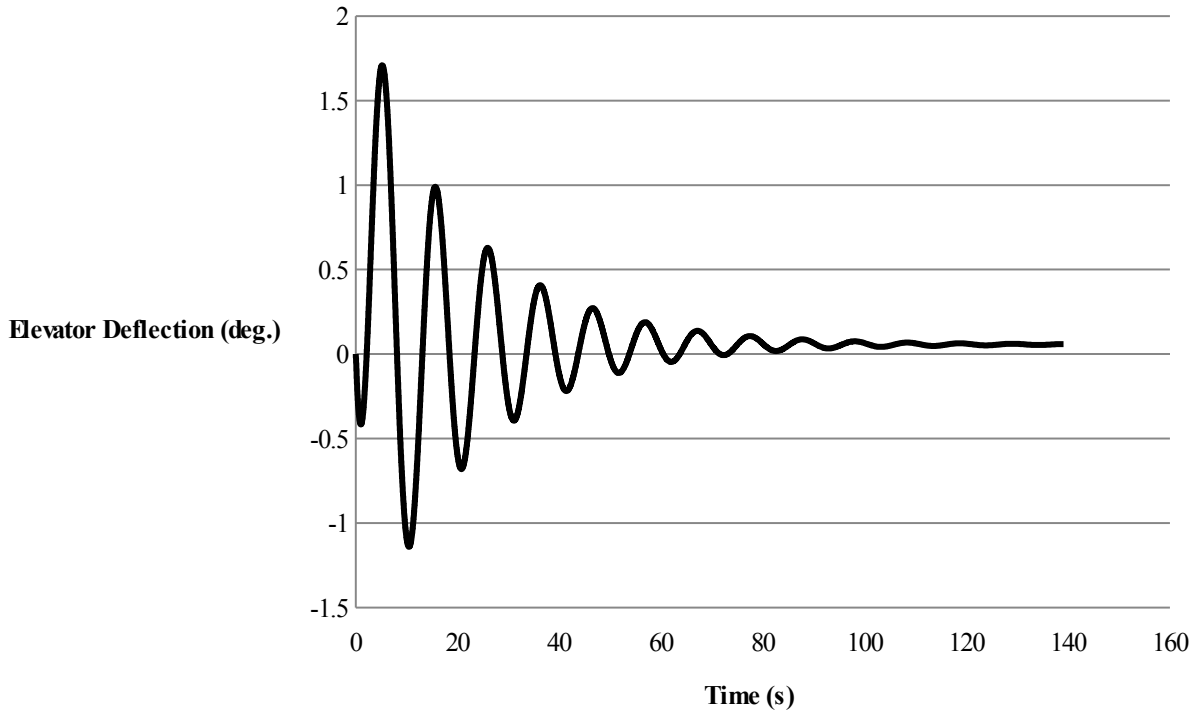


Fig. 46 Elevator deflection versus time using 6-DOF simulator for extended timeframe to view long term stability.

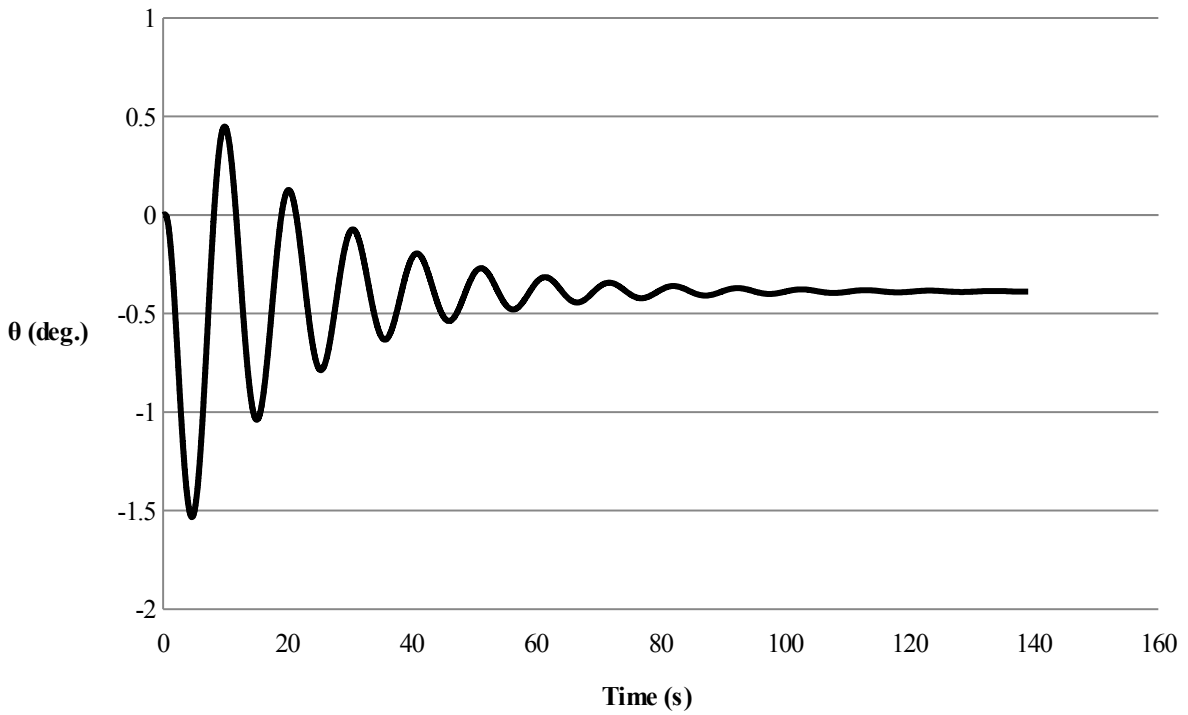


Fig. 47 Pitch deflection versus time using 6-DOF simulator for extended timeframe to view long term stability.

## Structural Analysis

A simple analysis of static loads on the main spar was conducted. The purpose was to gain a general insight into the maximum areas of stress, moment, and deflection. [17, 18, 19] As an initial assessment the forces and their affect on the spar were analyzed utilizing simple beam theory calculations performed by hand. The equations for the reaction forces, as well as the shear, moment and deflection equations as a function of x are shown below in Eq. 5 through Eq. 10 below.

$$R_A = -q_w l_w + W_{wl/wc} \quad (4)$$

$$M_A = \frac{-q_w l_w^2}{2} + W_{wl/wc} l_w - q_{wc} l_{wc} \sqrt{l_{wl}^2 + l_{wc}^2} - \frac{q_{wl} l_{wl}^2}{2} \quad ( \quad \text{SEQ Equation } \backslash^*$$

ARABIC 6 )

$$V_z = -R_A + q_w x \quad (5)$$

$$M_y = M_A - \frac{q_w x^2}{2} - R_A x \quad (6)$$

$$v' = \frac{1}{EI} \left( M_A x - \frac{R_A x^2}{2} - \frac{q x^3}{6} \right) \quad (7)$$

$$v = \frac{1}{EI} \left( \frac{M_A x^2}{2} - \frac{R_A x^3}{6} - \frac{q x^4}{24} \right) \quad (8)$$

Simple shear, moment, and deflection distribution diagrams are shown in Fig. 51 through Fig. 53.

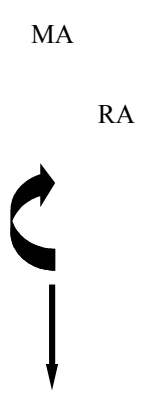


Fig. 48 Free body force diagram of static loading on C-wing of RBF1

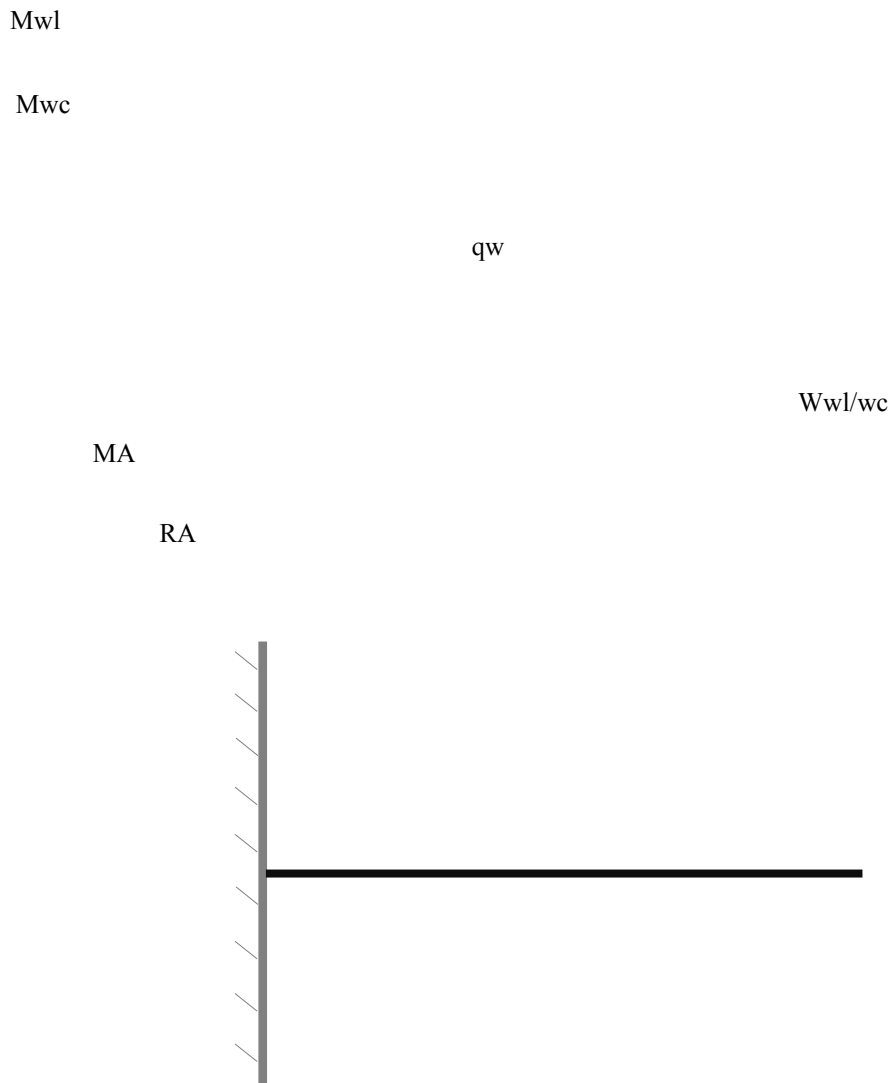


Fig. 49 Free body diagram of C-wing "beam" with all acting forces.

$M_y$

$V_z$

$M_A$

$R_A$

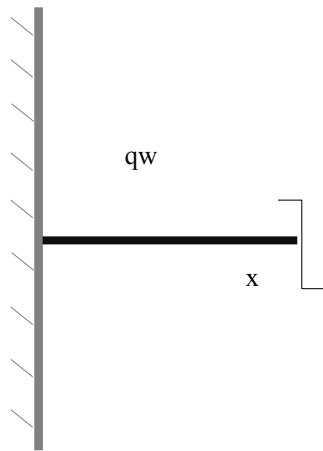


**Fig. 50 Free body diagram of cut section of C-wing "beam".**

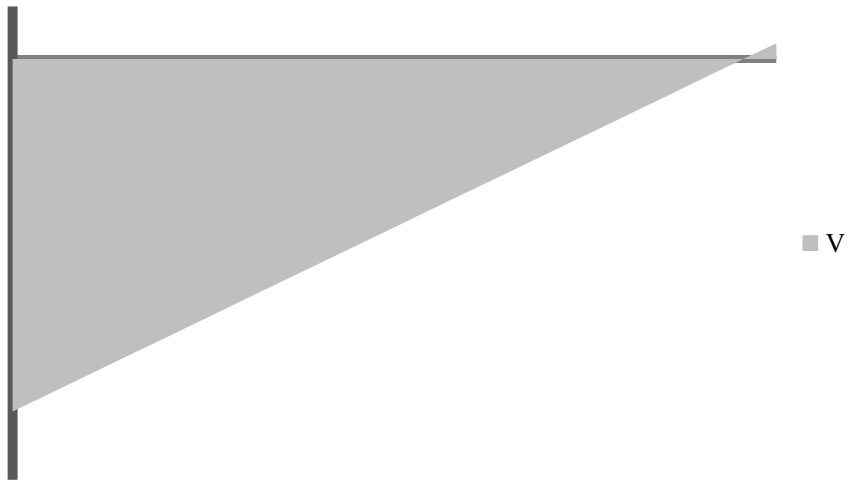


Fig. 51 Shear distribution diagram, assumed fixed beam, magnitude is not labeled but graph is within itself to scale.

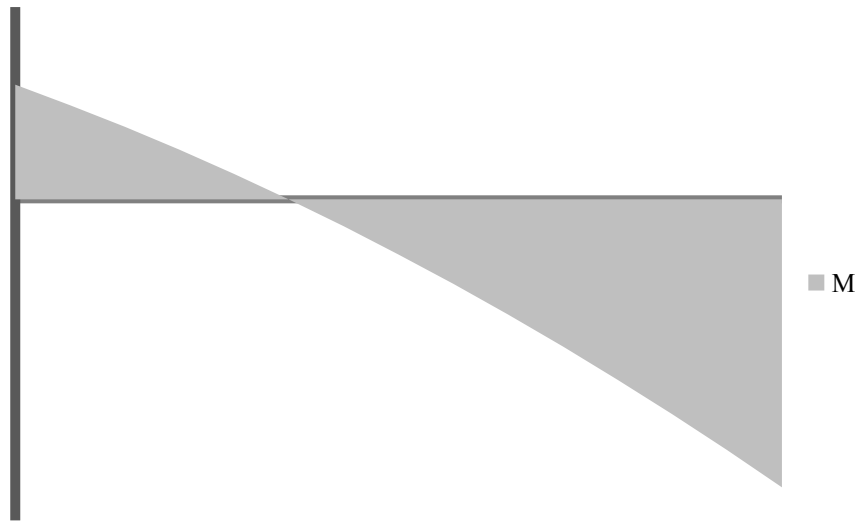


Fig. 52 Moment distribution diagram, assumed fixed beam, magnitude is not labeled but graph is within itself to scale.

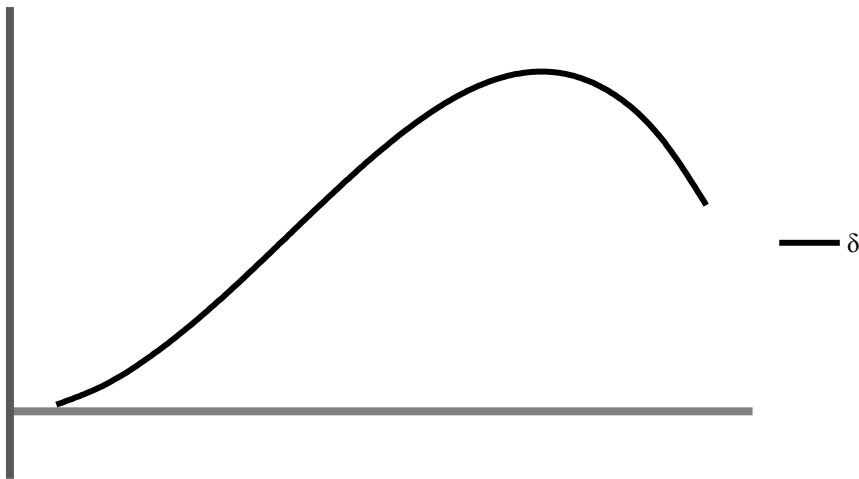


Fig. 53 Expected deflection diagram, assumed fixed beam, magnitude is not labeled but graph is within itself to scale.

Based on the equations and trends maximum shear occurs at the root of the wing, as expected. Maximum moment occurs at the tip of the wing and maximum deflection occurs at 73% half span (11 ft from the root of the wing).

### Final Thoughts on C-Wing

Though the C-wing configuration only slightly increases the span efficiency from a winglet-only design by 4% [7], the most profound advantage of the C-wing comes in the form of moment coefficient neutralization [8]. To achieve optimal span loading, the wing caps must produce a force in the downward direction. With proper design, that downward force can be located and scaled to cancel out the pitching moment of the aircraft, something normally

accomplished by the aircraft's tail. As such, the C-wing not only increases span efficiency, it coincidentally trims the aircraft without a trim drag penalty while eliminating the need and associated weight of a tail.

The question is begging to be asked: If the C-wing is so aerodynamically elegant, both increasing span efficiency while providing pitching moment trim in a perfectly synergic way; why is there not a single aircraft in existence using this configuration? There are three main reasons for this: It's a relatively new concept, its highly-coupled making design difficult, and it would be incredibly expensive to prototype because of its drastic departure from conventional aircraft design. Boeing and NASA's continued research into Blended Wing Body concepts, like the X-48, shows aircraft design is slowly migrating in the direction that most takes advantage of the C-wing's offerings. There is a significant chance that with the eventual advent of BWB aircraft in mainstream aviation, C-wing designs will become a reality soon thereafter.

### **Conclusion**

Though this project runs the gamut of aircraft design in hopes of breaking a world record, the use of the C-wing configuration is by far the most academically and technologically significant aspect of the RBF-1. With ever rising fuel prices coupled with the desire to minimize greenhouse gas emissions; efficiency is one of the most important design parameters for new aircraft. The C-wing configuration, especially used on tailless or blended wing body concepts, is very attractive for these reasons. As such, the humble flight of the RBF-1 could be the first demonstration of what will be a ubiquitous design and industry standard in the future.

### **Concept Evolution**

In Fig. 54 through Fig. 58 the evolution of the RBF-1 throughout the preliminary sizing and 3-D aerodynamic wing calculations is shown.



**Fig. 54 RBF-1 concept rendering Revision 1.**



**Fig. 55 RBF-1 concept rendering Revision 2.**

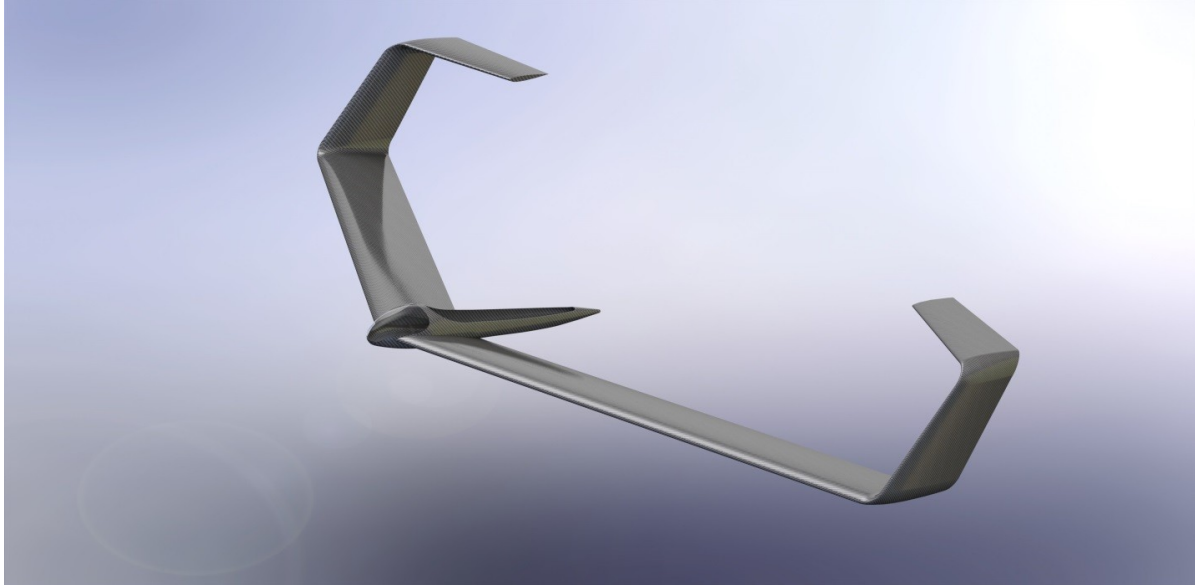


**Fig. 56 RBF-1 concept rendering Revision 5.**

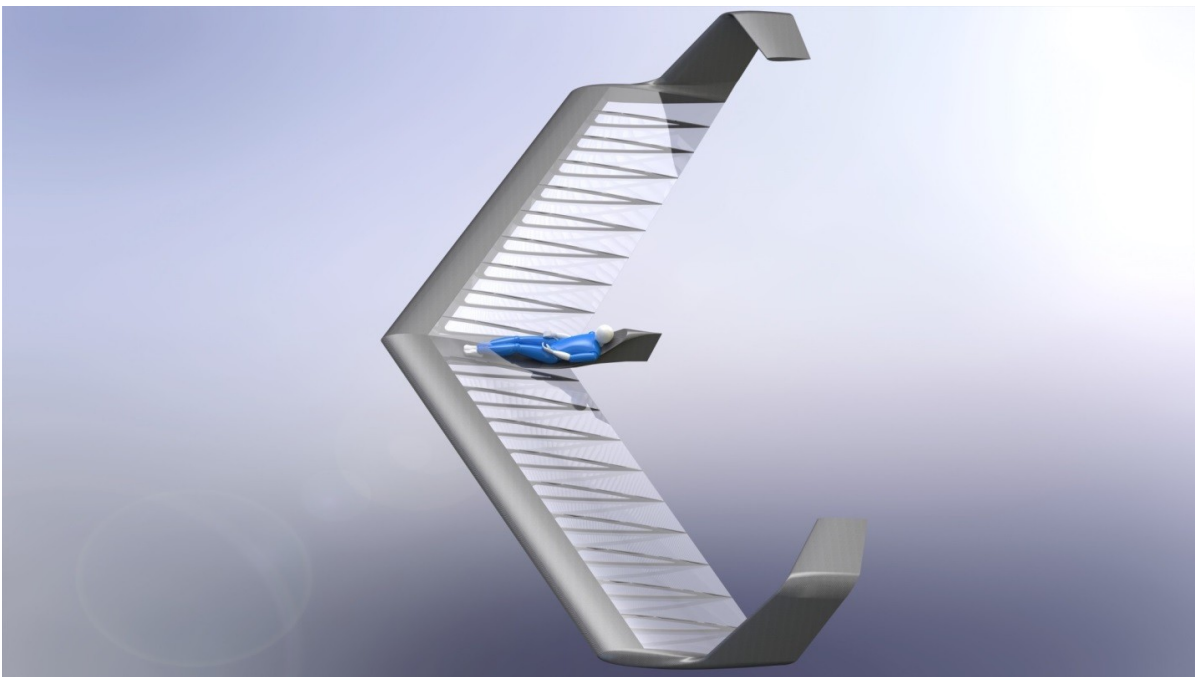


**Fig. 57 Larger wing area.**

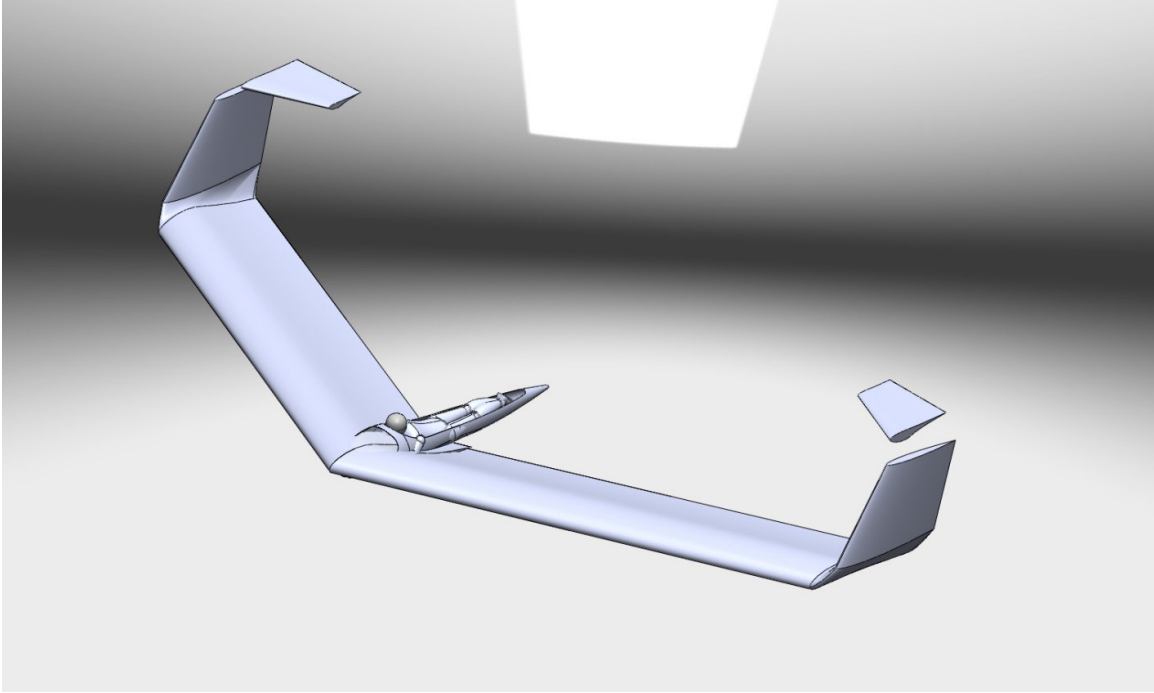


**Fig. 58** Wing cap version.

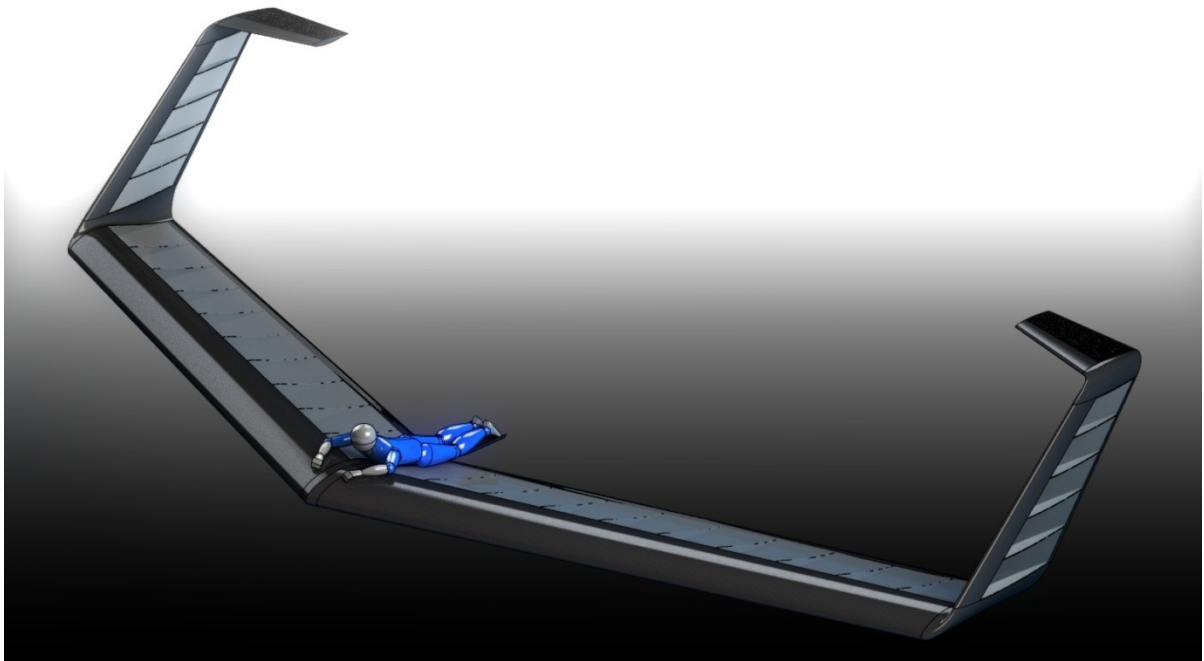


**Fig. 59** Final design of RBF-1.

## References

- [1] *Red Bull Flugtag*. (n.d.). Retrieved February 6, 2013, from <http://www.redbullflugtagusa.com/>
- [2] *Red Bull FAQ*. (2012, November 12). Retrieved February 6, 2013, from Red Bull Flugtag San Francisco: [http://www.redbullflugtagusa.com/doc/SF\\_2012\\_FAQ.pdf](http://www.redbullflugtagusa.com/doc/SF_2012_FAQ.pdf)
- [3] Kroo, I. (2000). *Design and Development of the Swift: A Foot-Launched Sailplane*. Stanford, CA: AIAA-00-4336.
- [4] Kroo, I. (2007, January). *Applied Aerodynamics: A Digital Textbook*. Retrieved February 10, 2013, from Desktop Aeronautics: <http://www.desktop.aero/appliedaero/preface/welcome.html>
- [5] Nickel, K. M. (1994). *Tailless Aircraft in Theory and Practice*. Burlington, MA: Butterworth Heinemann.
- [6] *Home Built Airplanes*. (n.d.). Retrieved February 11, 2013, from <http://www.homebuiltairplanes.com/forums/attachments/hangar-flying/3124d1235672974-flying-prone-img0073.jpg>
- [7] Kroo, I. (2005). *Nonplanar Wing Concepts for Increased Aircraft Efficiency*. Stanford, CA: Stanford University.
- [8] Ning, S. A. (2008). *Tip Extensions, Winglets, and C-wings: Conceptual Design and Optimization*. Stanford, CA: Stanford.
- [9] Liebeck, R. (1973). A Class of Airfoils Designed for High Lift in Incompressible Flow. *J. Aircraft*, 10 (10), 610-617.
- [10] Smith, A. (1975). High-Lift Aerodynamics. *J. Aircraft*, 12 (6), 501-530.
- [11] Henne, P. (1990). *Applied Computational Aerodynamics* (Vol. 125). Washington: AIAA.
- [12] Bushnell, D. M. (1990). *Viscous Drag Reduction in Boundary Layers* (Vol. 123). Washington: AIAA.
- [13] Drela, M. M. (1987). Viscous-Inviscid Analysis of Transonic and Low Reynolds Number Airfoils. *AIAA Journal*, 25 (10), 1347-1355.
- [14] Cebeci, T. (1999). *An Engineering Approach to the Calculation of Aerodynamic Flows*. Long Beach: Horizons Publishing Inc.
- [15] Astrom, K. J. (2002). *UCSB: Control System Design*. Retrieved February 11, 2013, from Lecture Notes for ME155A: <http://www.cds.caltech.edu/~murray/courses/cds101/fa02/caltech/astrom.html>
- [16] Mendoza, G. (2007). *Analysis of Flight Trajectories of an Aerodynamically Stabilized Ballistic Projectile*. Wichita: Wichita State University, Department of Mathematics and Statistics.

- [17] Agarwal, B., Broutman, L., & Chandrashekhara, K. (2006). *Analysis and Performance of Fiber Composites*. New Jersey: John Wiley and Sons.
- [18] Megson, T. (2007). *Aircraft Structures for Engineering Students*. Oxford: Butterworth-Heinemann.
- [19] Sun, C. (2006). *Mechanics of Aircraft Structures*. New York: John Wiley & Sons.

## Appendix

### 6 DOF Output Table

**Table 9 Output variables of 6 degree of freedom MATLAB program showing flight distance of 424 feet.**

Time (s)	Vel. (ft/s)	Dist. (ft)	Lat. Dist. (ft)	Ht. (ft)	$\alpha$ (deg)	Beta (deg)	$P_{dot}$	$Q_{dot}$	$R_{dot}$	$\Theta$ (deg)	Vert. Speed (ft/s)	Elevator Deflect. (deg)
0.0	30.0	0.0	0.0	-	0.0	0.0	0.0	0.0	0.0	0.0	0.0	0.0
				35.0								
0.1	30.0	1.5	0.0	-	1.4	0.0	0.0	0.0	0.0	0.0	0.7	0.0
				35.0								
0.1	29.9	3.0	0.0	-	2.6	0.0	0.0	0.0	0.0	0.0	1.4	-0.1
				34.9								
0.2	30.0	4.5	0.0	-	3.6	0.0	0.0	0.0	0.0	0.0	1.9	-0.1
				34.8								
0.2	30.0	6.0	0.0	-	4.5	0.0	0.0	0.0	0.0	0.0	2.3	-0.1
				34.7								
0.3	30.0	7.5	0.0	-	5.2	0.0	0.0	0.0	0.0	0.0	2.7	-0.2
				34.6								
0.3	30.1	9.0	0.0	-	5.7	0.0	0.0	0.0	0.0	0.0	3.0	-0.2
				34.5								
0.4	30.2	10.5	0.0	-	6.2	0.0	0.0	0.0	0.0	0.0	3.3	-0.2
				34.3								
0.4	30.2	12.0	0.0	-	6.6	0.0	0.0	0.0	0.0	0.0	3.5	-0.3
				34.1								
0.5	30.3	13.5	0.0	-	6.9	0.0	0.0	0.0	0.0	0.0	3.6	-0.3
				34.0								
0.5	30.4	15.0	0.0	-	7.1	0.0	0.0	0.0	0.0	0.0	3.8	-0.3
				33.8								
0.6	30.5	16.5	0.0	-	7.3	0.0	0.0	0.0	0.0	0.0	3.9	-0.3
				33.6								
0.6	30.6	18.0	0.0	-	7.5	0.0	0.0	0.0	0.0	0.0	4.0	-0.4
				33.4								
0.7	30.7	19.5	0.0	-	7.6	0.0	0.0	0.0	0.0	0.0	4.1	-0.4
				33.2								
0.7	30.8	21.1	0.0	-	7.6	0.0	0.0	0.0	0.0	0.0	4.1	-0.4
				33.0								
0.8	30.9	22.6	0.0	-	7.7	0.0	0.0	0.0	0.0	0.0	4.1	-0.4
				32.8								
0.8	31.0	24.1	0.0	-	7.7	0.0	0.0	0.0	0.0	0.0	4.2	-0.4
				32.6								
0.9	31.1	25.7	0.0	-	7.7	0.0	0.0	0.0	0.0	-0.1	4.2	-0.4
				32.4								
0.9	31.2	27.2	0.0	-	7.7	0.0	0.0	0.0	0.0	-0.1	4.2	-0.4
				32.2								
1.0	31.3	28.7	0.0	-	7.6	0.0	0.0	0.0	0.0	-0.1	4.2	-0.4
				31.9								
1.0	31.4	30.3	0.0	-	7.6	0.0	0.0	0.0	0.0	-0.1	4.2	-0.4
				31.7								
1.1	31.4	31.8	0.0	-	7.5	0.0	0.0	0.0	0.0	-0.1	4.2	-0.4
				31.5								
1.1	31.5	33.4	0.0	-	7.5	0.0	0.0	0.0	0.0	-0.1	4.2	-0.4
				31.3								
1.2	31.6	35.0	0.0	-	7.4	0.0	0.0	0.0	0.0	-0.1	4.1	-0.4
				31.1								
1.2	31.7	36.5	0.0	-	7.3	0.0	0.0	0.0	0.0	-0.2	4.1	-0.4
				30.9								
1.3	31.8	38.1	0.0	-	7.3	0.0	0.0	0.0	0.0	-0.2	4.1	-0.4
				30.7								
1.3	31.9	39.7	0.0	-	7.2	0.0	0.0	0.0	0.0	-0.2	4.1	-0.4
				30.5								
1.4	32.0	41.3	0.0	-	7.1	0.0	0.0	0.0	0.0	-0.2	4.1	-0.4
				30.3								

1.4	32.0	42.9	0.0	-	7.0	0.0	0.0	0.0	0.0	-0.2	4.0	-0.4
				30.1								
1.5	32.1	44.5	0.0	-	6.9	0.0	0.0	0.0	0.0	-0.2	4.0	-0.3
				29.9								
1.5	32.2	46.1	0.0	-	6.9	0.0	0.0	0.0	0.0	-0.3	4.0	-0.3
				29.7								
1.6	32.3	47.7	0.0	-	6.8	0.0	0.0	0.0	0.0	-0.3	4.0	-0.3
				29.5								
1.6	32.3	49.3	0.0	-	6.7	0.0	0.0	0.0	0.0	-0.3	3.9	-0.3
				29.3								
1.7	32.4	50.9	0.0	-	6.6	0.0	0.0	0.0	0.0	-0.3	3.9	-0.3
				29.1								
1.7	32.5	52.5	0.0	-	6.5	0.0	0.0	0.0	0.0	-0.4	3.9	-0.3
				28.9								
1.8	32.6	54.1	0.0	-	6.5	0.0	0.0	0.0	0.0	-0.4	3.9	-0.2
				28.7								
1.8	32.6	55.7	0.0	-	6.4	0.0	0.0	0.0	0.0	-0.4	3.9	-0.2
				28.5								
1.9	32.7	57.3	0.0	-	6.3	0.0	0.0	0.0	0.0	-0.4	3.8	-0.2
				28.3								
1.9	32.8	59.0	0.0	-	6.2	0.0	0.0	0.0	0.0	-0.5	3.8	-0.2
				28.1								
2.0	32.8	60.6	0.0	-	6.2	0.0	0.0	0.0	0.0	-0.5	3.8	-0.1
				27.9								
2.0	32.9	62.2	0.0	-	6.1	0.0	0.0	0.0	0.0	-0.5	3.8	-0.1
				27.7								
2.1	33.0	63.9	0.0	-	6.0	0.0	0.0	0.0	0.0	-0.5	3.8	-0.1
				27.6								
2.1	33.0	65.5	0.0	-	6.0	0.0	0.0	0.0	0.0	-0.6	3.8	0.0
				27.4								
2.2	33.1	67.1	0.0	-	5.9	0.0	0.0	0.0	0.0	-0.6	3.7	0.0
				27.2								
2.2	33.2	68.8	0.0	-	5.8	0.0	0.0	0.0	0.0	-0.6	3.7	0.0
				27.0								
2.3	33.2	70.4	0.0	-	5.8	0.0	0.0	0.0	0.0	-0.7	3.7	0.1
				26.8								
2.3	33.3	72.1	0.0	-	5.7	0.0	0.0	0.0	0.0	-0.7	3.7	0.1
				26.6								
2.4	33.4	73.7	0.0	-	5.6	0.0	0.0	0.0	0.0	-0.7	3.7	0.1
				26.4								
2.4	33.4	75.4	0.0	-	5.6	0.0	0.0	0.0	0.0	-0.7	3.7	0.2
				26.3								
2.5	33.5	77.1	0.0	-	5.5	0.0	0.0	0.0	0.0	-0.8	3.7	0.2
				26.1								
2.5	33.5	78.7	0.0	-	5.4	0.0	0.0	0.0	0.0	-0.8	3.6	0.2
				25.9								
2.6	33.6	80.4	0.0	-	5.4	0.0	0.0	0.0	0.0	-0.8	3.6	0.3
				25.7								
2.6	33.7	82.1	0.0	-	5.3	0.0	0.0	0.0	0.0	-0.9	3.6	0.3
				25.5								
2.7	33.7	83.7	0.0	-	5.3	0.0	0.0	0.0	0.0	-0.9	3.6	0.4
				25.3								
2.7	33.8	85.4	0.0	-	5.2	0.0	0.0	0.0	0.0	-0.9	3.6	0.4
				25.2								
2.8	33.8	87.1	0.0	-	5.2	0.0	0.0	0.0	0.0	-0.9	3.6	0.4
				25.0								
2.8	33.9	88.8	0.0	-	5.1	0.0	0.0	0.0	0.0	-1.0	3.6	0.5
				24.8								
2.9	33.9	90.5	0.0	-	5.1	0.0	0.0	0.0	0.0	-1.0	3.6	0.5
				24.6								
2.9	34.0	92.2	0.0	-	5.0	0.0	0.0	0.0	0.0	-1.0	3.6	0.5
				24.4								
3.0	34.0	93.9	0.0	-	5.0	0.0	0.0	0.0	0.0	-1.0	3.6	0.6
				24.3								
3.0	34.1	95.5	0.0	-	4.9	0.0	0.0	0.0	0.0	-1.1	3.5	0.6
				24.1								
3.1	34.1	97.2	0.0	-	4.9	0.0	0.0	0.0	0.0	-1.1	3.5	0.7
				23.9								

3.1	34.2	98.9	0.0	-	4.8	0.0	0.0	0.0	0.0	-1.1	3.5	0.7
				23.7								
3.2	34.3	100.6	0.0	-	4.8	0.0	0.0	0.0	0.0	-1.1	3.5	0.7
				23.6								
3.2	34.3	102.3	0.0	-	4.7	0.0	0.0	0.0	0.0	-1.2	3.5	0.8
				23.4								
3.3	34.4	104.1	0.0	-	4.7	0.0	0.0	0.0	0.0	-1.2	3.5	0.8
				23.2								
3.3	34.4	105.8	0.0	-	4.6	0.0	0.0	0.0	0.0	-1.2	3.5	0.9
				23.0								
3.4	34.5	107.5	0.0	-	4.6	0.0	0.0	0.0	0.0	-1.2	3.5	0.9
				22.9								
3.4	34.5	109.2	0.0	-	4.5	0.0	0.0	0.0	0.0	-1.3	3.5	0.9
				22.7								
3.5	34.6	110.9	0.0	-	4.5	0.0	0.0	0.0	0.0	-1.3	3.5	1.0
				22.5								
3.5	34.6	112.6	0.0	-	4.5	0.0	0.0	0.0	0.0	-1.3	3.5	1.0
				22.3								
3.6	34.7	114.4	0.0	-	4.4	0.0	0.0	0.0	0.0	-1.3	3.5	1.0
				22.2								
3.6	34.7	116.1	0.0	-	4.4	0.0	0.0	0.0	0.0	-1.3	3.5	1.1
				22.0								
3.7	34.7	117.8	0.0	-	4.3	0.0	0.0	0.0	0.0	-1.3	3.4	1.1
				21.8								
3.7	34.8	119.5	0.0	-	4.3	0.0	0.0	0.0	0.0	-1.4	3.4	1.1
				21.6								
3.8	34.8	121.3	0.0	-	4.3	0.0	0.0	0.0	0.0	-1.4	3.4	1.2
				21.5								
3.8	34.9	123.0	0.0	-	4.2	0.0	0.0	0.0	0.0	-1.4	3.4	1.2
				21.3								
3.9	34.9	124.7	0.0	-	4.2	0.0	0.0	0.0	0.0	-1.4	3.4	1.2
				21.1								
3.9	35.0	126.5	0.0	-	4.2	0.0	0.0	0.0	0.0	-1.4	3.4	1.3
				21.0								
4.0	35.0	128.2	0.0	-	4.1	0.0	0.0	0.0	0.0	-1.4	3.4	1.3
				20.8								
4.0	35.1	130.0	0.0	-	4.1	0.0	0.0	0.0	0.0	-1.5	3.4	1.3
				20.6								
4.1	35.1	131.7	0.0	-	4.0	0.0	0.0	0.0	0.0	-1.5	3.4	1.4
				20.5								
4.1	35.1	133.5	0.0	-	4.0	0.0	0.0	0.0	0.0	-1.5	3.4	1.4
				20.3								
4.2	35.2	135.2	0.0	-	4.0	0.0	0.0	0.0	0.0	-1.5	3.4	1.4
				20.1								
4.2	35.2	137.0	0.0	-	4.0	0.0	0.0	0.0	0.0	-1.5	3.3	1.4
				19.9								
4.3	35.3	138.7	0.0	-	3.9	0.0	0.0	0.0	0.0	-1.5	3.3	1.5
				19.8								
4.3	35.3	140.5	0.0	-	3.9	0.0	0.0	0.0	0.0	-1.5	3.3	1.5
				19.6								
4.4	35.4	142.2	0.0	-	3.9	0.0	0.0	0.0	0.0	-1.5	3.3	1.5
				19.4								
4.4	35.4	144.0	0.0	-	3.8	0.0	0.0	0.0	0.0	-1.5	3.3	1.5
				19.3								
4.5	35.4	145.8	0.0	-	3.8	0.0	0.0	0.0	0.0	-1.5	3.3	1.6
				19.1								
4.5	35.5	147.5	0.0	-	3.8	0.0	0.0	0.0	0.0	-1.5	3.3	1.6
				19.0								
4.6	35.5	149.3	0.0	-	3.7	0.0	0.0	0.0	0.0	-1.5	3.3	1.6
				18.8								
4.6	35.5	151.1	0.0	-	3.7	0.0	0.0	0.0	0.0	-1.5	3.3	1.6
				18.6								
4.7	35.6	152.8	0.0	-	3.7	0.0	0.0	0.0	0.0	-1.5	3.2	1.6
				18.5								
4.7	35.6	154.6	0.0	-	3.7	0.0	0.0	0.0	0.0	-1.5	3.2	1.6
				18.3								
4.8	35.6	156.4	0.0	-	3.6	0.0	0.0	0.0	0.0	-1.5	3.2	1.7
				18.1								

4.8	35.7	158.2	0.0	-	3.6	0.0	0.0	0.0	0.0	-1.5	3.2	1.7
				18.0								
4.9	35.7	159.9	0.0	-	3.6	0.0	0.0	0.0	0.0	-1.5	3.2	1.7
				17.8								
4.9	35.7	161.7	0.0	-	3.6	0.0	0.0	0.0	0.0	-1.5	3.2	1.7
				17.7								
5.0	35.8	163.5	0.0	-	3.6	0.0	0.0	0.0	0.0	-1.5	3.2	1.7
				17.5								
5.0	35.8	165.3	0.0	-	3.5	0.0	0.0	0.0	0.0	-1.5	3.2	1.7
				17.3								
5.1	35.8	167.1	0.0	-	3.5	0.0	0.0	0.0	0.0	-1.5	3.1	1.7
				17.2								
5.1	35.9	168.8	0.0	-	3.5	0.0	0.0	0.0	0.0	-1.5	3.1	1.7
				17.0								
5.2	35.9	170.6	0.0	-	3.5	0.0	0.0	0.0	0.0	-1.5	3.1	1.7
				16.9								
5.2	35.9	172.4	0.0	-	3.5	0.0	0.0	0.0	0.0	-1.5	3.1	1.7
				16.7								
5.3	36.0	174.2	0.0	-	3.4	0.0	0.0	0.0	0.0	-1.5	3.1	1.7
				16.6								
5.3	36.0	176.0	0.0	-	3.4	0.0	0.0	0.0	0.0	-1.5	3.1	1.7
				16.4								
5.4	36.0	177.8	0.0	-	3.4	0.0	0.0	0.0	0.0	-1.4	3.0	1.7
				16.3								
5.4	36.0	179.6	0.0	-	3.4	0.0	0.0	0.0	0.0	-1.4	3.0	1.7
				16.1								
5.5	36.1	181.4	0.0	-	3.4	0.0	0.0	0.0	0.0	-1.4	3.0	1.7
				16.0								
5.5	36.1	183.2	0.0	-	3.4	0.0	0.0	0.0	0.0	-1.4	3.0	1.7
				15.8								
5.6	36.1	185.0	0.0	-	3.4	0.0	0.0	0.0	0.0	-1.4	3.0	1.7
				15.7								
5.6	36.1	186.8	0.0	-	3.3	0.0	0.0	0.0	0.0	-1.4	3.0	1.7
				15.5								
5.7	36.1	188.6	0.0	-	3.3	0.0	0.0	0.0	0.0	-1.4	2.9	1.7
				15.4								
5.7	36.2	190.4	0.0	-	3.3	0.0	0.0	0.0	0.0	-1.3	2.9	1.6
				15.2								
5.8	36.2	192.2	0.0	-	3.3	0.0	0.0	0.0	0.0	-1.3	2.9	1.6
				15.1								
5.8	36.2	194.0	0.0	-	3.3	0.0	0.0	0.0	0.0	-1.3	2.9	1.6
				14.9								
5.9	36.2	195.8	0.0	-	3.3	0.0	0.0	0.0	0.0	-1.3	2.9	1.6
				14.8								
5.9	36.2	197.6	0.0	-	3.3	0.0	0.0	0.0	0.0	-1.3	2.9	1.6
				14.6								
6.0	36.2	199.4	0.0	-	3.3	0.0	0.0	0.0	0.0	-1.2	2.8	1.6
				14.5								
6.0	36.3	201.2	0.0	-	3.3	0.0	0.0	0.0	0.0	-1.2	2.8	1.5
				14.3								
6.1	36.3	203.0	0.0	-	3.3	0.0	0.0	0.0	0.0	-1.2	2.8	1.5
				14.2								
6.1	36.3	204.8	0.0	-	3.2	0.0	0.0	0.0	0.0	-1.2	2.8	1.5
				14.1								
6.2	36.3	206.6	0.0	-	3.2	0.0	0.0	0.0	0.0	-1.1	2.8	1.5
				13.9								
6.2	36.3	208.4	0.0	-	3.2	0.0	0.0	0.0	0.0	-1.1	2.8	1.5
				13.8								
6.3	36.3	210.3	0.0	-	3.2	0.0	0.0	0.0	0.0	-1.1	2.7	1.4
				13.7								
6.3	36.3	212.1	0.0	-	3.2	0.0	0.0	0.0	0.0	-1.1	2.7	1.4
				13.5								
6.4	36.3	213.9	0.0	-	3.2	0.0	0.0	0.0	0.0	-1.0	2.7	1.4
				13.4								
6.4	36.4	215.7	0.0	-	3.2	0.0	0.0	0.0	0.0	-1.0	2.7	1.3
				13.2								
6.5	36.4	217.5	0.0	-	3.2	0.0	0.0	0.0	0.0	-1.0	2.7	1.3
				13.1								

6.5	36.4	219.3	0.0	-	3.2	0.0	0.0	0.0	0.0	-1.0	2.6	1.3
				13.0								
6.6	36.4	221.1	0.0	-	3.2	0.0	0.0	0.0	0.0	-0.9	2.6	1.3
				12.8								
6.6	36.4	222.9	0.0	-	3.2	0.0	0.0	0.0	0.0	-0.9	2.6	1.2
				12.7								
6.7	36.4	224.8	0.0	-	3.2	0.0	0.0	0.0	0.0	-0.9	2.6	1.2
				12.6								
6.7	36.4	226.6	0.0	-	3.2	0.0	0.0	0.0	0.0	-0.8	2.6	1.2
				12.5								
6.8	36.4	228.4	0.0	-	3.2	0.0	0.0	0.0	0.0	-0.8	2.6	1.1
				12.3								
6.8	36.4	230.2	0.0	-	3.2	0.0	0.0	0.0	0.0	-0.8	2.5	1.1
				12.2								
6.9	36.4	232.0	0.0	-	3.2	0.0	0.0	0.0	0.0	-0.8	2.5	1.0
				12.1								
6.9	36.4	233.8	0.0	-	3.2	0.0	0.0	0.0	0.0	-0.7	2.5	1.0
				11.9								
7.0	36.4	235.6	0.0	-	3.2	0.0	0.0	0.0	0.0	-0.7	2.5	1.0
				11.8								
7.0	36.4	237.5	0.0	-	3.2	0.0	0.0	0.0	0.0	-0.7	2.5	0.9
				11.7								
7.1	36.4	239.3	0.0	-	3.2	0.0	0.0	0.0	0.0	-0.6	2.5	0.9
				11.6								
7.1	36.4	241.1	0.0	-	3.2	0.0	0.0	0.0	0.0	-0.6	2.4	0.9
				11.5								
7.2	36.4	242.9	0.0	-	3.2	0.0	0.0	0.0	0.0	-0.6	2.4	0.8
				11.3								
7.2	36.4	244.7	0.0	-	3.2	0.0	0.0	0.0	0.0	-0.6	2.4	0.8
				11.2								
7.3	36.4	246.5	0.0	-	3.3	0.0	0.0	0.0	0.0	-0.5	2.4	0.7
				11.1								
7.3	36.4	248.3	0.0	-	3.3	0.0	0.0	0.0	0.0	-0.5	2.4	0.7
				11.0								
7.4	36.4	250.2	0.0	-	3.3	0.0	0.0	0.0	0.0	-0.5	2.4	0.7
				10.9								
7.4	36.3	252.0	0.0	-	3.3	0.0	0.0	0.0	0.0	-0.4	2.3	0.6
				10.7								
7.5	36.3	253.8	0.0	-	3.3	0.0	0.0	0.0	0.0	-0.4	2.3	0.6
				10.6								
7.5	36.3	255.6	0.0	-	3.3	0.0	0.0	0.0	0.0	-0.4	2.3	0.5
				10.5								
7.6	36.3	257.4	0.0	-	3.3	0.0	0.0	0.0	0.0	-0.3	2.3	0.5
				10.4								
7.6	36.3	259.2	0.0	-	3.3	0.0	0.0	0.0	0.0	-0.3	2.3	0.4
				10.3								
7.7	36.3	261.0	0.0	-	3.3	0.0	0.0	0.0	0.0	-0.3	2.3	0.4
				10.2								
7.7	36.3	262.9	0.0	-	3.3	0.0	0.0	0.0	0.0	-0.3	2.3	0.4
				10.0								
7.8	36.3	264.7	0.0	-9.9	3.3	0.0	0.0	0.0	0.0	-0.2	2.3	0.3
7.8	36.3	266.5	0.0	-9.8	3.3	0.0	0.0	0.0	0.0	-0.2	2.2	0.3
7.9	36.3	268.3	0.0	-9.7	3.3	0.0	0.0	0.0	0.0	-0.2	2.2	0.2
7.9	36.2	270.1	0.0	-9.6	3.4	0.0	0.0	0.0	0.0	-0.1	2.2	0.2
8.0	36.2	271.9	0.0	-9.5	3.4	0.0	0.0	0.0	0.0	-0.1	2.2	0.1
8.0	36.2	273.7	0.0	-9.4	3.4	0.0	0.0	0.0	0.0	-0.1	2.2	0.1
8.1	36.2	275.5	0.0	-9.3	3.4	0.0	0.0	0.0	0.0	-0.1	2.2	0.1
8.1	36.2	277.3	0.0	-9.2	3.4	0.0	0.0	0.0	0.0	0.0	2.2	0.0
8.2	36.2	279.1	0.0	-9.0	3.4	0.0	0.0	0.0	0.0	0.0	2.2	0.0
8.2	36.2	280.9	0.0	-8.9	3.4	0.0	0.0	0.0	0.0	0.0	2.2	-0.1
8.3	36.1	282.7	0.0	-8.8	3.4	0.0	0.0	0.0	0.0	0.0	2.1	-0.1
8.3	36.1	284.5	0.0	-8.7	3.5	0.0	0.0	0.0	0.0	0.1	2.1	-0.2

8.4	36.1	286.3	0.0	-8.6	3.5	0.0	0.0	0.0	0.0	0.1	2.1	-0.2
8.4	36.1	288.1	0.0	-8.5	3.5	0.0	0.0	0.0	0.0	0.1	2.1	-0.2
8.5	36.1	289.9	0.0	-8.4	3.5	0.0	0.0	0.0	0.0	0.1	2.1	-0.3
8.5	36.1	291.7	0.0	-8.3	3.5	0.0	0.0	0.0	0.0	0.1	2.1	-0.3
8.6	36.0	293.5	0.0	-8.2	3.5	0.0	0.0	0.0	0.0	0.2	2.1	-0.3
8.6	36.0	295.3	0.0	-8.1	3.5	0.0	0.0	0.0	0.0	0.2	2.1	-0.4
8.7	36.0	297.1	0.0	-8.0	3.5	0.0	0.0	0.0	0.0	0.2	2.1	-0.4
8.7	36.0	298.9	0.0	-7.9	3.6	0.0	0.0	0.0	0.0	0.2	2.1	-0.5
8.8	36.0	300.7	0.0	-7.8	3.6	0.0	0.0	0.0	0.0	0.2	2.1	-0.5
8.8	35.9	302.5	0.0	-7.7	3.6	0.0	0.0	0.0	0.0	0.3	2.1	-0.5
8.9	35.9	304.3	0.0	-7.6	3.6	0.0	0.0	0.0	0.0	0.3	2.1	-0.6
8.9	35.9	306.1	0.0	-7.5	3.6	0.0	0.0	0.0	0.0	0.3	2.1	-0.6
9.0	35.9	307.9	0.0	-7.4	3.6	0.0	0.0	0.0	0.0	0.3	2.1	-0.6
9.0	35.9	309.7	0.0	-7.3	3.6	0.0	0.0	0.0	0.0	0.3	2.1	-0.7
9.1	35.8	311.5	0.0	-7.2	3.6	0.0	0.0	0.0	0.0	0.3	2.1	-0.7
9.1	35.8	313.3	0.0	-7.1	3.7	0.0	0.0	0.0	0.0	0.3	2.1	-0.7
9.2	35.8	315.1	0.0	-6.9	3.7	0.0	0.0	0.0	0.0	0.4	2.1	-0.8
9.2	35.8	316.8	0.0	-6.8	3.7	0.0	0.0	0.0	0.0	0.4	2.1	-0.8
9.3	35.8	318.6	0.0	-6.7	3.7	0.0	0.0	0.0	0.0	0.4	2.1	-0.8
9.3	35.7	320.4	0.0	-6.6	3.7	0.0	0.0	0.0	0.0	0.4	2.1	-0.8
9.4	35.7	322.2	0.0	-6.5	3.7	0.0	0.0	0.0	0.0	0.4	2.1	-0.9
9.4	35.7	324.0	0.0	-6.4	3.7	0.0	0.0	0.0	0.0	0.4	2.1	-0.9
9.5	35.7	325.8	0.0	-6.3	3.7	0.0	0.0	0.0	0.0	0.4	2.1	-0.9
9.5	35.7	327.5	0.0	-6.2	3.8	0.0	0.0	0.0	0.0	0.4	2.1	-0.9
9.6	35.7	329.3	0.0	-6.1	3.8	0.0	0.0	0.0	0.0	0.4	2.1	-0.9
9.6	35.6	331.1	0.0	-6.0	3.8	0.0	0.0	0.0	0.0	0.4	2.1	-1.0
9.7	35.6	332.9	0.0	-5.9	3.8	0.0	0.0	0.0	0.0	0.4	2.1	-1.0
9.7	35.6	334.7	0.0	-5.8	3.8	0.0	0.0	0.0	0.0	0.4	2.1	-1.0
9.8	35.6	336.4	0.0	-5.7	3.8	0.0	0.0	0.0	0.0	0.4	2.1	-1.0
9.8	35.6	338.2	0.0	-5.6	3.8	0.0	0.0	0.0	0.0	0.4	2.1	-1.0
9.9	35.5	340.0	0.0	-5.5	3.8	0.0	0.0	0.0	0.0	0.4	2.1	-1.1
9.9	35.5	341.8	0.0	-5.4	3.8	0.0	0.0	0.0	0.0	0.4	2.1	-1.1
10.0	35.5	343.5	0.0	-5.3	3.9	0.0	0.0	0.0	0.0	0.4	2.1	-1.1
10.0	35.5	345.3	0.0	-5.2	3.9	0.0	0.0	0.0	0.0	0.4	2.1	-1.1
10.1	35.5	347.1	0.0	-5.1	3.9	0.0	0.0	0.0	0.0	0.4	2.1	-1.1
10.1	35.5	348.8	0.0	-5.0	3.9	0.0	0.0	0.0	0.0	0.4	2.1	-1.1
10.2	35.5	350.6	0.0	-4.9	3.9	0.0	0.0	0.0	0.0	0.4	2.1	-1.1
10.2	35.4	352.4	0.0	-4.8	3.9	0.0	0.0	0.0	0.0	0.4	2.1	-1.1
10.3	35.4	354.2	0.0	-4.6	3.9	0.0	0.0	0.0	0.0	0.4	2.2	-1.1
10.3	35.4	355.9	0.0	-4.5	3.9	0.0	0.0	0.0	0.0	0.4	2.2	-1.1
10.4	35.4	357.7	0.0	-4.4	3.9	0.0	0.0	0.0	0.0	0.4	2.2	-1.1
10.4	35.4	359.5	0.0	-4.3	3.9	0.0	0.0	0.0	0.0	0.4	2.2	-1.1
10.5	35.4	361.2	0.0	-4.2	3.9	0.0	0.0	0.0	0.0	0.4	2.2	-1.1
10.5	35.4	363.0	0.0	-4.1	4.0	0.0	0.0	0.0	0.0	0.4	2.2	-1.1

10.6	35.3	364.7	0.0	-4.0	4.0	0.0	0.0	0.0	0.0	0.4	2.2	-1.1
10.6	35.3	366.5	0.0	-3.9	4.0	0.0	0.0	0.0	0.0	0.4	2.2	-1.1
10.7	35.3	368.3	0.0	-3.8	4.0	0.0	0.0	0.0	0.0	0.4	2.2	-1.1
10.7	35.3	370.0	0.0	-3.7	4.0	0.0	0.0	0.0	0.0	0.4	2.2	-1.1
10.8	35.3	371.8	0.0	-3.5	4.0	0.0	0.0	0.0	0.0	0.3	2.2	-1.1
10.8	35.3	373.6	0.0	-3.4	4.0	0.0	0.0	0.0	0.0	0.3	2.3	-1.1
10.9	35.3	375.3	0.0	-3.3	4.0	0.0	0.0	0.0	0.0	0.3	2.3	-1.1
10.9	35.3	377.1	0.0	-3.2	4.0	0.0	0.0	0.0	0.0	0.3	2.3	-1.1
11.0	35.3	378.8	0.0	-3.1	4.0	0.0	0.0	0.0	0.0	0.3	2.3	-1.1
11.0	35.3	380.6	0.0	-3.0	4.0	0.0	0.0	0.0	0.0	0.3	2.3	-1.1
11.1	35.3	382.4	0.0	-2.9	4.0	0.0	0.0	0.0	0.0	0.3	2.3	-1.1
11.1	35.2	384.1	0.0	-2.7	4.0	0.0	0.0	0.0	0.0	0.2	2.3	-1.1
11.2	35.2	385.9	0.0	-2.6	4.0	0.0	0.0	0.0	0.0	0.2	2.3	-1.0
11.2	35.2	387.6	0.0	-2.5	4.0	0.0	0.0	0.0	0.0	0.2	2.3	-1.0
11.3	35.2	389.4	0.0	-2.4	4.0	0.0	0.0	0.0	0.0	0.2	2.3	-1.0
11.3	35.2	391.1	0.0	-2.3	4.0	0.0	0.0	0.0	0.0	0.2	2.4	-1.0
11.4	35.2	392.9	0.0	-2.2	4.0	0.0	0.0	0.0	0.0	0.2	2.4	-1.0
11.4	35.2	394.7	0.0	-2.0	4.0	0.0	0.0	0.0	0.0	0.1	2.4	-1.0
11.5	35.2	396.4	0.0	-1.9	4.0	0.0	0.0	0.0	0.0	0.1	2.4	-0.9
11.5	35.2	398.2	0.0	-1.8	4.0	0.0	0.0	0.0	0.0	0.1	2.4	-0.9
11.6	35.2	399.9	0.0	-1.7	4.0	0.0	0.0	0.0	0.0	0.1	2.4	-0.9
11.6	35.2	401.7	0.0	-1.6	4.0	0.0	0.0	0.0	0.0	0.1	2.4	-0.9
11.7	35.2	403.4	0.0	-1.4	4.0	0.0	0.0	0.0	0.0	0.0	2.4	-0.9
11.7	35.2	405.2	0.0	-1.3	4.0	0.0	0.0	0.0	0.0	0.0	2.5	-0.8
11.8	35.2	407.0	0.0	-1.2	4.0	0.0	0.0	0.0	0.0	0.0	2.5	-0.8
11.8	35.2	408.7	0.0	-1.1	4.0	0.0	0.0	0.0	0.0	0.0	2.5	-0.8
11.9	35.2	410.5	0.0	-0.9	4.0	0.0	0.0	0.0	0.0	0.0	2.5	-0.8
11.9	35.2	412.2	0.0	-0.8	4.0	0.0	0.0	0.0	0.0	-0.1	2.5	-0.7
12.0	35.2	414.0	0.0	-0.7	4.0	0.0	0.0	0.0	0.0	-0.1	2.5	-0.7
12.0	35.2	415.7	0.0	-0.6	4.0	0.0	0.0	0.0	0.0	-0.1	2.5	-0.7
12.1	35.2	417.5	0.0	-0.4	4.0	0.0	0.0	0.0	0.0	-0.1	2.5	-0.7
12.1	35.2	419.2	0.0	-0.3	4.0	0.0	0.0	0.0	0.0	-0.2	2.5	-0.6
12.2	35.2	421.0	0.0	-0.2	4.0	0.0	0.0	0.0	0.0	-0.2	2.6	-0.6
12.2	35.2	422.8	0.0	-0.1	4.0	0.0	0.0	0.0	0.0	-0.2	2.6	-0.6
12.3	35.2	424.5	0.0	0.1	4.0	0.0	0.0	0.0	0.0	-0.2	2.6	-0.6

---

## MATLAB Code for 6 DOF Program Modified with Controller

```

%*****
% * Program : GliderSim.m
*
%
%*****
% * Function: Call xdot = Navigator(t,x)
*
% * Purpose : Track 6 DOF translational and rotational parameters for launched
uncontrolled glider *
% * States : 1 2 3 4 5 6 7 8 9 10 11 12 13 14 15 16
*
% * Uwind AOA Beta PB QB RB q1 q2 q3 q4 Xe Ye Ze Xedot Yedot Zedot
*
% * (Euler Parameters) (Tracking) (Ground Speed)
*
%
%*****
clear all
close all
tic
% // ***** Initial Conditions ***** //
Xeo = 0 ;
% X Initial Position WRT Earth (ft.)
Yeo = 0 ;
% Y Initial Position WRT Earth (ft.)
Zeo = -35 ;
% Z Initial Position WRT Earth (ft.) (- Up)
LaunchVelocity = 30 ;
% Launch Velocity (ft/sec.)
LaunchAngle = 0 ;
% Launch Angle (deg.)
Heading = 0 ;
% Launch Heading (deg.)
WindSpeed = 0;
% Wind Speed (deg.)
WindHeading = 180 ;
% Wind Heading (deg.)
dt = 0.05;
% Time step for numerical integration
slug = 0.0310809502;
MIC = 386.088;
%conversion for moment of interia from lb in to slug ft
Wt = 197.69422824 ;
% Weight (Lbs.)
Ixx = 6838.6606*slug*144 ; %
slug ft2 ***MARTIN*** MOI Taken at Output coordinate system
Iyy = 4096.86*slug*144 ;
% slug ft2
Izz = 10620*slug*144 ; %
slug ft2
Ixy = 0.00 ;
% slug ft2

```

```

Ixz                = 481.90768*slug*144                ;
% slug ft2
Iyz                = 0                                ;
% slug ft2
Geom.CG            = [ 47.16 0 4.15865 ]                ;
% Coordinates of CG (inches from tip of nose)***** Picked Ixx instead of Lxx
because of this*****
Geom.ARP           = [ 45.9445 0 0 ]                    ; %
Coordinates of aerodynamic reference point *****AERODYNAMIC REFERENCE*****
Geom.RefArea      = 17280                                ;
% Projected lifting surface area (sq. in.)
Geom.RefChord     = 51.43                                ;
% Reference chord (in.)
Geom.RefSpan      = 336                                  ;
% Reference span (in.)
OutputFileName = 'MyOutputFile.dat' ; % Name of output file

% *****
% // ***** End Of User Input ***** //
% *****
% *****
% * BEGIN ANALYSIS OF FLIGHT PATH *
% *****
% // ***** Set Initial Conditions (Quaternion definition from Robertson,
Stevens and others refer to q4 as q0) ***** //
DEo                = 0                                ;
% Initial elevon deflection (deg.)
rpd                = pi / 180                          ;
% Degrees per Radian
phio               = 0                                ;
% Initial Roll Angle (rad.)
thetao            = 0 * rpd                            ; %
Initial Pitch Angle (rad.) *****MODIFIED*****
psio               = Heading * rpd                    ;
% Initial Heading Angle (rad.)
wpsio             = WindHeading * rpd                 ;
% Initial Wind Heading (rad.)
dpsio             = psio - wpsio                      ;
% Heading angle between launch velocity and outside wind

TyPitch           = [ cos(thetao)    0    -sin(thetao)
                    0    1    0
                    sin(thetao)    0    cos(thetao) ] ;
% Y-Axis Transformation Rotation of Launch Angle

TzHeading         = [ cos(psio)    sin(psio)    0
                    -sin(psio)   cos(psio)    0
                    0    0    1 ] ;
% Z-Axis Transformation Rotation of Launch Heading

TzWindHead        = [ cos(wpsio)    sin(wpsio)    0
                    -sin(wpsio)   cos(wpsio)    0
                    0    0    1 ] ;
% Z-Axis Transformation from Air Mass to Earth Axis

```

```

TzdHeading          = [ cos(dpsio)    sin(dpsio)    0
                      -sin(dpsio)   cos(dpsio)    0
                      0              0              1      ] ;
% Z-Axis Transformation Rotation of Wind into Launch Direction (Body Axis)
WindSpeedE          = TzWindHead * [WindSpeed ; 0 ; 0] ;
% Velocity of Air Mass with Respect to Earth in Earth Axis
VelocityWo          = [LaunchVelocity ; 0 ; 0] ;
% Launch Velocity in Body Axis which is Equal to Wind Axis at Launch
WindVelWL           = TzdHeading * TyPitch' * [WindSpeed ; 0 ; 0] ;
% Velocity of Air Mass in Airplane Wind Axis at Launch
VelocityWL          = VelocityWo + WindVelWL ;
% Velocity of Aircraft wrt Air Mass at Launch
AOAo                = atan2(VelocityWL(3),VelocityWL(1))+thetao ;
% Delta AOA due to Outside Winds *****ADDED OFFSET FOR INTIAL INCLINATION OF
VEHICLE ON THE CART
Betao               = atan2(VelocityWL(2),VelocityWL(1)) ;
% Delta Beta due to Outside Winds
Uwindo              = sqrt(dot(VelocityWL,VelocityWL)) ;
% Velocity of Aircraft in Wind Axis WRT Air
VelocityEo          = TzHeading' * TyPitch' * VelocityWo ;
% Initial Velocity Vector (Rotation of Body Axis Launch Velocity)
I                   = [ Ixx Ixy Ixz
                      Ixy Iyy Iyz
                      Ixz Iyz Izz ] ;
% Inertia Matrix
InvI                 = inv(I) ;
% Inverse Inertia Matrix
qo                  = [sin(phio/2)*cos(thetao/2)*cos(psio/2) -
cos(phio/2)*sin(thetao/2)*sin(psio/2)
                      cos(phio/2)*sin(thetao/2)*cos(psio/2) +
sin(phio/2)*cos(thetao/2)*sin(psio/2)
                      cos(phio/2)*cos(thetao/2)*sin(psio/2) -
sin(phio/2)*sin(thetao/2)*cos(psio/2)
                      cos(phio/2)*cos(thetao/2)*cos(psio/2) +
sin(phio/2)*sin(thetao/2)*sin(psio/2)] ; % Initial Euler Parameters
(Quaternion)

Omegao              = [ 0 ; 0 ; 0 ] ;
% Initial Body Rates
EulerOffsetMatrix   = [ 0 -qo(3) qo(2)
                      qo(3) 0 -qo(1)
                      -qo(2) qo(1) 0 ] ;
% Euler Offset Matrix for Creating DCM (Transformation from Earth to Body
Coordinate Systems Using Quaternions)
EtoBDCM             = eye(3) + (EulerOffsetMatrix * EulerOffsetMatrix).*2 -
EulerOffsetMatrix.*(2*qo(4));
% Direccion Cosine Matrix (Rotation from Earth to Aircraft)

InitialConditions   = [ Uwindo
                      AOAO
                      Betao
                      Omegao
                      qo
                      Xeo
                      Yeo
                      Zeo

```

```

                                VelocityEo ] ;
% Assemble vector of initial conditions
% // ***** Run EOM Solver
[time,x,xdot,Euler,DE] =
Navigator(InitialConditions,dt,Geom,Wt,I,InvI,WindSpeedE,DEo) ;
% Solve EOMs
PrintArray = [time ; x(1,:) ; x(11,:) ; x(12,:) ; x(13,:) ;
x(2,)/rpd ; x(3,)/rpd ; ...
                                xdot(4,:) ; xdot(5,:) ; xdot(6,:) ;
Euler(2,)/rpd ; x(16,:) ; DE
                                ];
% Array of Outputs for Storing
fid = fopen(OutputFileName,'w');
fprintf(fid,'\n Time UW Xe Ye Ze AOA Beta
PBdot QBdot RBdot Pitch Angle Vert Speed DE');
fprintf(fid,'\n%8.4f %8.1f %8.1f %8.1f %8.1f %8.4f %8.4f %8.4f %8.4f %8.4f
%8.4f %8.4f %8.4f',PrintArray) ;
fclose(fid)
figure(1)
plot3(x(11,:),x(12,:),-x(13,:)) ;
title('Trajectory in Space') ;
xlabel('North Travel (ft)') ;
ylabel('East Travel (ft)') ;
zlabel('Altitude (ft)') ;
figure(2)
subplot(711) ;
plot(time,Euler(1,)./rpd) ;
title('Trajectory and Orientation') ;
ylabel('Phi (Deg.)') ;
subplot(712) ;
plot(time,Euler(2,)./rpd) ;
ylabel('Theta (Deg.)') ;
subplot(713) ;
plot(time,Euler(3,)./rpd) ;
ylabel('Psi (Deg.)') ;
subplot(714) ;
plot(time,-x(13,:)) ;
ylabel('Altitude (ft)') ;
subplot(715) ;
plot(time,x(11,:)) ;
ylabel('North (ft)') ;
subplot(716) ;
plot(time,x(12,:)) ;
ylabel('East (ft)') ;
subplot(717) ;
plot(time,x(2,)./rpd) ;
ylabel('AOA (deg)') ;
xlabel('Time (sec)') ;

%*****
% * Function: xdot = Navigator(t,x)
% *
% * Purpose : Track 6 DOF translational and rotational parameters for aircraft
% *
% * States : 1 2 3 4 5 6 7 8 9 10 11 12 13 14 15 16
% *

```

```

% * Uwind AOA Beta PB QB RB q1 q2 q3 q4 Xe Ye Ze Xedot Yedot Zedot
*
% * (Euler Parameters) (Tracking) (Ground Speed)
*
% * Notation: Parameter name followed by reference frame in which it is
expressed *
% * (S) = S/C axis, (B) = body axis, (W) = Wind Axis, (E) = Earth Axis
*
% * Ex.: ForceAeroS = Aero Force in S/C coordinates
*
% * EOMs : Forces are written in wind axis, Moments are written in body axis
*
%
*****
function [time,x,xdot,Euler,DEArray] =
Navigator(xo,dt,Geom,Wt,I,InvI,WindSpeedE,DE)
t = 0 ;
% Initiate time variable
rpd = pi / 180 ;
% Radians per Deg.
ii = 1 ;
% Begin Counter
x(:,ii) = xo ;
% Initialize State Vector
Crash = false ;
% Flag for Impact
C1 = -3*180/pi ;
;
C2 = 2 ;
ThetaTarget = -0.35 ;
ZeroController = [0 C1] ;
PoleController = [1 C2] ;
[A,B,C,D] = tf2ss(ZeroController,PoleController) ;
% xdot = -C2*x + 1*u, y = C1*x + 0*u.
Controller.A = A ;
Controller.B = B ;
Controller.C = C ;
Controller.D = D ;
xController = 0 ;
% Initialize the deviation controller
while ~Crash

DEArray(ii) = DE ;
q1 = x(7,ii) ;
% Euler Parameter q1 (Quaternion)
q2 = x(8,ii) ;
% Euler Parameter q1 (Quaternion)
q3 = x(9,ii) ;
% Euler Parameter q1 (Quaternion)
q4 = x(10,ii) ;
% Euler Parameter q1 (Quaternion)
Euler(1,ii) = atan2( (2*q3*q2 + 2*q1*q4), (1-2*q2*q2-2*q1*q1) ) ;
% Bank Angle
Euler(2,ii) = -asin( 2*q3*q1 - 2*q2*q4 ) ;
% Pitch Attitude Angle
Euler(3,ii) = atan2( (2*q2*q1 + 2*q3*q4), (1-2*q3*q3-2*q2*q2) ) ;

```

```

% Heading Angle
cxdot          = SolveEOM(t,x(:,ii),Geom,Wt,I,InvI,WindSpeedE,DE)
; % Find F(t(ii),x(ii)) (First Iteration)
xdot(:,ii)     = cxdot
; % Keep Accelerations at time step ii
k1x            = dt*cxdot
; % Delta x for first iteration
cxdot          = SolveEOM(t+0.5*dt,x(:,ii)
+0.5*k1x,Geom,Wt,I,InvI,WindSpeedE,DE) ;
% Find F(t(ii)+0.5*dt,x(ii)+0.5*k1) (Second Iteration)
k2x            = dt*cxdot
; % delta x for second iteration
cxdot          = SolveEOM(t+0.5*dt,x(:,ii)
+0.5*k2x,Geom,Wt,I,InvI,WindSpeedE,DE) ;
% Find F(t(ii)+0.5*dt,x(ii)+0.5*k2) (Third Iteration)
k3x            = dt*cxdot
; % delta x for third iteration
cxdot          = SolveEOM(t+dt,x(:,ii)+k3x,Geom,Wt,I,InvI,WindSpeedE,DE)
;
% Find F(t(ii)+dt,x(ii)+k3) (Fourth Iteration)
k4x            = dt*cxdot
; % delta x for fourth iteration
x(:,ii+1)      = x(:,ii) + 1/6*(k1x + 2*k2x + 2*k3x + k4x) ;
% Calculate x for t = t + dt
ThetaError     = Euler(2,ii)-ThetaTarget*rpdc ;
[DE,xController] = PIDController(xController,Controller,ThetaError,dt);
% Call Function which integrates the controller.
ii             = ii + 1 ;
% Increment time counter
t              = t + dt ;
% t = current time
if (ii > 2)    & (x(13,ii) >= 0), Crash = true; end ;
% Detect if Altitude < 0 (Recall +Ze is down)
if isnan(x(1,ii)) | isinf(x(1,ii)) , Crash = true; end ;
% Detects numerical problems
if Crash
    xdot(:,ii) = xdot(:,ii-1) ;
    Euler(:,ii) = Euler(:,ii-1) ;
    DEArray(ii) = DEArray(ii-1) ;
end ;
end ;
% End Runge-Kutta Solution
time          = [0:dt:dt*(ii-1)] ;
% Create Time Array
return

% ***** // PD Controller // *****
function [DE,xnew] = PIDController(x,Controller,ThetaError,dt)

    cxdot = ControllerFunction(Controller,x,ThetaError) ;
    k1x   = dt*cxdot ;
    cxdot = ControllerFunction(Controller,x+0.5*k1x,ThetaError);
    k2x   = dt*cxdot ;
    cxdot = ControllerFunction(Controller,x+0.5*k2x,ThetaError);
    k3x   = dt*cxdot ;

```

```

    cxdot = ControllerFunction(Controller,x+k3x,ThetaError)    ;
    k4x   = dt*cxdot                                         ;
    xnew  = x + 1/6*(k1x + 2*k2x + 2*k3x + k4x)              ;
    DE    = Controller.C * x + Controller.D * ThetaError    ;
function xdot = ControllerFunction(Controller,x,ThetaError)
    xdot  = Controller.A * x + Controller.B * ThetaError    ;
return

% ***** // Get External Forces // *****
function xdot = SolveEOM(t,x,Geom,Wt,I,InvI,WindSpeedE,DE)
UW = x( 1) ; % True velocity in wind axis
AOA = x( 2) ; % A/C Angle of Attack (Alpha)
Beta = x( 3) ; % A/C Angle of Sideslip
PB = x( 4) ; % Body axis roll rate
QB = x( 5) ; % Body axis pitch rate
RB = x( 6) ; % Body axis yaw rate
q1 = x( 7) ; % Euler Parameter q1 (Quaternion)
q2 = x( 8) ; % Euler Parameter q2 (Quaternion)
q3 = x( 9) ; % Euler Parameter q3 (Quaternion)
q4 = x(10) ; % Euler Parameter q4 (Quaternion)
XE = x(11) ; % Longitudinal displacement
YE = x(12) ; % Lateral displacement
ZE = x(13) ; % Vertical displacement
g = 32.174 ; % Acceleration of Gravity (ft/sec2)
% ***** // Prepare Data for EOMs // *****
TyAOA    = [ cos(AOA) 0 -sin(AOA)
             0      1  0
             sin(AOA) 0  cos(AOA) ] ;
% Y-Axis Transformation Rotation due to AOA
TzBeta   = [ cos(Beta) sin(Beta) 0
             -sin(Beta) cos(Beta) 0
             0          0      1 ] ;
% Z-Axis Transformation Rotation due to Beta
OmegaB   = [ 0 ; QB ; RB ] ;
% Airplane BODY axis rates

VelocityW = [ UW ; 0 ; 0 ] ;
% Airplane velocity in WIND axis
EulerOffsetMatrix = [ 0 -q3 q2
                     q3 0 -q1
                     -q2 q1 0 ] ;
% Euler Offset Matrix for Creating DCM (Transformation from Earth to Aircraft
Coordinate Systems Using Quaternions)
OmegaOffsetMatrixB = [ 0 -RB QB
                     RB 0 -PB
                     -QB PB 0 ] ;
% Offset Matrix for OmegaB
EtoBDCM = eye(3) + (EulerOffsetMatrix * EulerOffsetMatrix).*2 -
EulerOffsetMatrix.*(2*q4) ; % Direccion Cosine Matrix (Rotation from Earth to
Aircraft) % ***** // Calculate External Forces and Accelerations //
*****
[ExtForceCGW,ExtForceCGB,ExtMomentCGB] =
GetExternalForces(x,Geom,Wt,I,EtoBDCM,WindSpeedE,DE) ; % Calculate External
Forces and Moments % ***** // Translational EOM // *****
VelocitydotW = ExtForceCGW .* (g / Wt) ;

```

```

% Aircraft Acceleration in Wind Axis (Force EOM) % ***** // Rotational
EOMs // *****
wIw          = cross(OmegaB,I*OmegaB) ;
% Omega cross I*Omega
OmegadotB   = inv(I)*(ExtMomentCGB - wIw) ;
% Aircraft Body Axis Rotational Acceleration (Moment EOM)
QW          = -VelocitydotW(3) / UW ;
% Wind axis pitch rate
RW          = VelocitydotW(2) / UW ; % Wind axis yaw rate
AOAdot      = QB - ((PB*cos(AOA) + RB*sin(AOA))*sin(Beta) + QW) / cos(Beta) ;
% Rate of change of angle of attack
Betadot     = RW + PB*sin(AOA) - RB*cos(AOA) ;
% Rate of change of sideslip angle
% ***** // Four Variable Attitude Propagation // *****
QuaternionMatrix = [ q4 -q3 q2
                    q3 q4 -q1
                    -q2 q1 q4
                    -q1 -q2 -q3 ] ;
qdot        = (QuaternionMatrix * OmegaB) .* 0.5 ;
% Derivatives of Euler Parameters
% ***** // Navigation / Translation EOM // *****
VelocityE    = EtoBDCM' * TyAOA * TzBeta' * VelocityW ;
% Velocity in EARTH fixed axis (Recall Tz'(beta) = Tz(- beta)), Also EtoADCM'
= AtoEDCM
VelocitydotE = EtoBDCM' * TyAOA * TzBeta' * VelocitydotW ;
% Acceleration in EARTH fixed axis
% ***** // Create Derivative Vector // *****
xdot = [ VelocitydotW(1)
        AOAdot
        Betadot
        OmegadotB
        qdot
        VelocityE
        VelocitydotE] ;
% Derivative of state vector x
return
function [ExtForceCGW,ExtForceCGB,ExtMomentCGB] =
GetExternalForces(x,Geom,Wt,I,EtoBDCM,WindSpeedE,DE)
UW          = x( 1) ; % True velocity in wind axis
AOA         = x( 2) ; % A/C Angle of Attack (Alpha)
Beta        = x( 3) ; % A/C Angle of Sideslip
PB          = x( 4) ; % Body axis roll rate
QB          = x( 5) ; % Body axis pitch rate
RB          = x( 6) ; % Body axis yaw rate
Alt         = -x(13) ; % Altitude = -ZE
Sref = Geom.RefArea ;
bref = Geom.RefSpan ;
cref = Geom.RefChord ;
% // ***** Incorporate Effect of Velocity of Air Mass ***** //
TyAOA      = [ cos(AOA) 0 -sin(AOA)
              0 1 0
              sin(AOA) 0 cos(AOA) ] ;
% Y-Axis Transformation Rotation due to AOA
TzBeta     = [ cos(Beta) sin(Beta) 0
              -sin(Beta) cos(Beta) 0
              0 0 1 ] ;

```

```

% Z-Axis Transformation Rotation due to Beta
WindSpeedW = TzBeta*TyAOA'*EtoBDCM*WindSpeedE ;
% Velocity of Air Mass wrt "Wind Axis" (Before Wind Axis is Updated due to
Velocity of Air Mass)
VelocityAMW = [UW ; 0 ; 0] + WindSpeedW ;
% Velocity of Aircraft wrt Air Mass in "Wind Axis" (Before Wind Axis is
Updated due to Velocity of Air Mass)
dAOA = atan2(VelocityAMW(3),VelocityAMW(1)) ;
% Delta AOA due to Outside Winds
dBeta = atan2(VelocityAMW(2),VelocityAMW(1)) ;
% Delta Beta due to Outside Winds
UW = sqrt(dot(VelocityAMW,VelocityAMW)) ;
% Velocity of Aircraft in Wind Axis WRT Air Mass
AOA = AOA + dAOA ;
% New AOA wrt Air Mass
Beta = Beta + dBeta ;
% New Beta wrt Air Mass
% Because AOA and Beta are updated, all subsequent Wind Axis are true Axis in
the Direction of Relative Wind
% // ***** Aerodynamic Forces and Moments S&C Axis ***** //
%[Mach,QPSI,vfps,KTAS,KEAS,KCAS] = SpeedConv(UW,Alt,'VFPS') ; % Convert speeds
Mach = 0.0 ;
% ****ADDED BY MENDOZA TO FIX ABOVE CODE****
vfps = UW ;
% ****ADDED BY MENDOZA TO FIX ABOVE CODE****
QPSI = 0.5*0.0023769*vfps^2/144 ;
% ****ADDED BY MENDOZA TO FIX ABOVE CODE****

[CL,CD,Cm,Cn,Cy,Clp,Cmq,Cnr] = GetAerodynamicData(Mach,AOA,Beta,DE); % Get
Aerodynamic Coeff.
FxAeroS = -CD *QPSI*Sref ;
% Drag coefficient with sign swapped as positive X is forward
FyAeroS = Cy *QPSI*Sref ;
% Lateral load coefficient
FzAeroS = -CL *QPSI*Sref ;
% Lift coefficient with sign swapped as positive Z is down
Helix = bref / (2 * UW * 12) ;
% Helix Angle for Dynamic Derivatives (bwinch/2vips)
GxAeroS = ( 0*Clp*PB*Helix )*QPSI*Sref*bref ;
% Rolling Moment Buildup (S/C Axis)
GyAeroS = (Cm + Cmq*QB*Helix )*QPSI*Sref*cref ;
% Pitching Moment Buildup (S/C Axis)
GzAeroS = (Cn + Cnr*RB*Helix )*QPSI*Sref*cref ;
% Yawing Moment Buildup (S/C Axis)
FAeroS = [ FxAeroS ; FyAeroS ; FzAeroS ] ;
% Force Vector S/C Axis
GAeroS = [ GxAeroS ; GyAeroS ; GzAeroS ] ;
% Moment Vector S/C Axis
% // ***** Prepare Direction Cosine Matrices ***** //
TyAOA = [ cos(AOA) 0 -sin(AOA)
0 1 0
sin(AOA) 0 cos(AOA) ] ;
% Y-Axis Transformation Rotation due to AOA
TzBeta = [ cos(Beta) sin(Beta) 0
-sin(Beta) cos(Beta) 0
0 0 1 ] ;

```

```

% Z-Axis Transformation Rotation due to Beta
% // ***** Calculate NET Forces in WIND Axis ***** //
Ty180 = [-1 0 0
0 1 0
0 0 -1] ; % Rotation from aircraft to body axis
WeightE = [ 0 ; 0 ; Wt] ;
% Airplane weight in EARTH axis (Recall Earth Axis +Z Down)
WeightW = TzBeta*TyAOA'*EtoBDCM*WeightE ;
% Rotate Weight Vector into WIND Axis (Recall TyAOA' = Ty(-AOA))
FAeroW = TzBeta*FAeroS ;
% Rotate Aerodynamic Force Vector into WIND Axis
ExtForceCGW = FAeroW + WeightW ;
% Calculate External Forces in WIND Axis
ExtForceCGB = TyAOA * TzBeta' * ExtForceCGW ;
% Calculate External Forces in BODY Axis
% // ***** Calculate NET Moments in BODY Axis ***** //
CGtoARPA = Geom.ARP - Geom.CG ;
% Calculate Radius From CG to A/C Ref Point (In Aircraft Coordinates)
CGtoARPB = Ty180*CGtoARPA' ;
% Rotate Radius into Body Axis (Recall Body +X fwd and +Z down)
FAeroB = TyAOA*FAeroS ;
% Rotate FAeroS into Body Axis
GAeroB = TyAOA*GAeroS ;
% Rotate GAeroS into Body Axis, at airplane reference point
GAeroB(1) = 0 ;
% Eliminate Rolling Moments due to Symmetry
%Projectile Trajectory
ExtMomentCGB = GAeroB + cross(CGtoARPB,FAeroB); % Aerodynamic Moments About CG
%fprintf('ForceCGW: %8.0f %8.0f %8.0f ForceCGB: %8.0f %8.0f %8.0f MomentCGB:
%8.0f %8.0f %8.0f AOA:
%8.4f\n',[ExtForceCGW;ExtForceCGB;ExtMomentCGB;AOA*180/pi]);
return
function [CL,CD,Cm,Cn,CY,Clp,Cmq,Cnr] = GetAerodynamicData(Mach,AOA,Beta,DE)
AOA = AOA * 180/pi;
Beta = Beta * 180/pi;
if abs(AOA) > 180, AOA = AOA - sign(AOA) *(floor(AOA /360)+1)*360; end; %
Quadrant Check
if abs(Beta) > 180, Beta = Beta - sign(Beta)*(floor(Beta/360)+1)*360; end; %
Quadrant Check
if abs(AOA) == 360, AOA = 0; end ;
if abs(Beta) == 360, Beta = 0; end ;
% AOA, CL, CD, Cm
PitchData = [-180 0.000 0.013 0.000
-176 0.192 0.028 0.012
-172 0.384 0.140 0.024
-168 0.624 0.290 0.036
-166 0.702 0.400 0.048
-164 0.546 0.520 0.038
-162 0.480 0.650 0.029
-140 0.144 0.850 0.010
-120 0.058 0.990 0.010
-90 0.000 1.080 0.020
-60 -0.120 0.990 0.020
-40 -0.300 0.850 0.020
-18 -1.000 0.650 0.060
-16 -1.050 0.520 0.080

```

% RBF1-1 Opti.03

```
-12.0 -0.24140133718635662 0.02815444745556085
0.05153076102356748
-11.0 -0.1597652054275452 0.026523759831385024 0.049361575530642625
-10.0 -0.07747820862425675 0.02529209506029148 0.04679253872171702
-9.0 0.005412443003358988 0.024490776465914334 0.04382660532606242
-8.0 0.08885777916436356 0.02414978008104369 0.04046722195305117
-7.0 0.1728071510366291 0.02429764696478459 0.03671832316408968
-6.0 0.2572083168731749 0.024961399491036675 0.03258432670509867
-5.0 0.3420075315159022 0.026166461729841908 0.028070127946159488
-4.0 0.4271496396714796 0.027936584061692915 0.023181093582643992
-3.0 0.5125781728038253 0.030293772183624893 0.017923054652977784
-2.0 0.5982354494861905 0.03325822068070915 0.0123022989243337
-1.0 0.6840626790371863 0.03684825134527275 0.0063255626911313855
0.0 0.7700000682428392 0.04108025642824139 2.2023899793456214E-8
1.0 0.8559869309436856 0.04596864700292472 -0.0066667165009592156
2.0 0.9419618002441997 0.051525806612368434 -0.013666625566046534
3.0 1.027862543082335 0.05776205035830546 -0.020991267352824552
4.0 1.1136264768804884 0.06468558957390692 -0.028631804240332803
5.0 1.1991904879856226 0.07230250220491516 -0.03657900994901448
6.0 1.2844911515955282 0.08061670900510866 -0.04482328111731043
7.0 1.3694648528600222 0.08962995563290953 -0.053354649299367285
8.0 1.4540479088398615 0.09934180071668629 -0.06216279337232686
9.0 1.538176691002002 0.10974960993711758 -0.07123705234143815
10.0 1.6217877479273368 0.1208485561560245 -0.08056643853074642
11.0 1.7048179279059503 0.1326316256024124 -0.09013965114649185
12.0 1.7872045010950337 0.1450896301080989 -0.09994509019967583
13.0 0 0.15821122536729154 -0.10997087077351317
14.0 0 0.17198293517680585 -0.12020483762081682
15.0 0 0.23343708145739983 -0.12406313421356047
16.0 0 0.24988489267729347 -0.13387295095336418
17.0 0 0.26689165103997325 -0.14380964165019328
18.0 0 0.2844320704653487 -0.15386116139397985
19.0 0 0.3024790231177442 -0.1640153237150806
```

% End RBF1-1 Data

```
40 0 0.850 -0.020
60 0 0.990 -0.020
90 0.000 1.080 -0.020
120 -0.058 0.990 -0.010
140 -0.144 0.850 -0.010
162 -0.480 0.650 -0.029
164 -0.546 0.520 -0.038
166 -0.702 0.400 -0.048
168 -0.624 0.290 -0.036
172 -0.384 0.140 -0.024
176 -0.192 0.028 -0.012
180 0.000 0.013 0.000 ] ;
```

```
YawData = [ -180 0.000 0.013 0.000
-176 0.192 0.028 0.012
-172 0.384 0.140 0.024
-168 0.624 0.290 0.036
-166 0.702 0.400 0.048
-164 0.546 0.520 0.038
```

```

-162 0.480 0.650 0.029
-140 0.144 0.850 0.010
-120 0.058 0.990 0.010
-90 0.000 1.080 0.020
-60 -0.120 0.990 0.020
-40 -0.300 0.850 0.020
-18 -1.000 0.650 0.060
-16 -1.050 0.520 0.080
-14 -1.350 0.400 0.100
-12 -1.200 0.290 0.075
-8 -0.800 0.140 0.050
-4 -0.400 0.028 0.025
0 0.000 0.013 0.000
4 0.400 0.028 -0.025
8 0.800 0.140 -0.050
12 1.200 0.290 -0.075
14 1.350 0.400 -0.100
16 1.050 0.520 -0.080
18 1.000 0.650 -0.060
40 0.300 0.850 -0.020
60 0.120 0.990 -0.020
90 0.000 1.080 -0.020
120 -0.058 0.990 -0.010
140 -0.144 0.850 -0.010
162 -0.480 0.650 -0.029
164 -0.546 0.520 -0.038
166 -0.702 0.400 -0.048
168 -0.624 0.290 -0.036
172 -0.384 0.140 -0.024
176 -0.192 0.028 -0.012
180 0.000 0.013 0.000 ] ; % Beta, CY, CD, Cn

%GE Mendoza
%Projectile Trajectory
Cmq = -2 / sqrt(1 - Mach^2) ; % Pitching moment due to pitch rate (damping)
Cnr = -2 / sqrt(1 - Mach^2) ; % Yawing moment due to yaw rate (damping)
Clp = -1 / sqrt(1 - Mach^2) ; % Rolling moment due to roll rate (damping)
CLde = -0.0045 ; % Lift due to elevon deflection (per deg.)
CDde = 9.04191E-05 ; % Drag due to elevon deflection (per
deg.)
Cmde = 0.008414 ; % Pitching moment due to elevon deflection (per
deg.)
% // ***** Interpolate Data ***** //
CL = (interp1(PitchData(:,1),PitchData(:,2),AOA) + Cmde*DE) / sqrt(1 -
Mach^2); % Lift Coeff.
CDaoa = interp1(PitchData(:,1),PitchData(:,3),AOA) / sqrt(1 - Mach^2);
% Drag Coeff.
Cm = (interp1(PitchData(:,1),PitchData(:,4),AOA) + Cmde*DE) / sqrt(1 - Mach^2);
% Pitching Moment Coeff.
CY = interp1(YawData(:,1),YawData(:,2),Beta)*-1 / sqrt(1 - Mach^2);
% Side Force Coeff.
CDbeta = interp1(YawData(:,1),YawData(:,3),Beta) / sqrt(1 - Mach^2);
% Drag Coeff.
Cn = interp1(YawData(:,1),YawData(:,4),Beta)*-1 / sqrt(1 - Mach^2);
% Yawing Moment Coeff.
CD = CDaoa + CDbeta + CDde*DE;

```

```
% Sum of Drag due to AOA, Beta, and DE  
return
```